Geophysical Journal International

Geophys. J. Int. (2012) **189,** 1635–1666 doi: 10.1111/j.1365-246X.2012.05435.x

Kinematic time migration and demigration of reflections in pre-stack seismic data

Einar Iversen,[1] Martin Tygel,[2] Bjørn Ursin[3] and Maarten V. de Hoop[4]

[1]*NORSAR, Gunnar Randers vei* 15, P.O. Box 53, 2027 *Kjeller, Norway. E-mail: einar@norsar.no*
[2]*State University of Campinas (UNICAMP), Department of Applied Mathematics, R. Sérgio Buarque de Holanda* 651, 13083-859 *Campinas SP, Brazil*
[3]*Norwegian University of Science and Technology (NTNU), Department of Petroleum Engineering and Applied Geophysics, S.P. Andersensvei* 15A, NO-7491 *Trondheim, Norway*
[4]*Center for Computational and Applied Mathematics, Purdue University,* 150 N. *University Street, West Lafayette* IN 47907, *USA*

Accepted 2012 February 24. Received 2012 February 24; in original form 2011 September 29

SUMMARY

In kinematic time migration one maps the time, slope and curvature characteristics of seismic reflection events, referred to as reflection-time parameters, from the recording domain of the seismic data to the time-migration domain. The inverse process is kinematic time demigration. We generalize kinematic time migration and demigration in several respects: the reflection-time parameters may belong to arbitrary source–receiver offsets; local heterogeneity of the time-migration velocity model is accounted for; the mapping operations do not depend specifically on the type of diffraction-time function and the parametrization of the velocity model. Time-migration and time-demigration spreading matrices are obtained as byproducts of the mapping operations. These matrices yield a paraxial expression for the connection between midpoint and image-point gather locations of mapped reflection events. Also, we obtain the time-migration counterpart of the so-called second duality theorem in Kirchhoff depth migration. Diffractions and reflections are assumed to be without conversion, and sources and receivers are located along the same measurement surface. Our framework enables the identification of a full set of first- and second-order reflection-time parameters from time-migrated seismic data followed by a kinematic demigration to the recording domain. The idea of this route is to 'undo' eventual errors introduced by time migration and result in reliable estimation of recording-domain invariants, that is, parameters insensitive to the time-migration velocity model. The developed concepts associated with time migration are of interest in reflection seismic and global earth applications. Two numerical examples demonstrate the potential of kinematic time migration and demigration techniques in seismic time imaging and velocity-model building.

Key words: Image processing; Numerical approximations and analysis; Tomography; Body waves; Computational seismology; Wave scattering and diffraction.

1 INTRODUCTION

Time migration has been widely applied by the seismic processing industry for decades and still holds the position as the most frequently used imaging technique. Considering research and development, however, the situation is different: there, most of the resources are devoted to depth-migration methods. Although time migration has clear limitations with respect to lateral velocity variations (e.g. Robein 2003) it also has, in particular, two great advantages over depth migration: (i) time migration is normally a much faster process; (ii) the problem of estimating a velocity model for time migration is, in general, well posed.

The final goal of the seismic processing sequence is to obtain a well focused and accurately located image in depth. However, because of the difficulties involved in estimating a reliable depth-migration velocity model and a depth image of sufficient quality, it is often preferred to perform interpretation of geological structures on time-migrated images. In this way, the ill-posed part of the imaging process can be postponed until more information is available. This probably explains why time migration is still attractive, in spite of its known weaknesses.

Time migration transforms seismic data from the domain of its recording coordinates to another domain in time, the time-migration domain. Both data domains are 5-D, assuming maximal acquisition geometry. The process has an inverse counterpart, time demigration, which transforms data from the migration domain to the recording domain. The analogous processes of depth migration and demigration are well established in the seismic literature. The combination of them to solve a number of imaging problems is referred to as a 'unified approach to seismic reflection imaging' in the companion

papers Hubral *et al.* (1996) and Tygel *et al.* (1996). A review of this approach is presented in Schleicher *et al.* (2007).

Considering waves of light, the Dutch physicist Christiaan Huygens proposed (in *Traité de la Lumière*, 1690) that every point to which a luminous disturbance reaches becomes a source of a spherical wave, and the sum of these secondary waves determines the form of the wave at any subsequent time. This important observation, known as *Huygens' principle*, forms the basis of today's techniques for seismic modelling and imaging. The secondary sources are then considered as potential diffraction points, distributed continuously within the (depth) region of interest. One particular approach to time migration, the *diffraction stack method* (Lindsey & Hermann 1970), performs summation along diffraction curves and may be said to represent a direct application of Huygens' principle. For a historical overview of diffraction stack and other methods for time migration, the reader is referred to, for example Yilmaz (2000, 2001) or Robein (2003). Bancroft (2007) also reviews time-migration approaches and divides them into two categories: (i) pseudo pre-stack time migration, which refers to a computationally cheap route via dip-moveout processing; and (ii) full pre-stack time migration. Only full pre-stack time migration is considered in this paper.

Full pre-stack time migration is conventionally conducted using an explicit two-way diffraction-time function specified in the time-migration domain. Thereby, the diffraction-time function is directly related to a migration-velocity model in this domain. The 'elementary diffraction time', that is, the two-way time from source to receiver via a single diffraction point in the subsurface, is a function of two basic quantities, source–receiver offset and migration aperture, which are defined specifically below. One example is the classic double-square-root function (e.g. Claerbout 1985), which is exact for a homogeneous isotropic medium. When assuming small offsets or apertures, this function is well approximated by a corresponding single-square-root function (Hubral & Krey 1980). For large offsets or apertures, however, it is often necessary to use more sophisticated traveltime functions (e.g. Alkhalifah 2000; Tsvankin 2005; Ursin & Stovas 2006). This will typically be a consequence of lateral velocity variations or anisotropy in the underlying (depth) medium. Because of the historical role of the classic single- and double-square-root functions in time-migration algorithms, we find it useful to discuss them explicitly below.

It is remarked that when performing *time* migration (in the standard way) to one specific output point, it suffices to evaluate the time-migration velocity model only at that location. On the other hand, when performing *depth* migration in a similar manner, a minimum requirement is that the depth–velocity model can be accessed everywhere in a certain wave-propagation volume encapsulating the output point and the relevant source–receiver locations. We find this to be an often overlooked difference between time and depth migration.

The classic approach to reduce noise and retrieve velocity-sensitive information from recorded pre-stack seismic data is common-midpoint (CMP) stacking (Mayne 1962). With this method, stacking over source–receiver offsets is done separately for gathers of traces corresponding to a common source–receiver midpoint. Before stacking one performs velocity analysis (Taner & Koehler 1969) and *normal-moveout* (NMO) correction. In recent years, there has been a development of a suite of processing techniques utilizing that coherent local reflection events in the recording domain of the seismic data constitute a (hyper)surface, often referred to as the *common reflection surface* (CRS). From such surfaces one can estimate time, slope and curvature characteristics of the local events. These 'reflection-time parameters' (or CRS parameters) can be used for multi-midpoint stacking (or CRS stacking, Jäger *et al.* 2001; Duveneck 2004). Therefore, with the introduction of the reflection-surface concept the stacking process is no longer limited to separate CMP gathers.

In CRS processing it is common to assume that the reflection-time parameters belong to zero offset; we shall however abandon this restriction in the current paper and allow the reference offset to be finite (non-zero). For CRS processing in the finite-offset situation, see, for example, Zhang *et al.* (2001). Reflection-time parameters in the recording domain are *invariants*, that is, they are independent with respect to the migration-velocity model in time or depth. This property makes these parameters very attractive for the purpose of estimating or updating such models. Recent research is utilizing the CRS concept also in the context of time migration (e.g. Dell & Gajewski 2011). In the time-migration domain, the CRS is generally more well behaved and more easily identified than in the recording domain, because of less noise, structures looking more like geology and collapse of diffractions (fully or partially).

Based on spherically symmetric models, the analogues of stacking and the notion of CMP have been developed also in global earth applications. Here, epicentral distance plays the role of source–receiver offset; bounce points play the role of midpoints. Shearer (1991) pioneers the use of stacking methods for global data sets. He introduces an approach using a reference phase to normalize the amplitude and phase of each seismogram and a median filter over nearby bins to enhance the coherence. It performs well in practice at long periods ($\geq$15 s) because the timing differences due to the ellipticity and 3-D spatial variations are generally less than the dominant period of such data. Stacking along theoretical (differential) traveltime curves corresponding with basic Kirchhoff migration is further developed by Flanagan & Shearer (1998). Alternative stacking methods have been developed and applied to facilitate the observation of secondary phases (Deuss *et al.* 2000). Chambers *et al.* (2005) carry out the stacking in the time-slowness domain relative to a reference epicentral distance and also use a convolutional model to estimate reflectivity. In the context of this paper, the developed concepts associated with time migration have potential global earth applications.

Pre-stack time migration and demigration have kinematic equivalents referred to as 'kinematic time migration' and 'kinematic time demigration', applicable when coherent reflection events are present in the seismic data. The philosophy behind these techniques is depicted in Fig. 1, for a certain constant source–receiver offset: a reflector in depth can be considered as a continuum of diffraction points (brown dots)—each point gives rise to an elementary diffraction-time function (grey). The diffraction-time response of the entire reflector has the reflection-time function (red) in the recording domain as its envelope. In the time-migration domain, the reflection-time function (blue) represents a continuum of all the minima of the elementary diffraction-time functions. Kinematic time migration is to map a local reflection event with (recording) time T^X posted in the midpoint X to a new (migrated) time $\mathcal{T}^M$ in the point M^{CIG}—the points X and M^{CIG} are both located in a horizontal plane, Σ. The inverse process is kinematic time demigration. Both processes require knowledge of local slopes in the seismic data (Douma & de Hoop 2006; Schleicher *et al.* 2009). In the following, a point of the type M^{CIG}, which localizes a common-image gather of the migrated seismic data, is referred to as a 'common-image point'.

Fig. 1 also introduces the 'diffraction isochron', which is an important concept inherent to seismic imaging. For a specific couple

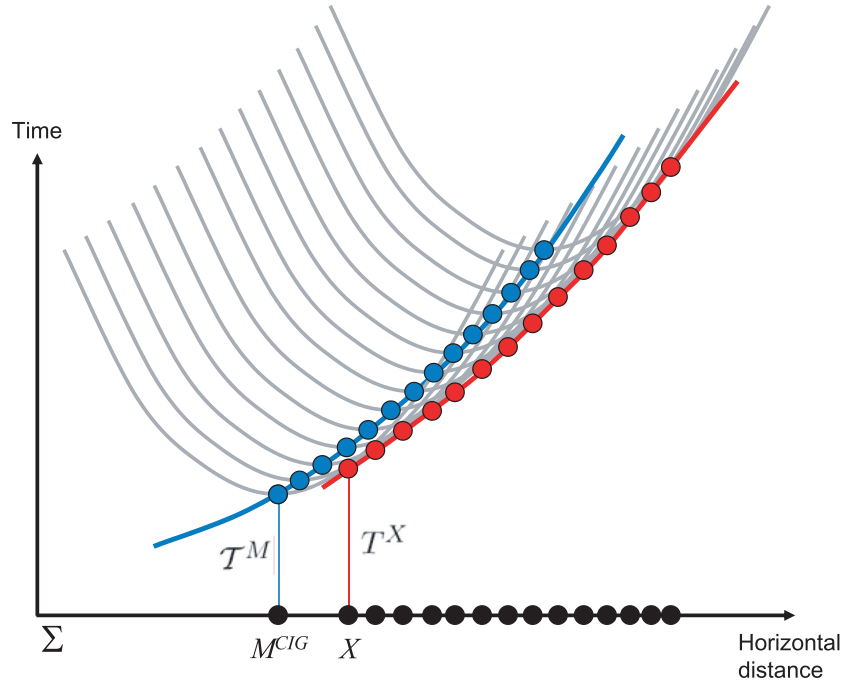

(a)

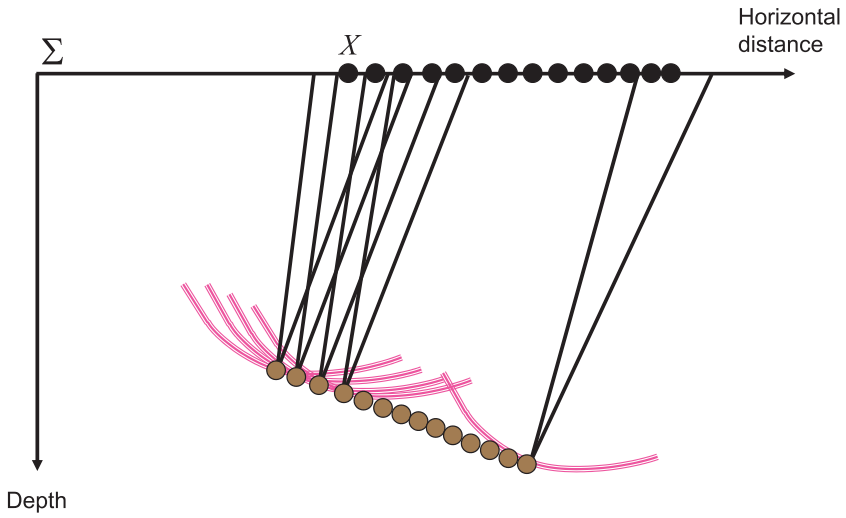

(b)

Figure 1. (a) Considering a given constant offset, the collection of elementary diffraction-time functions (grey) for a given reflector in depth has the reflection-time function (red) in the recording domain as its envelope. Each output location of a classic time-migration process corresponds to minimum diffraction time between a uniquely defined diffraction point in depth and a planar horizontal reference (datum) surface, Σ. The reflection-time function (blue) in the time-migration domain represents a continuum of such elementary diffraction-time minima. Kinematic time migration is to map a local reflection event with (recording) time T^X posted in the midpoint X to a new (migrated) time $\mathcal{T}^M$ in the common-image point M^{CIG}. The inverse process is called kinematic time demigration. (b) Discrete diffraction points (brown) forming the reflector and some of the associated constant-offset ray paths (black). Also indicated are diffraction isochrons (pink), along which the diffraction time for a certain X is constant and equal to the corresponding reflection time T^X.

of source and receiver locations, or equivalently, for a fixed offset and a fixed midpoint, X, the diffraction isochron is defined as the surface of constant diffraction time (i.e. the surface for which the diffraction time equals the constant time T^X signified in Fig. 1).

The counterpart of kinematic time migration for mapping into depth, kinematic depth migration (or 'map migration'), uses the same input reflection-time parameters to yield local reflector depth, dips, and curvatures (Shah 1973; Kleyn 1977; Hubral & Krey 1980; Gjøystdal & Ursin 1981; Ursin 1982b; Iversen & Gjøystdal 1996; Iversen 2004; Douma & de Hoop 2006; Stolk *et al.* 2009). It is also possible to do a corresponding time-to-depth mapping directly from the time-migration domain using image rays (Hubral 1977; Hubral & Krey 1980). This approach is, however, known to have more limited applicability than kinematic depth migration, as a result of the limitations inherent to conventional time migration. Some recent achievements in image-ray mapping are described by Tygel *et al.* (2012).

One can probably consider a graphical technique for migration (Bleistein *et al.* 2001, p. 10), applied before the introduction of computers, as the first approach to kinematic time or depth migration. By that method, a zero-offset reflector image is constructed geometrically as the envelope of semicircles. Whitcombe (1994) introduces kinematic time demigration for the zero-offset situation and demonstrates mapping of time and slope parameters under the assumption of locally constant migration velocities. Söllner & Andersen (2005) describe zero-offset kinematic migration/demigration of time and slope parameters under a ray-theoretical perspective, so that the resulting mapping equations are expressed in terms of surface-to-surface ray paraxial matrices of normal and image rays. Robein (2003, p. 435) points out that Whitcombe (1994)'s equations were published relatively recently and are thus overlooked by many users. Furthermore, he states: 'Note, moreover, that these published equations must be updated to take account of time and space variability of the migration-velocity field in 3-D'. In the methodology part below, one key objective is to present such updated equations.

In this paper, we extend previous approaches to kinematic time migration and demigration of reflection-time parameters so that the parameter estimation and the mapping operations can be performed for any constant source–receiver offset, not just zero offset. In addition to mapping the reflection time and its slopes, we provide the option of mapping the full set of reflection-time second-derivatives. To improve accuracy the local heterogeneity of the time-migration velocity model is accounted for. The derived mapping formulas do not depend explicitly on the type of diffraction-time function and the parametrization of the velocity model.

In typical applications of the presented methodology one would start by time-migrating the seismic data using a preliminary time-migration velocity model. The purpose is to utilize the fact that identification of seismic reflection events is generally much more easily done in the migration domain than in the recording domain, even if the time-migration velocity model is not optimal. For each selected event we estimate local reflection-time parameters, which are subsequently kinematically demigrated to the recording domain. In this demigration operation one should use the same time-migration velocity model as in the original migration of the seismic data. The idea is that this will undo eventual errors introduced by the migration and result in reliable estimation of reflection-time invariants (e.g. Robein 2003). Knowing such invariants the ground is prepared for the important applications time-migration and depth-migration tomography. For an overview regarding velocity-model building in time or depth, see Robein (2003) and Jones (2010). Recent approaches to estimate the time-migration velocity model can be found in, for example, Fomel (2003, 2007), Cooke *et al.* (2009) and Dell & Gajewski (2011).

In the approaches to kinematic time migration and demigration presented below the time-migration velocity model is assumed known. We discuss how this model can be obtained at the very end of the methodology part, supported by two numerical examples. Our paper is focused on kinematic (or geometric) aspects of time migration and demigration. For completeness, Appendix A provides a brief treatment also of important dynamic aspects, using concepts and notation from microlocal analysis. One important observation in this context is that the kinematics of time migration is not completely detached from its dynamics. In particular, for a reliable estimation of reflection-time parameters at finite offsets in the time-migration domain it is essential that the time-migrated data have been properly compensated for stretch effects. The relevant stretch factor is introduced in Appendix A. In addition, we provide there an independent derivation of the basic conditions for kinematic time migration and demigration formulated in the main text.

In the following, we first describe the involved coordinates of the recording and time-migration domains of the seismic data, the principles of pre-stack time migration, the properties of the diffraction-time function, the underlying time-migration velocity model, and the reflection-time parameters in the two data domains. Thereafter, kinematic migration and demigration is presented in the same order as they appear in the natural application sequence outlined above, namely, with demigration coming before migration.

Table 1 gives an overview of most mathematical symbols used in the paper. To distinguish between vector and matrix entities that are zero, we use the notations $\mathbf{0}$ and $\mathbf{O}$ for, respectively, the zero vector of dimension 2 and the zero matrix of size 2×2. The symbol $\mathbf{I}$ signifies the 2×2 identity matrix. Moreover, some mathematical quantities may take the roles both as independent and dependent variables. We separate these two situations by marking the independent quantity (e.g. $\mathbf{x}$) and the function (e.g. $\hat{\mathbf{x}}$) without and with a hat, respectively. In the figures illustrating the methodology, quantities belonging to the recording, time-migration and depth-migration domains are shown, respectively, in red, blue and brown.

2 COORDINATE SYSTEMS FOR RECORDED AND MIGRATED SEISMIC DATA

A fixed Cartesian coordinate system (ξ_1, ξ_2, ξ_3) is used for describing the 3-D depth domain. We use the convention of collecting the first two of these coordinates in the vector $\boldsymbol{\xi}$. The horizontal plane $\xi_3 = 0$ is the measurement surface, Σ, where all sources and receivers of the seismic experiment are located. For an outline of the involved lateral coordinates, see Fig. 2. The recording of seismic data can then be described in terms of the 5-D domain $(\mathbf{s}, \mathbf{r}, t)$, where $\mathbf{s}$ and $\mathbf{r}$ are two-component vectors defining the positions of any source point, S, and receiver point, R, situated along Σ, and t is the recording time. The vectors $\mathbf{s}$ and $\mathbf{r}$ both belong to the Cartesian sub-coordinate system (ξ_1, ξ_2). The three coordinates of a common-source (or common-shot) gather are $(\mathbf{r}, t)$, given that the source coordinates, $\mathbf{s}$, are fixed. Conversely, for fixed receiver coordinates, $\mathbf{r}$, the coordinate space $(\mathbf{s}, t)$ constitutes a common-receiver gather.

The midpoint, X, between source and receiver shall be specified by the two-component vector $\mathbf{x}$. We also use half-offset coordinates,

Table 1. Overview of mathematical symbols used in the paper. For vector and matrix quantities the dimension is specified.

Quantity	Dimension	Description
(ξ_1, ξ_2, ξ_3)	3	Cartesian coordinate system
$\boldsymbol{\xi}$	2	Lateral position vector, (with components ξ_1 and ξ_2)
ξ_3		General depth coordinate
Σ		Measurement and migration datum surface, $\xi_3 = 0$
t		Recording time
ω		Angular frequency
S		Source point in the surface Σ
$\mathbf{s}$	2	Lateral position vector for the point S
R		Receiver point in the surface Σ
$\mathbf{r}$	2	Lateral position vector for the point R
X		Source–receiver midpoint in the surface Σ; common midpoint-gather location
$\mathbf{x}$	2	Lateral position vector for the point X
$\mathbf{h}$	2	Source–receiver half-offset vector
$d(\mathbf{h}, \mathbf{x}, t)$		Recorded seismic data
$D(\mathbf{h}, \mathbf{x}, \omega)$		Frequency spectrum of the data $d(\mathbf{h}, \mathbf{x}, t)$
$s(t)$		Wavelet
$S(\omega)$		Frequency spectrum of the wavelet $s(t)$
$A(\mathbf{h}, \mathbf{x})$		Reflection amplitude
τ		Migration time
υ		Frequency variable in the time-migration domain
M^{CIG}		Image point in the surface Σ; time-migration common image-gather location
$\mathbf{m}$	2	Lateral position vector for the point M^{CIG}
$d^M(\mathbf{h}, \mathbf{m}, \tau)$		Time-migrated seismic data
$\tilde{d}(\mathbf{h}, \mathbf{x}, t)$		Time-demigrated seismic data
$W(\mathbf{h}, \mathbf{x}, \mathbf{m}, \tau, \omega)$		Frequency-dependent weight function
$K_{DS}(\mathbf{h}, \mathbf{x}, \mathbf{m}, \tau)$		Frequency-independent weight function
z		Migration depth
$d^D(\mathbf{h}, \boldsymbol{\xi}, z)$		Depth-migrated seismic data
D		Depth point
D^{CIG}		Point resulting when projecting the point D vertically into the surface Σ; depth-migration common image-gather location
D_0		Depth point corresponding to a zero-offset reflection in a common-midpoint gather at X
X_0		Point in the surface Σ corresponding to a zero-offset reflection at the depth point D
$\mathbf{a}$	2	Time-migration aperture vector
$\mathbf{h}^S$	2	Source-offset vector
$\mathbf{h}^R$	2	Receiver-offset vector
T_0^S		One-way traveltime between the points S and D, for coinciding points S and R
T_0^R		One-way traveltime between the points R and D, for coinciding points S and R
$T^S(\mathbf{h}^S, \mathbf{m}, T_0^S)$		Source-time function
$T^R(\mathbf{h}^R, \mathbf{m}, T_0^R)$		Receiver-time function
$T^D(\mathbf{h}, \mathbf{a}, \mathbf{m}, \tau)$		Diffraction-time function
u, u^τ		Diffraction-time partial derivative scalars
$\mathbf{q}^h, \mathbf{q}^a, \mathbf{q}^m, \mathbf{u}^h, \mathbf{u}^a, \mathbf{u}^m$	2	Diffraction-time partial derivative vectors
$\mathbf{U}^{hh}, \mathbf{U}^{aa}, \mathbf{U}^{mm}$	2×2	Diffraction-time partial derivative matrices
$\mathbf{U}^{ha}, \mathbf{U}^{hm}, \mathbf{U}^{am}$	2×2	Diffraction-time partial derivative matrices
$\mathbf{U}^{ah}, \mathbf{U}^{mh}, \mathbf{U}^{ma}$	2×2	Diffraction-time partial derivative matrices
$\boldsymbol{\alpha}$	7	Domain vector of the function T^D
$N^{\mathcal{V}}$		Number of parameters comprising the time-migration velocity model
$\mathcal{V}_i(\mathbf{m}, \tau)$		Parameters of the time-migration velocity model, for $i = 1, 2, \ldots, N^{\mathcal{V}}$
$\mathbf{S}^M(\mathbf{m}, \tau)$	2×2	Time-migration matrix
θ^a		Angle specifying the direction of vector $\mathbf{a}$
$\mathbf{e}(\theta^a)$	2	Unit vector corresponding to vector $\mathbf{a}$
$V^M(\theta^a, \mathbf{m}, \tau)$		Direction-dependent time-migration velocity
$T(\mathbf{h}, \mathbf{x})$		Reflection-time function in the recording domain
$\bar{\mathbf{x}}$	4	Domain vector of the function T
T^X		Reflection-time parameter scalar in the recording domain
$\mathbf{p}^h, \mathbf{p}^x$	2	Reflection-time parameter vectors in the recording domain

Table 1. (*Continued.*)

Quantity	Dimension	Description
$\mathbf{M}^{hh}$, $\mathbf{M}^{hx}$, $\mathbf{M}^{xx}$	2×2	Reflection-time parameter matrices in the recording domain
$\bar{\mathbf{p}}$	4	Reflection-time parameter vector in the recording domain
$\bar{\mathbf{M}}$	4×4	Reflection-time parameter matrix in the recording domain
$\mathbf{S}^{\mathrm{NMO}}(\mathbf{x})$	2×2	Normal-moveout matrix
θ^h		Angle specifying the direction of vector $\mathbf{h}$
$\mathbf{e}(\theta^h)$	2	Unit vector corresponding to vector $\mathbf{h}$
$v^{\mathrm{NMO}}(\theta^h, \mathbf{x})$		Direction-dependent normal-moveout velocity
$\mathcal{T}(\mathbf{h}, \mathbf{m})$		Reflection-time function in the time-migration domain
$\bar{\mathbf{m}}$	4	Domain vector of the function $\mathcal{T}$
$\mathcal{T}^M$		Reflection-time parameter scalar in the time-migration domain
$\boldsymbol{\psi}^h$, $\boldsymbol{\psi}^m$	2	Reflection-time parameter vectors in the time-migration domain
$\boldsymbol{\mathcal{M}}^{hh}$, $\boldsymbol{\mathcal{M}}^{hm}$, $\boldsymbol{\mathcal{M}}^{mm}$	2×2	Reflection-time parameter matrices in the time-migration domain
$\bar{\boldsymbol{\psi}}$	4	Reflection-time parameter vector in the time-migration domain
$\bar{\boldsymbol{\mathcal{M}}}$	4×4	Reflection-time parameter matrix in the time-migration domain
$\mathbf{K}^{ha}$, $\mathbf{K}^{am}$, $\mathbf{L}^{hh}$, $\mathbf{L}^{hm}$, $\mathbf{L}^{mm}$	2×2	Auxiliary matrices in kinematic migration/demigration of reflection-time second derivatives
$\mathbf{Y}$	2×2	Matrix in the time-migration domain associated with curvatures of the diffraction isochron
$\mathbf{X}^h$, $\mathbf{X}^m$	2×2	Time-demigration spreading matrices
$\boldsymbol{\mathcal{X}}^h$, $\boldsymbol{\mathcal{X}}^x$	2×2	Time-migration spreading matrices
F		Extended time-demigration operator
F^*		Extended time-migration operator
ϕ		Phase function
$\mathbf{0}$	2	Zero vector
$\mathbf{O}$	2×2	Zero matrix
$\mathbf{I}$	2×2	Identity matrix

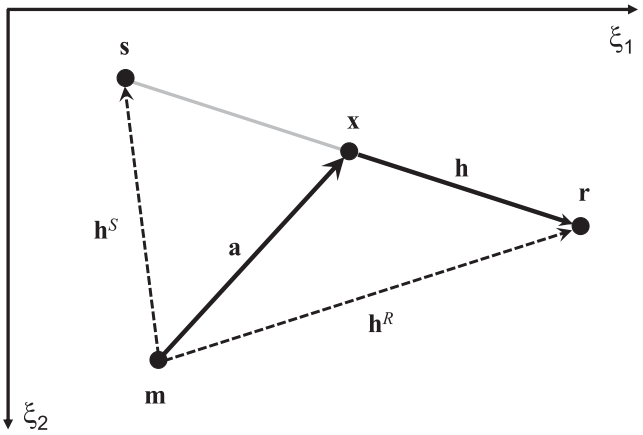

Figure 2. Lateral coordinates **s**, **r**, **x** and **m** of source point (S), receiver point (R), midpoint (X) and common-image point (M^{CIG}), respectively. Also indicated are aperture (**a**), half-offset (**h**), source-offset ($\mathbf{h}^S$) and receiver-offset ($\mathbf{h}^R$) vectors.

h, such that **h** and **x** satisfy the linear transformation

$$\mathbf{h} = \frac{1}{2}(\mathbf{r} - \mathbf{s}), \qquad \mathbf{x} = \frac{1}{2}(\mathbf{r} + \mathbf{s}). \tag{1}$$

In the following, the recording domain is considered as (**h**, **x**, t). In this domain, recorded seismic data are assumed given in the scalar form $d(\mathbf{h}, \mathbf{x}, t)$. A CMP gather of the data $d(\mathbf{h}, \mathbf{x}, t)$ is a subset for which the midpoint vector, **x**, is fixed. The internal coordinates of each CMP gather are therefore (**h**, t). Likewise, for a common-offset gather of $d(\mathbf{h}, \mathbf{x}, t)$ the half-offset vector **h** is constant and the internal coordinates of the gather are (**x**, t). Note that one could eventually have defined the half-offset vector with opposite sign, $\mathbf{h} = (\mathbf{s} - \mathbf{r})/2$, as in Ursin (1982a). If this option is preferred, one can still utilize the equations derived in this paper, but all occurrences of **h** must then be substituted by $-\mathbf{h}$.

Consider an arbitrary depth point, D, with lateral coordinate vector $\boldsymbol{\xi}$ and vertical coordinate (depth) $\xi_3 = z$. In a common-offset depth migration of the data $d(\mathbf{h}, \mathbf{x}, t)$, one computes an image $d^D(\mathbf{h}, \boldsymbol{\xi}, z)$ for each half-offset **h**. The depth-migration domain is then (**h**, $\boldsymbol{\xi}$, z), where $\boldsymbol{\xi}$ specifies the depth migration common-image point, D^{CIG}, in the surface Σ. The point D^{CIG} is located vertically above the point D. The coordinates ($\boldsymbol{\xi}$, z) and (**h**, z) define, respectively, common-offset gathers and common-image gathers of the depth-migrated seismic data.

Analogously to the above considerations, time migration of the data $d(\mathbf{h}, \mathbf{x}, t)$ yields a time-migrated data set, $d^M(\mathbf{h}, \mathbf{m}, \tau)$, defined in the time-migration domain (**h**, **m**, τ). Here, τ is the migration time, and the vector **m** specifies the time-migration common-image point, M^{CIG}, also located in the surface Σ. The common-image points M^{CIG} and D^{CIG} for time and depth migration usually do not coincide; this will be explained in the next section. A basic assumption behind the introduction of the time-migration domain is that the mapping between the coordinates ($\boldsymbol{\xi}$, z) and (**m**, τ) is one-to-one. The migration time τ is considered as a pseudo-depth variable, and as such, we have $\tau = 0$ along the surface Σ. The coordinates (**m**, τ) and (**h**, τ) appear in, respectively, common-offset gathers and common-image gathers of the time-migrated seismic data.

The difference

$$\mathbf{a} = \mathbf{x} - \mathbf{m}, \tag{2}$$

is referred to as the aperture vector for time migration. In the migration process, the vector **a** spans the set of all input locations, **x**, that contributes to the image at the output location, **m**. This set of locations **x** is commonly referred to as the time-migration aperture.

For given coordinates **s**, **r** and **m** we define the source-offset vector, $\mathbf{h}^S$, and the receiver-offset vector, $\mathbf{h}^R$, by

$$\mathbf{h}^S = \mathbf{s} - \mathbf{m}, \qquad \mathbf{h}^R = \mathbf{r} - \mathbf{m}. \tag{3}$$

Using eq. (1) in eq. (3) and also taking into account eq. (2) yields

$$\mathbf{h}^S = \mathbf{a} - \mathbf{h}, \qquad \mathbf{h}^R = \mathbf{a} + \mathbf{h}. \tag{4}$$

3 TIME MIGRATION OF PRE-STACK SEISMIC DATA

The traveltime from source to receiver via a diffraction point in the subsurface is a fundamental entity in seismic time and depth migration. It is common to express this two-way diffraction time, T^D, as the sum of two one-way times,

$$T^D = T^S + T^R. \tag{5}$$

Here, the 'source time' T^S is the traveltime of a hypothetical wave (Green's function) propagating between the source point and the diffraction point, and the 'receiver time' T^R is the corresponding traveltime from the receiver point to the diffraction point. The actual arguments to be chosen for the functions T^S, T^R and T^D will depend on the type of migration (time or depth) and the type of 'common' partial images to be created. In the following our studies are limited to symmetric source- and receiver waves, which means that (i) the underlying types of wave propagation and polarization for the one-way times T^S and T^R are the same, for example, so that both correspond to P waves or both correspond to S waves and (ii) the sources and receivers are situated on the same measurement surface, Σ. Moreover, by considering only isolated branches of functions T^S, T^R and T^D in a common-offset context, the diffraction time for depth migration can be specified with the arguments $(\mathbf{h}, \mathbf{x}, \boldsymbol{\xi}, z)$.

The purpose of time migration is to provide meaningful seismic images that look like geology in depth, but such that the resulting images are still constituted by traces in time. Time migration normally uses an explicit diffraction-time function. Given that a unique relationship exists between the coordinates $(\boldsymbol{\xi}, z)$ and $(\mathbf{m}, \tau)$, the diffraction-time function can be expressed in the form

$$t = T^D(\mathbf{h}, \mathbf{a}, \mathbf{m}, \tau), \tag{6}$$

with the aperture vector **a** defined in eq. (2).

Taking as input seismic data $d(\mathbf{h}, \mathbf{x}, t)$ with frequency spectrum $D(\mathbf{h}, \mathbf{x}, \omega)$ and also a given frequency-dependent weight function, $W(\mathbf{h}, \mathbf{x}, \mathbf{m}, \tau, \omega)$, one can outline diffraction-stack time migration for constant offset **h** and output location $(\mathbf{m}, \tau)$ by the integrations

$$d^M(\mathbf{h}, \mathbf{m}, \tau) = \int\int W^*(\mathbf{h}, \mathbf{m} + \mathbf{a}, \mathbf{m}, \tau, \omega)\, D(\mathbf{h}, \mathbf{m} + \mathbf{a}, \omega) \times \exp\left[-\imath\omega T^D(\mathbf{h}, \mathbf{a}, \mathbf{m}, \tau)\right] \mathrm{d}\mathbf{a}\, \mathrm{d}\omega, \tag{7}$$

see eqs (A1)–(A3). Here, superscript $*$ stands for complex conjugate. We note that Kirchhoff depth migration has been formulated previously (Schleicher *et al.* 2007, p. 195, eq. 5) with a frequency-independent weight function, K_{DS}, which serves to compensate depth-migrated primary reflections for geometric spreading. Thereby, the depth-migrated amplitudes are anticipated to become a better measure of the reflectivity. Corresponding compensation of time-migration amplitudes is outside the scope of this paper; nevertheless, we observe that the weight functions W and K_{DS} can be connected in the time-migration domain by taking

$$W^*(\mathbf{h}, \mathbf{x}, \mathbf{m}, \tau, \omega) = \frac{1}{4\pi^2}\, \imath\omega\, K_{DS}(\mathbf{h}, \mathbf{x}, \mathbf{m}, \tau). \tag{8}$$

In 2-D and 3-D pre-stack time migration, eq. (7) integrates, respectively, over diffraction-time curves and diffraction-time surfaces.

It is common to formulate the function T^D for a single diffraction point D such that the common-image point M^{CIG} will be situated vertically above D (at the projection point D^{CIG}) if the underlying depth-velocity model is homogeneous. However, when considering symmetric waves in isotropic media, Hubral (1977) showed that the points M^{CIG} and D^{CIG} generally do not coincide in the presence of lateral velocity variations. Rather, the point D will be connected to the surface Σ by a generally non-straight and non-vertical *image ray*. This situation is depicted in Fig. 3. The emergence point M^{CIG} of the image ray on Σ corresponds to minimum two-way time for the diffraction generated at the point D. We therefore consider the coordinate vector **m** of point M^{CIG} defined by stationarity of the function T^D, namely,

$$\frac{\partial T^D}{\partial \mathbf{a}}(\mathbf{h} = \mathbf{0}, \mathbf{a} = \mathbf{0}, \mathbf{m}, \tau) = \mathbf{0}. \tag{9}$$

The assumption of one-to-one correspondence $(\boldsymbol{\xi}, z) \leftrightarrow (\mathbf{m}, \tau)$ mentioned above implies that the image-ray field cannot contain caustics.

For anisotropic media there are additional concerns, arising from the fact that diffraction-time functions used in classic time-migration approaches are symmetric in **h** and **a**. These symmetry properties are exemplified in Section 4. In particular, if the point D^{CIG} is to be situated vertically above point D in a homogeneous anisotropic medium, the slowness surface has to be laterally symmetric in any plane containing the vertical axis. As a consequence, image-ray paths will be vertical lines for constant medium parameters. When medium parameters are varying, the ray paths will still be normal to the surface Σ as in the isotropic situation. This inherent constraint on slowness-surface symmetry means that a classic time-migration approach may still be adequate for transversely isotropic media with a vertical symmetry axis (VTI media) and for orthorhombic media with symmetry planes aligned with the main coordinate planes of the (ξ_1, ξ_2, ξ_3) coordinate system.

On the other hand, it is clear that the classic approach may easily yield significant time-migration errors if the slowness surface is laterally asymmetric. Such asymmetry is formed, for example, by a tilted transversely isotropic medium. To quantify to what extent lateral slowness-surface asymmetries are acceptable is not a subject of this paper. In the following, we do not introduce specific restrictions regarding heterogeneity or anisotropy. One basic requirement that always has to be fulfilled, however, is the absence of caustics in the diffraction-time field.

4 DIFFRACTION-TIME FUNCTION FOR TIME MIGRATION

We discuss the properties of diffraction-time functions used in time migration.

4.1 Diffraction-time partial derivatives

For the kinematic migration and demigration processes described below we need the diffraction time T^D and its partial derivatives evaluated for specific values of half-offset, **h**, aperture, **a**, image-gather location, **m**, and migration time, τ. The diffraction-time

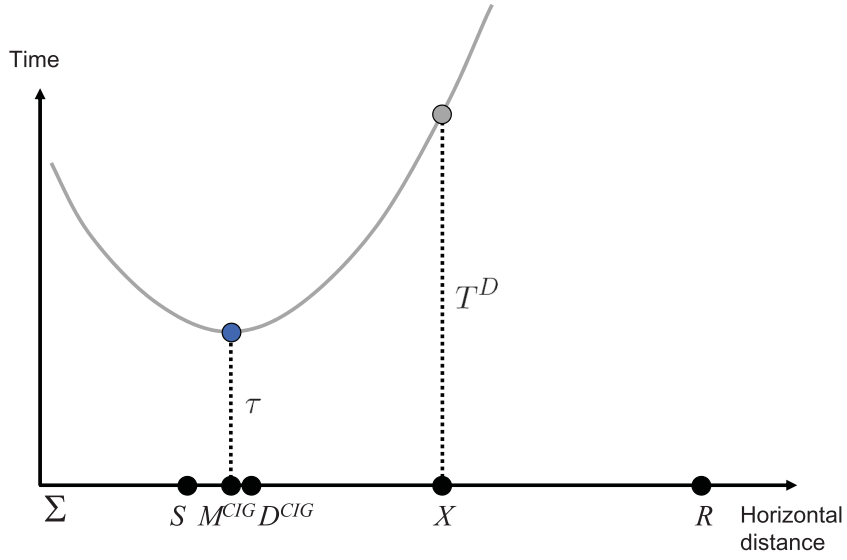

(a)

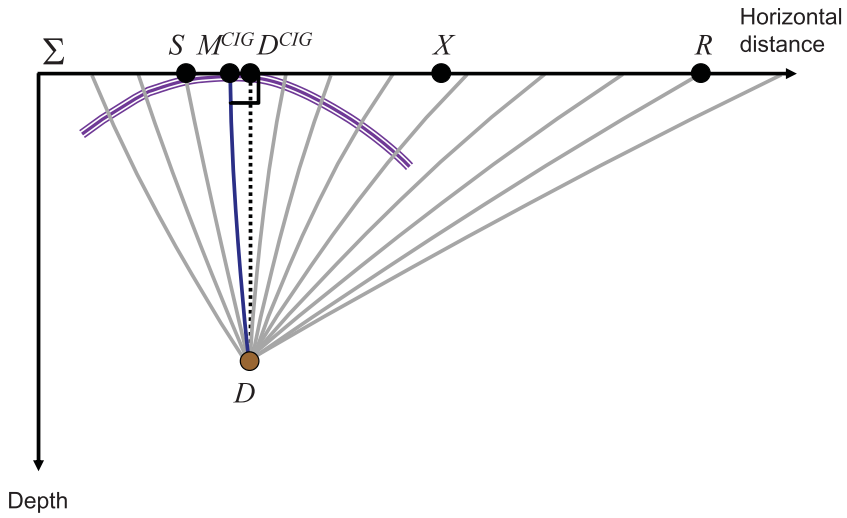

(b)

Figure 3. Diffraction-time concept in classic pre-stack time migration, illustrated under the assumption that the involved time- and depth-migration velocity models give rise to identical diffraction-time functions: (a) diffraction-time curve (grey) for a single depth point, D, with the time T^D marked (grey dot) for a midpoint (X) between selected source (S) and receiver (R) points; (b) corresponding diffraction ray paths (grey) and the associated diffraction wavefront (purple). The diffraction point D is imaged at the location M^{CIG} and time τ (blue dot) in the time-migration domain, for which the diffraction-time function has a minimum. The points D and M^{CIG} are uniquely connected by an image ray (dark blue). The vertical projection (dotted black line) of point D to its lateral position in the time-migration domain, D^{CIG}, is indicated.

partial derivatives are written in the notation

$$
\begin{aligned}
u &= \frac{\partial T^D}{\partial \tau}, \\
\mathbf{q}^h &= \frac{\partial T^D}{\partial \mathbf{h}}, \qquad \mathbf{q}^a = \frac{\partial T^D}{\partial \mathbf{a}}, \qquad \mathbf{q}^m = \frac{\partial T^D}{\partial \mathbf{m}}, \\
u^\tau &= \frac{\partial^2 T^D}{\partial \tau^2}, \\
\mathbf{u}^h &= \frac{\partial^2 T^D}{\partial \mathbf{h} \partial \tau}, \qquad \mathbf{u}^a = \frac{\partial^2 T^D}{\partial \mathbf{a} \partial \tau}, \qquad \mathbf{u}^m = \frac{\partial^2 T^D}{\partial \mathbf{m} \partial \tau}, \\
\mathbf{U}^{hh} &= \frac{\partial^2 T^D}{\partial \mathbf{h} \partial \mathbf{h}^T}, \qquad \mathbf{U}^{aa} = \frac{\partial^2 T^D}{\partial \mathbf{a} \partial \mathbf{a}^T}, \qquad \mathbf{U}^{mm} = \frac{\partial^2 T^D}{\partial \mathbf{m} \partial \mathbf{m}^T}, \\
\mathbf{U}^{ha} &= \frac{\partial^2 T^D}{\partial \mathbf{h} \partial \mathbf{a}^T}, \qquad \mathbf{U}^{hm} = \frac{\partial^2 T^D}{\partial \mathbf{h} \partial \mathbf{m}^T}, \qquad \mathbf{U}^{am} = \frac{\partial^2 T^D}{\partial \mathbf{a} \partial \mathbf{m}^T}, \\
\mathbf{U}^{ah} &= \mathbf{U}^{ha\,T}, \qquad \mathbf{U}^{mh} = \mathbf{U}^{hm\,T}, \qquad \mathbf{U}^{ma} = \mathbf{U}^{am\,T}.
\end{aligned}
\tag{10}
$$

To better visualize the properties of these quantities, we introduce a seven-component column vector, $\boldsymbol{\alpha} = (h_1, h_2, a_1, a_2, m_1, m_2, \tau)^T$, containing the arguments of the diffraction-time function, so that the complete set of first and second derivatives of function T^D is given by a seven-component gradient vector and a symmetric 7×7 matrix,

$$\frac{\partial T^D}{\partial \boldsymbol{\alpha}} = \begin{pmatrix} \mathbf{q}^h \\ \mathbf{q}^a \\ \mathbf{q}^m \\ u \end{pmatrix}, \qquad \frac{\partial^2 T^D}{\partial \boldsymbol{\alpha} \partial \boldsymbol{\alpha}^T} = \begin{pmatrix} \mathbf{U}^{hh} & \mathbf{U}^{ha} & \mathbf{U}^{hm} & \mathbf{u}^h \\ \cdot & \mathbf{U}^{aa} & \mathbf{U}^{am} & \mathbf{u}^a \\ \cdot & \cdot & \mathbf{U}^{mm} & \mathbf{u}^m \\ \cdot & \cdot & \cdot & u^\tau \end{pmatrix}. \tag{11}$$

To emphasize symmetry, elements of the lower triangular part of matrix $\partial^2 T^D / \partial \boldsymbol{\alpha} \partial \boldsymbol{\alpha}^T$ are only indicated by dots. It is remarked that the quantity u in eqs (10) and (11) yields the stretch of the time coordinate in time migration or time demigration of seismic data (see also Appendix A).

4.2 Properties of the diffraction-time function

The diffraction-time function $T^D(\mathbf{h}, \mathbf{a}, \mathbf{m}, \tau)$ has some general properties that are independent of the actual function representation. Considering symmetric diffractions, one immediate observation is that the function T^D has to be symmetric in the variable $\mathbf{h}$, that is, we always have

$$T^D(\mathbf{h}, \mathbf{a}, \mathbf{m}, \tau) = T^D(-\mathbf{h}, \mathbf{a}, \mathbf{m}, \tau). \tag{12}$$

The reason is reciprocity: the diffraction time is the same if source and receiver positions are interchanged. As a consequence, the partial derivatives with respect to half-offset coordinates vanish at zero offset,

$$\frac{\partial T^D}{\partial \mathbf{h}}(\mathbf{h} = \mathbf{0}, \mathbf{a}, \mathbf{m}, \tau) = \mathbf{0}. \tag{13}$$

Eq. (13) has the implication that also mixed partial second derivatives involving half-offset $\mathbf{h}$ vanish for $\mathbf{h} = \mathbf{0}$. The set of diffraction-time partial derivatives in eq. (11) at zero offset ($\mathbf{h} = \mathbf{0}$) and generally non-zero aperture ($\mathbf{a} \neq \mathbf{0}$) can therefore be written

$$\frac{\partial T^D}{\partial \boldsymbol{\alpha}} = \begin{pmatrix} \mathbf{0} \\ \mathbf{q}^a \\ \mathbf{q}^m \\ u \end{pmatrix}, \qquad \frac{\partial^2 T^D}{\partial \boldsymbol{\alpha} \partial \boldsymbol{\alpha}^T} = \begin{pmatrix} \mathbf{U}^{hh} & \mathbf{O} & \mathbf{O} & \mathbf{0} \\ \cdot & \mathbf{U}^{aa} & \mathbf{U}^{am} & \mathbf{u}^a \\ \cdot & \cdot & \mathbf{U}^{mm} & \mathbf{u}^m \\ \cdot & \cdot & \cdot & u^\tau \end{pmatrix}. \tag{14}$$

Consistently with the above discussions it is assumed that the source- and receiver-time functions T^S and T^R in eq. (5) are single-valued. We express them as

$$T^S\left(\mathbf{h}^S, \mathbf{m}, T_0^S\right), \qquad T^R\left(\mathbf{h}^R, \mathbf{m}, T_0^R\right), \tag{15}$$

where $\mathbf{h}^S$ and $\mathbf{h}^R$ are source- and receiver-offset vectors (eqs 3 and 4), and T_0^S and T_0^R are source and receiver times corresponding to the situations $\mathbf{h}^S = \mathbf{0}$ and $\mathbf{h}^R = \mathbf{0}$. Since source points, receiver points and migration output locations belong to the same surface, Σ, the migration time is related to the diffraction time via

$$\tau \equiv T_0^S + T_0^R = T^D(\mathbf{h} = \mathbf{0}, \mathbf{a} = \mathbf{0}, \mathbf{m}, \tau). \tag{16}$$

Symmetric wave propagation implies that $T_0^S = T_0^R = \tau/2$. As a consequence, the diffraction-time function can be written in the form

$$T^D(\mathbf{h}, \mathbf{a}, \mathbf{m}, \tau) = T^S\left(\mathbf{a} - \mathbf{h}, \mathbf{m}, \frac{\tau}{2}\right) + T^R\left(\mathbf{a} + \mathbf{h}, \mathbf{m}, \frac{\tau}{2}\right). \tag{17}$$

The standard approach in time migration is to assume a certain analytic relationship for $(T^S)^2$ and $(T^R)^2$ expressed in terms of coefficients evaluated at $\mathbf{a} = \mathbf{h} = \mathbf{0}$. Such coefficients have a simple relationship to the parameters of the time-migration velocity model, which has to be known.

Differentiation of eq. (17) twice with respect to $\mathbf{a}$ and $\mathbf{h}$ yields

$$\frac{\partial^2 T^D}{\partial \mathbf{a} \partial \mathbf{a}^T}(\mathbf{h}, \mathbf{a}, \mathbf{m}, \tau) = \frac{\partial^2 T^D}{\partial \mathbf{h} \partial \mathbf{h}^T}(\mathbf{h}, \mathbf{a}, \mathbf{m}, \tau) \quad \text{or}$$
$$\mathbf{U}^{aa}(\mathbf{h}, \mathbf{a}, \mathbf{m}, \tau) = \mathbf{U}^{hh}(\mathbf{h}, \mathbf{a}, \mathbf{m}, \tau). \tag{18}$$

In other words, for the function T^D in eq. (17) the matrices $\mathbf{U}^{aa}$ and $\mathbf{U}^{hh}$ are always equal. Based on eq. (18) we define a symmetric 2×2 matrix

$$\mathbf{S}^M(\mathbf{m}, \tau) \equiv \frac{1}{4}\tau \mathbf{U}^{aa}(\mathbf{h} = \mathbf{0}, \mathbf{a} = \mathbf{0}, \mathbf{m}, \tau)$$
$$= \frac{1}{4}\tau \mathbf{U}^{hh}(\mathbf{h} = \mathbf{0}, \mathbf{a} = \mathbf{0}, \mathbf{m}, \tau), \tag{19}$$

which is useful in derivations below. It is referred to as the time-migration matrix. We observe that matrix $\mathbf{S}^M$ is a function of the three (volume) variables (m_1, m_2, τ) and has unit of squared slowness. Matrix $\mathbf{S}^M$ is proportional to the wavefront curvature matrix of a wave diffracting at the depth point D (Fig. 3) and emerging to the surface Σ at the point M^{CIG}. As such, matrix $\mathbf{S}^M$ has to comply with the requirement that the diffracted wave field does not contain caustics. This requirement ensures, as mentioned earlier, that the correspondence between the points D and M^{CIG} is one to one. On this background both eigenvalues of $\mathbf{S}^M$ must be positive in the context of 3-D post- or pre-stack time migration.

It is inherent to conventional time migration that the diffraction-time function T^D has one and only one apex in the coordinates $\mathbf{h}$ and $\mathbf{a}$. This apex is located at $(\mathbf{h} = \mathbf{0}, \mathbf{a} = \mathbf{0}, \mathbf{m}, \tau)$ and yields a considerably simplified set of diffraction-time partial derivatives. For $\mathbf{h} = \mathbf{a} = \mathbf{0}$ the gradients with respect to $\mathbf{h}$ and $\mathbf{a}$ are zero (eqs 9 and 13), and eq. (16) is satisfied. As a consequence, all mixed-term second derivatives of T^D involving $\mathbf{h}$ or $\mathbf{a}$ are zero; the same is true for all first- and second-order partial derivatives involving $\mathbf{m}$. In addition, we have $\partial T^D/\partial \tau = 1$ and $\partial^2 T^D/\partial \tau^2 = 0$. In summary, we find that the set of diffraction-time partial derivatives at $\mathbf{h} = \mathbf{a} = \mathbf{0}$ has the structure

$$\frac{\partial T^D}{\partial \boldsymbol{\alpha}} = \begin{pmatrix} \mathbf{0} \\ \mathbf{0} \\ \mathbf{0} \\ 1 \end{pmatrix}, \qquad \frac{\partial^2 T^D}{\partial \boldsymbol{\alpha} \partial \boldsymbol{\alpha}^T} = \begin{pmatrix} \frac{4}{\tau}\mathbf{S}^M & \mathbf{O} & \mathbf{O} & \mathbf{0} \\ \cdot & \frac{4}{\tau}\mathbf{S}^M & \mathbf{O} & \mathbf{0} \\ \cdot & \cdot & \mathbf{O} & \mathbf{0} \\ \cdot & \cdot & \cdot & 0 \end{pmatrix}. \tag{20}$$

4.3 Example 1: double-square-root function

One common realization of diffraction time is the double-square-root function based on exact traveltime equations for P- or S-wave propagation in a homogeneous isotropic medium. The diffraction time is obtained as $T^D = T^S + T^R$ (see eq. 17) with one-way times

T^S and T^R specified by

$$T^S = \sqrt{\frac{\tau^2}{4} + (\mathbf{a}-\mathbf{h})^T\,\mathbf{S}^M(\mathbf{m},\tau)\,(\mathbf{a}-\mathbf{h})},$$
$$T^R = \sqrt{\frac{\tau^2}{4} + (\mathbf{a}+\mathbf{h})^T\,\mathbf{S}^M(\mathbf{m},\tau)\,(\mathbf{a}+\mathbf{h})}. \quad (21)$$

Matrix $\mathbf{S}^M$ has been defined in eq. (19). The double-square-root function T^D is symmetric not only in the variable $\mathbf{h}$ but also in $\mathbf{a}$, so that

$$T^D(\mathbf{h},\mathbf{a},\mathbf{m},\tau) = T^D(\mathbf{h},-\mathbf{a},\mathbf{m},\tau). \quad (22)$$

4.4 Example 2: single-square-root function

Another example of diffraction-time functions is the single-square-root approximation. Following Hubral & Krey (1980) we can express it as

$$T^D(\mathbf{h},\mathbf{a},\mathbf{m},\tau) = \sqrt{\tau^2 + 4\mathbf{a}^T\mathbf{S}^M(\mathbf{m},\tau)\,\mathbf{a} + 4\mathbf{h}^T\mathbf{S}^M(\mathbf{m},\tau)\,\mathbf{h}}. \quad (23)$$

As opposed to the double-square-root function, which uses eq. (21), the single-square-root function in eq. (23) is not exact for non-zero apertures and offsets in homogeneous isotropic media. At zero aperture or at zero offset, however, the single and double square-root formulas are identical. One can see immediately that the symmetry properties in eqs (12) and (22) hold for the single-square-root approximation.

It is easy to verify that eq. (23) exhibits the property of eq. (18) for $\mathbf{h} = \mathbf{a} = \mathbf{0}$ but not for arbitrary $\mathbf{h}$ and $\mathbf{a}$. The latter is explained by the underlying assumption of eq. (18), namely, that the diffraction time is expressed as the explicit sum of the two one-way times in eq. (17).

5 TIME-MIGRATION VELOCITY MODEL

The complete set of parameters required for time migration is referred to as the time-migration velocity model or to just as the time-migration velocity, in the case of a mono-parametric representation. Following common practise, the model is defined in the time-migration coordinates $(\mathbf{m},\tau)$, so that the model parameters do not depend on offset. To permit formulations of kinematic migration and demigration that do not rely on a particular model parametrization, we use the general form

$$\mathcal{V}_i(\mathbf{m},\tau), \qquad i = 1,2,\ldots,N^{\mathcal{V}}, \quad (24)$$

where $N^{\mathcal{V}}$ is the number of parameters. One possibility is to use the symmetric 2×2 matrix $\mathbf{S}^M$, defined in eq. (19), as a basis for defining the parameters $(\mathcal{V}_i)$. When using conventional double-square-root or single-square-root diffraction-time functions it is sufficient to consider three model parameters, for example, $\mathcal{V}_1 = S^M_{11}$; $\mathcal{V}_2 = S^M_{22}$; $\mathcal{V}_3 = S^M_{12} = S^M_{21}$.

From eq. (19) we recall that matrix $\mathbf{S}^M$ corresponds to second-order derivatives of diffraction time with respect to aperture $\mathbf{a}$ or half-offset $\mathbf{h}$ at the apex point, for which $\mathbf{a} = \mathbf{0}$ and $\mathbf{h} = \mathbf{0}$. A natural extension of the set of model parameters in eq. (24) to $N^{\mathcal{V}} > 3$ would be to define $\mathcal{V}_i$ in terms of diffraction-time partial derivatives of higher order than two.

Matrix $\mathbf{S}^M$ has historically been related to a location- and direction-dependent time-migration velocity $V^M(\theta^a,\mathbf{m},\tau)$ corresponding to small apertures and offsets, such that (Hubral & Krey 1980; Iversen & Tygel 2008)

$$\left[V^M(\theta^a,\mathbf{m},\tau)\right]^{-2} = \mathbf{e}(\theta^a)^T\,\mathbf{S}^M(\mathbf{m},\tau)\,\mathbf{e}(\theta^a). \quad (25)$$

Here, the directional dependency of V^M is specified in terms of the two-component unit vector $\mathbf{e}(\theta^a) = (\cos\theta^a,\ \sin\theta^a)^T$, which corresponds to a normalization of the aperture vector $\mathbf{a}$. Observe that it would be formally equivalent to specify V^M using instead a similar unit vector $\mathbf{e}(\theta^h)$ obtained by a normalization of the half-offset vector $\mathbf{h}$. It is not equally practical, though, as pre-stack time migration is commonly done separately for constant-offset subcubes of the seismic data set.

For a fixed location $(\mathbf{m},\tau)$ eq. (25) yields the *time-migration ellipse* with coefficients specified by the time-migration matrix $\mathbf{S}^M$. The restriction of function V^M to small apertures and offsets comes from its relation to second-derivatives of diffraction time evaluated at $\mathbf{h} = \mathbf{a} = \mathbf{0}$, see eq. (19).

6 REFLECTION TIME

In the recording and migration domains we introduce two single-valued reflection-time functions corresponding to symmetrically reflected waves,

$$t = T(\mathbf{h},\mathbf{x}), \qquad \tau = \mathcal{T}(\mathbf{h},\mathbf{m}). \quad (26)$$

The first of these is historically known as a CRS belonging to a pre-stack seismic data set; the second function yields the corresponding CRS in the time-migration domain. The CRSs $T(\mathbf{h},\mathbf{x})$ and $\mathcal{T}(\mathbf{h},\mathbf{x})$ can be parameterized locally in terms of reflection-time parameters, which is the subject of the following subsections. The connection between the reflection-time functions in eq. (26) and the diffraction-time function discussed previously is indicated in Fig. 1.

6.1 Reflection-time parameters in the recording domain

The vector couple $(\mathbf{h},\mathbf{x})$ specifies traces within the recording domain. In equations below we equivalently refer to such traces using the four-component column vector $\bar{\mathbf{x}} = (h_1,h_2,x_1,x_2)^T$. For a reflection event at a given trace location, $(\mathbf{h},\mathbf{x})$, we associate a number of reflection-time parameters, namely: reflection time, $T^X = T(\mathbf{h},\mathbf{x})$, slope (first-derivative) vectors $\mathbf{p}^h = \partial T/\partial\mathbf{h}$, $\mathbf{p}^x = \partial T/\partial\mathbf{x}$, and second-derivative matrices $\mathbf{M}^{hh} = \partial^2 T/\partial\mathbf{h}\partial\mathbf{h}^T$, $\mathbf{M}^{hx} = \partial^2 T/\partial\mathbf{h}\partial\mathbf{x}^T$, $\mathbf{M}^{xx} = \partial^2 T/\partial\mathbf{x}\partial\mathbf{x}^T$. For a better overview the latter first- and second-derivative parameters can be collected in a four-component vector, $\bar{\mathbf{p}}$, and a 4×4 matrix, $\bar{\mathbf{M}}$, as follows (Ursin 1982a; Gjøystdal *et al.* 1984):

$$\bar{\mathbf{p}} = \frac{\partial T}{\partial\bar{\mathbf{x}}} = \begin{pmatrix}\mathbf{p}^h\\ \mathbf{p}^x\end{pmatrix}, \qquad \bar{\mathbf{M}} = \frac{\partial^2 T}{\partial\bar{\mathbf{x}}\partial\bar{\mathbf{x}}^T} = \begin{pmatrix}\mathbf{M}^{hh} & \mathbf{M}^{hx}\\ \mathbf{M}^{hx\,T} & \mathbf{M}^{xx}\end{pmatrix}. \quad (27)$$

The quantities in eq. (27) shall be understood as functions of $\mathbf{h}$ and $\mathbf{x}$.

Reciprocity of symmetric reflections implies that

$$T(\mathbf{h},\mathbf{x}) = T(-\mathbf{h},\mathbf{x}). \quad (28)$$

As a consequence, the following partial derivatives involving half offset vanish at zero offset,

$$\frac{\partial T}{\partial\mathbf{h}}(\mathbf{h}=\mathbf{0},\mathbf{x}) = \mathbf{0}, \qquad \frac{\partial^2 T}{\partial\mathbf{h}\partial\mathbf{x}^T}(\mathbf{h}=\mathbf{0},\mathbf{x}) = \mathbf{O}. \quad (29)$$

These properties determine the classic CRS parameters (e.g. Ursin 1982a; Duveneck 2004) and yield vector $\bar{\mathbf{p}}$ and matrix $\bar{\mathbf{M}}$ as

$$\bar{\mathbf{p}} = \begin{pmatrix} \mathbf{0} \\ \mathbf{p}^x \end{pmatrix}, \qquad \bar{\mathbf{M}} = \begin{pmatrix} \mathbf{M}^{hh} & \mathbf{O} \\ \mathbf{O} & \mathbf{M}^{xx} \end{pmatrix}, \tag{30}$$

where all parameters correspond to $(\mathbf{h} = \mathbf{0}, \mathbf{x})$.

The reflection-time parameters constituting the second-derivative matrix $\mathbf{M}^{hh}$ evaluated for $\mathbf{h} = \mathbf{0}$ have a particular interpretation in terms of NMO velocity. To aid this interpretation we introduce a 2×2 'NMO matrix' with the unit of squared slowness,

$$\mathbf{S}^{\mathrm{NMO}}(\mathbf{x}) \equiv \frac{1}{4} T(\mathbf{h} = \mathbf{0}, \mathbf{x})\, \mathbf{M}^{hh}(\mathbf{h} = \mathbf{0}, \mathbf{x}). \tag{31}$$

In general there are no restrictions on the signs of the eigenvalues of matrix $\mathbf{S}^{\mathrm{NMO}}$. If both eigenvalues are positive, however, it is useful to relate matrix $\mathbf{S}^{\mathrm{NMO}}$ to a direction-dependent and surface-specific NMO velocity $v^{\mathrm{NMO}}(\theta^h, \mathbf{x})$ associated with small offsets, such that (Hubral & Krey 1980; Iversen 2006)

$$\left[v^{\mathrm{NMO}}(\theta^h, \mathbf{x})\right]^{-2} = \mathbf{e}(\theta^h)^T\, \mathbf{S}^{\mathrm{NMO}}(\mathbf{x})\, \mathbf{e}(\theta^h). \tag{32}$$

Here, $\mathbf{e}(\theta^h)$ is the unit vector $(\cos\theta^h, \sin\theta^h)^T$ corresponding to normalization of the vector $\mathbf{h}$. In the case of a fixed midpoint location, $\mathbf{x}$, eq. (32) constitutes the *NMO ellipse* (Grechka & Tsvankin 2002). The association of parameter v^{NMO} with small offsets comes from the connection to second-derivatives of reflection time evaluated at zero offset (eq. 31).

Matrix $\mathbf{S}^{\mathrm{NMO}}$ is a function of the two (surface) variables (x_1, x_2). As such, it is essential to recognize that matrix $\mathbf{S}^{\mathrm{NMO}}$ is a surface function, in contrast to the time-migration matrix, $\mathbf{S}^M$, which is a volume function. By imposing strong limitations on the shape of (depth) reflectors, however, it is possible to consider also the NMO matrix (and corresponding angle-dependent NMO velocity) as a volume function, that is, as a single-valued function of the variables (x_1, x_2, t). The key point here is that normal rays from reflectors do not form caustics.

Using eq. (30) one can restate Ursin's (1982a) approximation of the CRS with coefficients evaluated at zero offset $(\mathbf{h} = \mathbf{0})$ and a reference CMP location $(\mathbf{x} = \mathbf{x}_0)$ as

$$\begin{aligned} T(\mathbf{h}, \mathbf{x})^2 = &\left[T^X + (\mathbf{x} - \mathbf{x}_0)^T \mathbf{p}^x\right]^2 \\ &+ T^X \left[\mathbf{h}^T\, \mathbf{M}^{hh}\, \mathbf{h} + (\mathbf{x} - \mathbf{x}_0)^T\, \mathbf{M}^{xx}\, (\mathbf{x} - \mathbf{x}_0)\right]. \end{aligned} \tag{33}$$

6.2 Reflection-time parameters in the time-migration domain

In the time-migration domain, each trace is uniquely specified by the vector couple $(\mathbf{h}, \mathbf{m})$ or by the equivalent four-component vector $\bar{\mathbf{m}} = (h_1, h_2, m_1, m_2)^T$. For a migrated reflection event at a certain trace location, $(\mathbf{h}, \mathbf{m})$, we consider the following reflection-time parameters: migrated reflection time, $\mathcal{T}^M = \mathcal{T}(\mathbf{h}, \mathbf{m})$, slope vectors $\boldsymbol{\psi}^h = \partial\mathcal{T}/\partial\mathbf{h}$, $\boldsymbol{\psi}^m = \partial\mathcal{T}/\partial\mathbf{m}$, and second-derivative matrices $\boldsymbol{\mathcal{M}}^{hh} = \partial^2\mathcal{T}/\partial\mathbf{h}\partial\mathbf{h}^T$, $\boldsymbol{\mathcal{M}}^{hm} = \partial^2\mathcal{T}/\partial\mathbf{h}\partial\mathbf{m}^T$, $\boldsymbol{\mathcal{M}}^{mm} = \partial^2\mathcal{T}/\partial\mathbf{m}\partial\mathbf{m}^T$. As in the recording domain, it is convenient to assemble the first- and second-derivative parameters in a four-component vector and a 4×4 matrix,

$$\bar{\boldsymbol{\psi}} = \frac{\partial\mathcal{T}}{\partial\bar{\mathbf{m}}} = \begin{pmatrix} \boldsymbol{\psi}^h \\ \boldsymbol{\psi}^m \end{pmatrix}, \quad \bar{\boldsymbol{\mathcal{M}}} = \frac{\partial^2\mathcal{T}}{\partial\bar{\mathbf{m}}\partial\bar{\mathbf{m}}^T} = \begin{pmatrix} \boldsymbol{\mathcal{M}}^{hh} & \boldsymbol{\mathcal{M}}^{hm} \\ \boldsymbol{\mathcal{M}}^{hm\,T} & \boldsymbol{\mathcal{M}}^{mm} \end{pmatrix}. \tag{34}$$

The parameters in eq. (34) are considered functions of $\mathbf{h}$ and $\mathbf{m}$.

As will be proved in the derivation of eqs (61) and (62) below, the entities $\boldsymbol{\psi}^h$ and $\boldsymbol{\mathcal{M}}^{hm}$ are zero when $\mathbf{h} = \mathbf{0}$. The natural definition of (zero-offset) CRS parameters in the time-migration domain is therefore

$$\bar{\boldsymbol{\psi}} = \begin{pmatrix} \mathbf{0} \\ \boldsymbol{\psi}^m \end{pmatrix}, \qquad \bar{\boldsymbol{\mathcal{M}}} = \begin{pmatrix} \boldsymbol{\mathcal{M}}^{hh} & \mathbf{O} \\ \mathbf{O} & \boldsymbol{\mathcal{M}}^{mm} \end{pmatrix}, \tag{35}$$

where all parameters are evaluated for $(\mathbf{h} = \mathbf{0}, \mathbf{m})$. An ideal pre-stack time-migration result would imply that the entities $\boldsymbol{\psi}^h$, $\boldsymbol{\mathcal{M}}^{hh}$, and $\boldsymbol{\mathcal{M}}^{hm}$ are zero for all $(\mathbf{h}, \mathbf{m})$. When this is not the case one can use observations of such parameters to update the time-migration velocity model, applying the so-called extension principle (Stolk *et al.* 2009).

The slope vector $\boldsymbol{\psi}^m$ of the reflection in the time-migration domain is connected to the reflector normal in the depth-migration domain. This reflector normal can be obtained after a simultaneous construction of the image ray and (depth) velocities along it (Hubral & Krey 1980; Cameron *et al.* 2007; Iversen & Tygel 2008; Tygel *et al.* 2012). Using also the matrix $\boldsymbol{\mathcal{M}}^{mm}$ it is possible to estimate the reflector curvature.

As in eq. (33) one can form an approximation of the CRS in the time-migration domain using the coefficients in eq. (35), corresponding to zero offset $(\mathbf{h} = \mathbf{0})$ and a reference common-image gather location $(\mathbf{m} = \mathbf{m}_0)$, such that

$$\begin{aligned} \mathcal{T}(\mathbf{h}, \mathbf{x})^2 = &\left[\mathcal{T}^M + (\mathbf{m} - \mathbf{m}_0)^T \boldsymbol{\psi}^m\right]^2 \\ &+ \mathcal{T}^M \left[\mathbf{h}^T\, \boldsymbol{\mathcal{M}}^{hh}\, \mathbf{h} + (\mathbf{m} - \mathbf{m}_0)^T\, \boldsymbol{\mathcal{M}}^{mm}\, (\mathbf{m} - \mathbf{m}_0)\right]. \end{aligned} \tag{36}$$

7 KINEMATIC TIME DEMIGRATION

We consider the situation that a pre-stack seismic data set has been migrated using a known time-migration velocity model, $(\mathcal{V}_i)$. This model is not necessarily the optimal one, but it is assumed sufficiently accurate to yield well-defined coherent reflection events within common-offset subsets of the data. We further assume that a picking process has been applied, and that a set of reflection-time parameters, as specified in eq. (34), has been estimated. These known reflection-time parameters shall now be mapped from the migration domain to the recording domain by kinematic time demigration, to yield the output parameter set in eq. (27). The process relies on the computation of first- and second order partial derivatives of the known diffraction-time function, T^D, see eq. (10). We shall need access to first- and second-order partial derivatives of each model parameter $\mathcal{V}_i$ with respect to the coordinates $\mathbf{m}$ and τ within the time-migration domain. The flow of the kinematic time-demigration process is outlined in Fig. 4.

In a demigration of parameters corresponding to migrated reflection time $\mathcal{T}(\mathbf{h}, \mathbf{m})$ the output trace location $(\mathbf{h}, \mathbf{x})$ is assumed to have a single-valued relationship to the input trace location $(\mathbf{h}, \mathbf{m})$ such that

$$\mathbf{x} = \hat{\mathbf{x}}(\mathbf{h}, \mathbf{m}). \tag{37}$$

Because of the functional relationship in eq. (37), the aperture vector $\mathbf{a}$ in eq. (2) will also be a function of $\mathbf{m}$ and $\mathbf{h}$, given by

$$\mathbf{a} = \hat{\mathbf{a}}(\mathbf{h}, \mathbf{m}) = \hat{\mathbf{x}}(\mathbf{h}, \mathbf{m}) - \mathbf{m}. \tag{38}$$

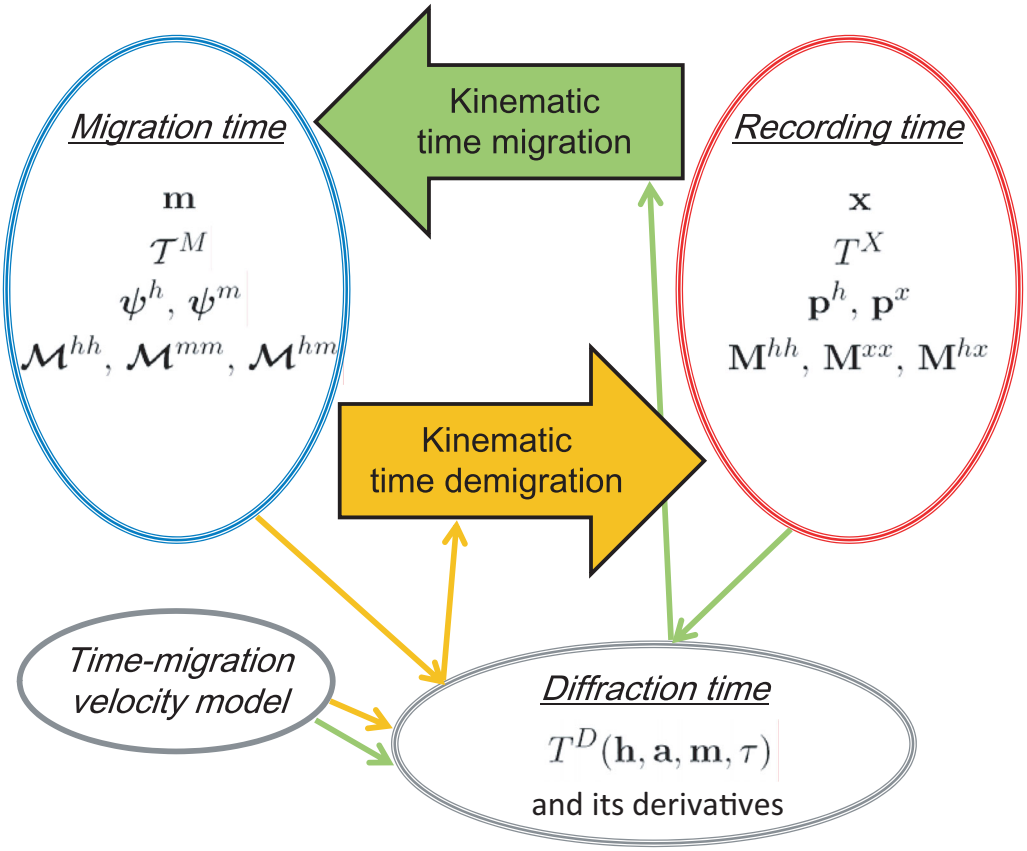

Figure 4. Kinematic time migration (green) and demigration (orange) processes for constant offset with indicated input and output reflection-time parameters. The processes estimates the aperture vector and a number of diffraction-time partial derivatives using the given input parameters and the known time-migration velocity model. Tiny arrows in the appropriate colour (green or orange) signify the data flow.

7.1 Basic conditions

Consider now a reflected wave

$$d(\mathbf{h}, \mathbf{x}, t) = A(\mathbf{h}, \mathbf{x})\, s\,[t - T(\mathbf{h}, \mathbf{x})] \tag{39}$$

with amplitude $A(\mathbf{h}, \mathbf{x})$, traveltime $T(\mathbf{h}, \mathbf{x})$, and wavelet $s(t)$. We let $S(\omega)$ denote the Fourier transform of $s(t)$. When the time-migration eq. (7) is applied to this data for fixed coordinates $(\mathbf{h}, \mathbf{m}, \tau)$, we obtain

$$d^M(\mathbf{h}, \mathbf{m}, \tau) = \iint W^*(\mathbf{h}, \mathbf{m} + \mathbf{a}, \mathbf{m}, \tau, \omega)\, A(\mathbf{h}, \mathbf{m} + \mathbf{a})$$
$$\times\ S(\omega)\, \exp\left\{-\imath\omega\left[T^D(\mathbf{h}, \mathbf{a}, \mathbf{m}, \tau) - T(\mathbf{h}, \mathbf{m} + \mathbf{a})\right]\right\} \mathrm{d}\mathbf{a}\, \mathrm{d}\omega, \tag{40}$$

since $\mathbf{x} = \mathbf{m} + \mathbf{a}$. Furthermore, for $\mathbf{m}$ constant we have $\partial/\partial\mathbf{x} = \partial/\partial\mathbf{a}$. Applying the method of stationary phase (e.g. Treves 1980; Bleistein 1984; Stamnes 1986) and using that $\tau = \mathcal{T}(\mathbf{h}, \mathbf{m})$, it follows that the stationary point $\hat{\mathbf{a}}(\mathbf{h}, \mathbf{m})$ of the aperture integral in eq. (40) satisfies the conditions

$$T(\mathbf{h}, \hat{\mathbf{x}}) = T^D[\mathbf{h}, \hat{\mathbf{x}} - \mathbf{m}, \mathbf{m}, \mathcal{T}(\mathbf{h}, \mathbf{m})], \tag{41}$$

$$\frac{\partial T}{\partial \mathbf{x}}(\mathbf{h}, \hat{\mathbf{x}}) = \frac{\partial T^D}{\partial \mathbf{a}}[\mathbf{h}, \hat{\mathbf{x}} - \mathbf{m}, \mathbf{m}, \mathcal{T}(\mathbf{h}, \mathbf{m})]. \tag{42}$$

An independent derivation is given in Appendix A. For each constant half-offset vector, $\mathbf{h}$, eqs (41)–(42) express, first, that the time of the diffraction-time function must equal the reflection time corresponding to the output trace location $(\mathbf{h}, \mathbf{x}) = [\mathbf{h}, \hat{\mathbf{x}}(\mathbf{h}, \mathbf{m})]$ and, secondly, that the diffraction-time function is required tangential to the reflection time branch at the same location. The two conditions are completely general and can thus be used for any type of diffraction-time function.

Fig. 5 outlines how a finite-offset reflection posted in the point M^{CIG} and time $\mathcal{T}^M$ in the time-migration domain is mapped to the point X and time T^X by time demigration to the recording domain. The reflection point D is connected to the time-migration domain via an image ray. For the idealized situation that the involved velocity models for time and depth migration yield identical diffraction-time functions, we will have consistency between kinematic *time* demigration (of the reflection in the point M^{CIG} at the time $\mathcal{T}^M$) and kinematic *depth* demigration (of the reflection in the point D): the output location in the recording domain will be the same in both situations. In the kinematic depth demigration, the point D is connected to the recording domain via the reflected ray SDR. Given a perfect depth-migration velocity model, so that the point D does not change with offset, the ray SDR will coincide with the normal ray X_0DX_0 in the zero-offset situation.

7.2 Demigrated position, reflection time and reflection slopes

In this and the following subsections we establish a general framework for kinematic time demigration. Details of the derivations are given in Appendix B.

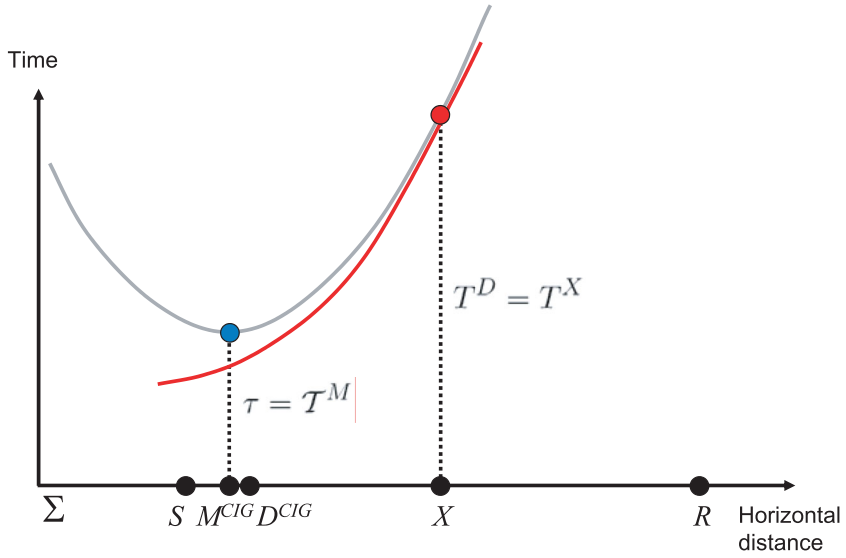

(a)

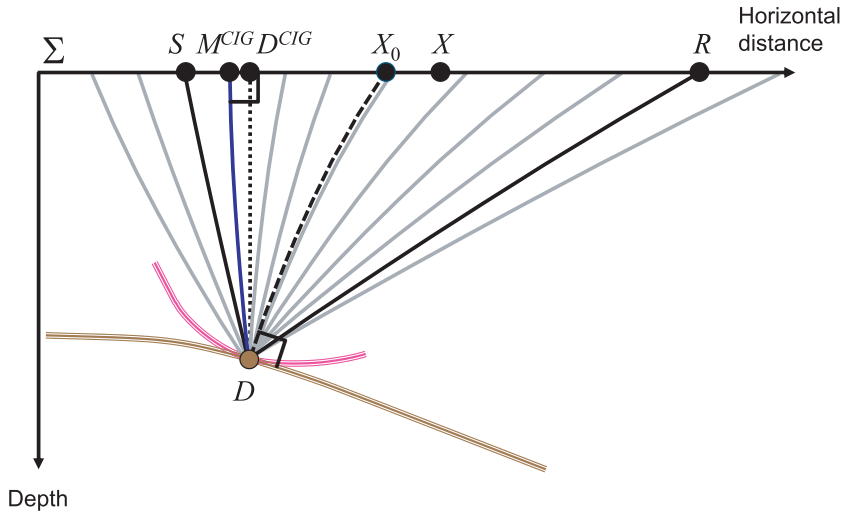

(b)

Figure 5. Special situation of Fig. 3 where a specular reflection occurs at the point D: (a) a finite-offset reflection posted in the point M^{CIG} and time $\mathcal{T}^M$ (blue dot) in the time-migration domain is mapped to the point X and time T^X (red dot) by kinematic time demigration. The reflection-time function (red curve) in the recording domain is indicated; (b) in kinematic depth demigration based on the introduced reflector (brown), the point D is mapped to the recording domain via the reflected ray *SDR* (solid black). Also shown is the diffraction isochron (pink) associated with this ray. The ray X_0DX_0 (dashed black) represents a 'degeneration' of the ray *SDR* to the zero-offset situation, given that the point D does not change with offset. As in Fig. 3, the involved time- and depth-migration velocity models are assumed to yield identical diffraction-time functions.

In the first subsection of Appendix B we derive the so-called *consistency equation*

$$\frac{\partial T^D}{\partial \mathbf{a}}[\mathbf{h}, \hat{\mathbf{a}}, \mathbf{m}, \mathcal{T}(\mathbf{h}, \mathbf{m})] - \frac{\partial T^D}{\partial \mathbf{m}}[\mathbf{h}, \hat{\mathbf{a}}, \mathbf{m}, \mathcal{T}(\mathbf{h}, \mathbf{m})] = \frac{\partial T^D}{\partial \tau}[\mathbf{h}, \hat{\mathbf{a}}, \mathbf{m}, \mathcal{T}(\mathbf{h}, \mathbf{m})] \frac{\partial \mathcal{T}}{\partial \mathbf{m}}(\mathbf{h}, \mathbf{m}), \tag{43}$$

which can be solved to provide the aperture vector, $\hat{\mathbf{a}} = \hat{\mathbf{x}} - \mathbf{m}$. Once we know this vector, the computation of the output time $T^X = T^D[\mathbf{h}, \hat{\mathbf{a}}, \mathbf{m}, \mathcal{T}(\mathbf{h}, \mathbf{m})]$ (eq. 41) and the output slope vector $\mathbf{p}^x = \partial T^D/\partial \mathbf{a}[\mathbf{h}, \hat{\mathbf{a}}, \mathbf{m}, \mathcal{T}(\mathbf{h}, \mathbf{m})]$ (eq. 42) is usually straightforward.

Naturally, the complexity of the algorithm required to compute $\hat{\mathbf{a}}$ will depend on the form of the diffraction-time function, T^D. Some forms of T^D yield analytical solutions for $\hat{\mathbf{a}}$; others not. In particular, as is discussed further below, $\hat{\mathbf{a}}$ can be obtained analytically under the assumption of single-square-root diffraction time and a homogeneous time-migration velocity model. For given coordinates $(\mathbf{h}, \mathbf{m})$ and time $\tau = \mathcal{T}(\mathbf{h}, \mathbf{m})$, eq. (43) is considered in the form $f_i(\mathbf{a}) = 0$, $i = 1, 2$, with the goal of computing a root, $\mathbf{a} = \hat{\mathbf{a}}$,

numerically. In this respect, one possible approach is the Newton–Raphson method, starting by assuming some trial solution for $\hat{\mathbf{a}}$ which complies with eq. (43) only approximately, and then iterate until consistency is achieved within some predefined numerical limit. Given a physically meaningful solution $\hat{\mathbf{a}}$, one can proceed to obtain demigrated time, slopes and second derivatives.

We have already seen that the slope vector $\mathbf{p}^x$ can be computed from eq. (42) when vector $\hat{\mathbf{a}}$ is known. There is an alternative way to compute $\mathbf{p}^x$, provided by eq. (B4), which can be restated as

$$\mathbf{p}^x = \mathbf{q}^m + u\,\boldsymbol{\psi}^m, \tag{44}$$

where eq. (10) defines the involved diffraction-time partial derivatives $\mathbf{q}^m$ and u. Eq. (44) relates the slope $\boldsymbol{\psi}^m$ in the time-migration domain to the slope $\mathbf{p}^x$ in the recording domain. Computation of the diffraction-time partial derivatives $\mathbf{q}^m$ and u requires the knowledge of the vector $\hat{\mathbf{a}}$. Similarly, eq. (B7) shows that the slopes $\boldsymbol{\psi}^h$ and $\mathbf{p}^h$ are related by

$$\mathbf{p}^h = \mathbf{q}^h + u\,\boldsymbol{\psi}^h, \tag{45}$$

with $\mathbf{q}^h$ defined by eq. (10).

7.3 Demigrated reflection-time second derivatives

Assuming that the output point $(\mathbf{h}, \hat{\mathbf{x}}, T^X)$ from kinematic time demigration is known, one can map the second derivatives $\bar{\boldsymbol{\mathcal{M}}} \rightarrow \bar{\mathbf{M}}$ by the following set of equations,

$$\mathbf{M}^{hh} = u\,\boldsymbol{\mathcal{M}}^{hh} + \mathbf{L}^{hh} - \left(u\,\boldsymbol{\mathcal{M}}^{hm} + \mathbf{L}^{hm} - \mathbf{K}^{ha}\right)(u\,\boldsymbol{\mathcal{M}}^{mm} - \mathbf{Y})^{-1} \times \left(u\,\boldsymbol{\mathcal{M}}^{hm} + \mathbf{L}^{hm} - \mathbf{K}^{ha}\right)^T, \tag{46}$$

$$\mathbf{M}^{hx} = \mathbf{K}^{ha} - \left(u\,\boldsymbol{\mathcal{M}}^{hm} + \mathbf{L}^{hm} - \mathbf{K}^{ha}\right) \times (u\,\boldsymbol{\mathcal{M}}^{mm} - \mathbf{Y})^{-1}\,(\mathbf{K}^{am} - \mathbf{U}^{aa})^T, \tag{47}$$

$$\mathbf{M}^{xx} = \mathbf{U}^{aa} - (\mathbf{K}^{am} - \mathbf{U}^{aa})\,(u\,\boldsymbol{\mathcal{M}}^{mm} - \mathbf{Y})^{-1}\,(\mathbf{K}^{am} - \mathbf{U}^{aa})^T. \tag{48}$$

For derivation, we refer to the reader to the second subsection of Appendix B. The mapping relations (46)–(48) include a number of auxiliary 2×2 matrices, defined in terms of diffraction-time partial derivatives (eq. 10) and reflection-time slopes $\bar{\boldsymbol{\psi}}$ in the time-migration domain (eq. 34),

$$\begin{aligned}
\mathbf{K}^{ha} &= \mathbf{U}^{ha} + \boldsymbol{\psi}^h \mathbf{u}^{a\,T}, \qquad \mathbf{K}^{am} = \mathbf{U}^{am} + \mathbf{u}^a \boldsymbol{\psi}^{m\,T},\\
\mathbf{L}^{hh} &= \mathbf{U}^{hh} + \boldsymbol{\psi}^h \mathbf{u}^{h\,T} + \mathbf{u}^h \boldsymbol{\psi}^{h\,T} + u^\tau\,\boldsymbol{\psi}^h \boldsymbol{\psi}^{h\,T},\\
\mathbf{L}^{hm} &= \mathbf{U}^{hm} + \boldsymbol{\psi}^h \mathbf{u}^{m\,T} + \mathbf{u}^h \boldsymbol{\psi}^{m\,T} + u^\tau\,\boldsymbol{\psi}^h \boldsymbol{\psi}^{m\,T},\\
\mathbf{L}^{mm} &= \mathbf{U}^{mm} + \boldsymbol{\psi}^m \mathbf{u}^{m\,T} + \mathbf{u}^m \boldsymbol{\psi}^{m\,T} + u^\tau\,\boldsymbol{\psi}^m \boldsymbol{\psi}^{m\,T},
\end{aligned} \tag{49}$$

and also the matrix

$$\mathbf{Y} = \mathbf{K}^{am} + \mathbf{K}^{am\,T} - (\mathbf{U}^{aa} + \mathbf{L}^{mm}). \tag{50}$$

Among these, the matrices $\mathbf{L}^{mm}$, $\mathbf{L}^{hh}$ and $\mathbf{Y}$ are symmetric.

Concerning physical interpretation of eqs (46)–(48), additional insight is provided from the second duality theorem in Kirchhoff depth migration (Schleicher *et al.* 2007, p. 159). This theorem relates second-order traveltime derivatives corresponding to reflection ($\mathbf{M}^{xx}$) and diffraction ($\mathbf{U}^{aa}$), at the location $(\mathbf{h}, \mathbf{x})$ of the recording domain, to curvatures of the reflector and the diffraction isochron, at the point D in the depth-migration domain (see Fig. 5). Eq. (48) can be viewed as the time-migration counterpart of the (depth-migration) second duality theorem in Schleicher *et al.* (2007). In the context of time migration, the matrices $\boldsymbol{\mathcal{M}}^{mm}$ and $\mathbf{Y}$ can thus be interpreted, respectively, in terms of curvatures of the reflector and the diffraction isochron.

To first order, the change in the output position $\hat{\mathbf{x}}$ can be described as

$$\Delta\hat{\mathbf{x}} = \mathbf{X}^h \Delta\mathbf{h} + \mathbf{X}^m \Delta\mathbf{m}, \tag{51}$$

with 2×2 matrices $\mathbf{X}^h$ and $\mathbf{X}^h$ given by

$$\mathbf{X}^h = \frac{\partial\hat{\mathbf{x}}}{\partial\mathbf{h}^T} = \left(\frac{\partial\hat{x}_i}{\partial h_j}\right), \qquad \mathbf{X}^m = \frac{\partial\hat{\mathbf{x}}}{\partial\mathbf{m}^T} = \left(\frac{\partial\hat{x}_i}{\partial m_j}\right). \tag{52}$$

The matrices $\mathbf{X}^h$ and $\mathbf{X}^m$ are characterizing the mapping of position coordinates performed by the time-demigration process. Moreover, $\mathbf{X}^h$ and $\mathbf{X}^m$ have similarities with paraxial (spreading) matrices known from ray theory. For these reasons, we refer to them as 'time-demigration spreading matrices'. Considering a specific reflection event, $\mathbf{X}^h$ and $\mathbf{X}^m$ describe first-order changes of the CMP location as a result of changing, respectively, the half-offset vector and the common-image gather location, while the other entity (common-image point and half offset) is kept constant. Using eq. (51), the first-order change of the output four-component trace location in the recording domain, $\hat{\bar{\mathbf{x}}}$, relative to the input four-component trace location in the time-migration domain, $\bar{\mathbf{m}}$, can be expressed in the form

$$\Delta\hat{\bar{\mathbf{x}}} = \begin{pmatrix} \mathbf{I} & \mathbf{O} \\ \mathbf{X}^h & \mathbf{X}^m \end{pmatrix} \Delta\bar{\mathbf{m}}. \tag{53}$$

The mapping operation $\bar{\boldsymbol{\mathcal{M}}} \rightarrow \bar{\mathbf{M}}$ yields the time-demigration spreading matrices in eq. (52) as byproducts (see Appendix B),

$$\mathbf{X}^h = -(\mathbf{K}^{am} - \mathbf{U}^{aa})^{-T} \left(u\,\boldsymbol{\mathcal{M}}^{hm} + \mathbf{L}^{hm} - \mathbf{K}^{ha}\right)^T, \tag{54}$$

$$\mathbf{X}^m = -(\mathbf{K}^{am} - \mathbf{U}^{aa})^{-T}\,(u\,\boldsymbol{\mathcal{M}}^{mm} - \mathbf{Y}). \tag{55}$$

From eq. (55) one can observe that the matrix $u\,\boldsymbol{\mathcal{M}}^{mm} - \mathbf{Y}$ is not necessarily invertible. In a caustic situation, matrix $\mathbf{X}^m$ will have determinant equal zero, and the inverse $(u\,\boldsymbol{\mathcal{M}}^{mm} - \mathbf{Y})^{-1}$ can not be computed. Application of mapping eqs (46)–(48) is therefore limited to cases where matrix $\mathbf{X}^m$ is non-singular.

7.4 Kinematic demigration from focused migrated images

If the time migration of the seismic data resulted in perfect focusing (no residual moveout after the migration), all derivatives of the migrated reflection time $\mathcal{T}$ with respect to half offset are zero. As a consequence, the matrices in eq. (49) are subjected to simplifications

$$\mathbf{K}^{ha} = \mathbf{U}^{ha}, \qquad \mathbf{L}^{hh} = \mathbf{U}^{hh}, \qquad \mathbf{L}^{hm} = \mathbf{U}^{hm} + \mathbf{u}^h \boldsymbol{\psi}^{m\,T}, \tag{56}$$

while eqs (45)–(47) and (54) reappear in idealized versions as

$$\mathbf{p}^h = \mathbf{q}^h, \tag{57}$$

$$\mathbf{M}^{hh} = \mathbf{U}^{hh} - \left(\mathbf{U}^{hm} - \mathbf{U}^{ha} + \mathbf{u}^h \boldsymbol{\psi}^{m\,T}\right)(u\,\boldsymbol{\mathcal{M}}^{mm} - \mathbf{Y})^{-1} \times \left(\mathbf{U}^{hm} - \mathbf{U}^{ha} + \mathbf{u}^h \boldsymbol{\psi}^{m\,T}\right)^T, \tag{58}$$

$$\mathbf{M}^{hx} = \mathbf{K}^{ha} - \left(\mathbf{U}^{hm} - \mathbf{U}^{ha} + \mathbf{u}^h \boldsymbol{\psi}^{m\,T}\right) \times (u\,\boldsymbol{\mathcal{M}}^{mm} - \mathbf{Y})^{-1}\,(\mathbf{K}^{am} - \mathbf{U}^{aa})^T, \tag{59}$$

$$\mathbf{X}^h = -(\mathbf{K}^{am} - \mathbf{U}^{aa})^{-T} \left(\mathbf{U}^{hm} - \mathbf{U}^{ha} + \mathbf{u}^h \boldsymbol{\psi}^{m\,T}\right)^T. \tag{60}$$

In eq. (57), the vector $\mathbf{p}^h$ represents the reflection slope at half-offset $\mathbf{h}$ within a CMP gather of time-demigrated seismic data at the location $\hat{\mathbf{x}}$. The matrix $\mathbf{M}^{hh}$ in eq. (58) yields the associated (time) 'curvature' of the NMO function within that gather. We observe that the slopes of the diffraction time and the reflection time with respect to $\mathbf{h}$ are equal. But this occurs only if the original time migration gave zero residual moveout.

7.5 Demigration at zero offset

In the zero-offset situation the diffraction-time partial derivatives satisfy eq. (14), while the reflection-time function T exhibits the properties in eq. (30). This yields $\mathbf{u}^h = \mathbf{0}$; $\mathbf{q}^h = \mathbf{0}$; $\mathbf{p}^h = \mathbf{0}$, and also $\mathbf{U}^{ha} = \mathbf{U}^{hm} = \mathbf{O}$; $\mathbf{M}^{hx} = \mathbf{O}$. Using eq. (45) it follows that

$$\boldsymbol{\psi}^h = \mathbf{0}. \tag{61}$$

In other words, at zero offset in the migration domain the slope of the reflection-time function is zero, regardless of the type of diffraction-time function and the parametrization of the time-migration velocity model. A further consequence is that $\mathbf{K}^{ha} = \mathbf{L}^{hm} = \mathbf{O}$, and from eqs (46), (47) and (54) we therefore obtain

$$\boldsymbol{\mathcal{M}}^{hm} = \mathbf{O}, \tag{62}$$

$$\mathbf{X}^h = \mathbf{O}, \tag{63}$$

$$\mathbf{M}^{hh} = u\,\boldsymbol{\mathcal{M}}^{hh} + \mathbf{U}^{hh}. \tag{64}$$

For a perfectly focused migration result at zero offset, we have $\boldsymbol{\mathcal{M}}^{hh} = \mathbf{O}$, so eq. (64) simplifies to

$$\mathbf{M}^{hh} = \mathbf{U}^{hh}. \tag{65}$$

Eq. (65) states that the second derivatives of reflection and diffraction time with respect to $\mathbf{h}$ are equal for $\mathbf{h} = \mathbf{0}$, a property known as the NIP-wave theorem (Chernyak & Gritsenko 1979; Hubral & Krey 1980). In the framework of second-order approximations this means that the traveltimes along the reflected and diffracted ray trajectories in Fig. 6, *SDR* and SD_0R, can be considered equal.

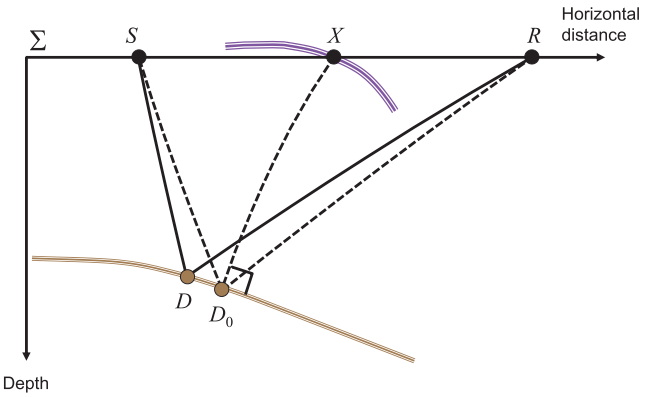

Figure 6. The NIP-wave theorem implies, under the assumption of traveltime approximations of second order, that the traveltimes along the reflected ray trajectory *SDR* (solid black) and the diffracted ray trajectory SD_0R (dashed black) can be taken as equal. For small offsets, the theorem justifies to estimate approximate (second-order) reflection times within a common-midpoint gather at X, based on the wavefront curvatures of the NIP wave (indicated in purple), which is considered originating as a point explosion in the reflector point D_0. The two-way normal ray trajectory associated with the (one-way) NIP wave is XD_0X (dashed black).

8 KINEMATIC TIME MIGRATION

Our approach to kinematic migration is structured in a similar way as the kinematic demigration approach described above. A schematic overview is depicted in Fig. 4. The input reflection-time parameters to kinematic migration are exactly those that were output from kinematic demigration, namely, the time function T and its first- and second-derivative parameters in eq. (27). These parameters are assumed known for a certain trace location $(\mathbf{h}, \mathbf{x})$ in the recording domain. However, since the time-migration velocity model is specified in the migration domain, not in the recording domain, the partial derivatives of the diffraction-time function T^D are inherently expressed in terms of the *output point* $(\mathbf{h}, \mathbf{m}, \tau)$ of the kinematic migration and not the input point, $(\mathbf{h}, \mathbf{x}, t)$. In order to solve this fundamental problem, it is necessary to compute the output point before proceeding to kinematic mapping of first- and second-order reflection-time parameters. Apart from trivial situations (e.g. assuming homogeneous time-migration velocity and single-square-root diffraction time) the computation of the output point will have to be done numerically.

In a kinematic migration corresponding to a reflection-time branch $T(\mathbf{h}, \mathbf{x})$ in the recording domain the output trace location $(\mathbf{h}, \mathbf{m})$ is assumed to have a single-valued relationship to the input trace location $(\mathbf{h}, \mathbf{x})$ such that

$$\mathbf{m} = \hat{\mathbf{m}}(\mathbf{h}, \mathbf{x}). \tag{66}$$

The aperture function $\hat{\mathbf{a}}$ introduced in eq. (38) is redefined accordingly to read

$$\mathbf{a} = \hat{\mathbf{a}}(\mathbf{h}, \mathbf{x}) = \mathbf{x} - \hat{\mathbf{m}}(\mathbf{h}, \mathbf{x}). \tag{67}$$

The migration output location, $\hat{\mathbf{m}}$, will generally have to be found numerically, while the mapping of all first and second-derivative parameters can be performed by means of explicit formulas. For kinematic migration under the assumption of perfect focusing the mapping equations involving half offset are the same as for kinematic demigration, see eqs (56)–(60) and (65).

8.1 Migrated position, reflection time, and reflection slopes

The basic conditions in eqs (41)–(42) formulated for kinematic demigration have to be satisfied also for kinematic migration. Hence, the output time $\hat{\tau}$ and the corresponding aperture vector $\hat{\mathbf{a}}$ have to comply with the relations

$$T(\mathbf{h}, \mathbf{x}) = T^D(\mathbf{h}, \hat{\mathbf{a}}, \mathbf{x} - \hat{\mathbf{a}}, \hat{\tau}), \tag{68}$$

$$\frac{\partial T}{\partial \mathbf{x}}(\mathbf{h}, \mathbf{x}) = \frac{\partial T^D}{\partial \mathbf{a}}(\mathbf{h}, \hat{\mathbf{a}}, \mathbf{x} - \hat{\mathbf{a}}, \hat{\tau}). \tag{69}$$

The latter system of three component equations can be worked on iteratively until one finds a solution for $\hat{\tau}$ and $\hat{\mathbf{a}}$ (and therefore also $\hat{\mathbf{m}} = \mathbf{x} - \hat{\mathbf{a}}$). Thereby, we are ready to compute all the diffraction-time partial derivatives in eq. (10). The sought reflection time in the migration domain is retrieved as the solution $\mathcal{T}^M = \hat{\tau}$.

From eqs (44) and (45) it is clear that slopes $\bar{\boldsymbol{\psi}}$ in the time-migration domain can be computed from slopes $\bar{\mathbf{p}}$ in the recording domain using

$$\boldsymbol{\psi}^h = \frac{1}{u}(\mathbf{p}^h - \mathbf{q}^h), \qquad \boldsymbol{\psi}^m = \frac{1}{u}(\mathbf{p}^x - \mathbf{q}^m). \tag{70}$$

Knowing the slopes $\bar{\boldsymbol{\psi}}$, and the diffraction-time partial derivatives in eq. (10), we have sufficient information to compute all the auxiliary 2×2 matrices in eq. (49) and the matrix $\mathbf{Y}$ in eq. (50).

8.2 Migrated reflection-time second derivatives

The next step is to map reflection-time second derivatives $\bar{\mathbf{M}} \rightarrow \bar{\boldsymbol{\mathcal{M}}}$ from the recording domain to the time-migration domain. We achieve this by reversing the transformations in eqs (46)–(48) and taking advantage of intermediate results in Appendix B. This yields

$$\begin{aligned}
\boldsymbol{\mathcal{M}}^{hh} &= \frac{1}{u}\left[\mathbf{M}^{hh} - \mathbf{L}^{hh}\right. \\
&\quad \left. - \left(\mathbf{M}^{hx} - \mathbf{K}^{ha}\right)\left(\mathbf{M}^{xx} - \mathbf{U}^{aa}\right)^{-1}\left(\mathbf{M}^{hx} - \mathbf{K}^{ha}\right)^{T}\right], \\
\boldsymbol{\mathcal{M}}^{hm} &= \frac{1}{u}\left[\mathbf{L}^{hm} - \mathbf{K}^{ha} + \left(\mathbf{M}^{hx} - \mathbf{K}^{ha}\right)\right. \\
&\quad \left. \times \left(\mathbf{M}^{xx} - \mathbf{U}^{aa}\right)^{-1}\left(\mathbf{K}^{am} - \mathbf{U}^{aa}\right)\right], \\
\boldsymbol{\mathcal{M}}^{mm} &= \frac{1}{u}\left[\mathbf{Y} - \left(\mathbf{K}^{am} - \mathbf{U}^{aa}\right)^{T}\left(\mathbf{M}^{xx} - \mathbf{U}^{aa}\right)^{-1}\left(\mathbf{K}^{am} - \mathbf{U}^{aa}\right)\right].
\end{aligned} \tag{71}$$

For a particular reflection event, the change of output position $\hat{\mathbf{m}}$ is given to first order by

$$\Delta\hat{\mathbf{m}} = \boldsymbol{\mathcal{X}}^{h}\Delta\mathbf{h} + \boldsymbol{\mathcal{X}}^{x}\Delta\mathbf{x} \tag{72}$$

where the two 2×2 'time-migration spreading matrices' $\boldsymbol{\mathcal{X}}^{h}$ and $\boldsymbol{\mathcal{X}}^{x}$ have the definitions

$$\boldsymbol{\mathcal{X}}^{h} = \frac{\partial\hat{\mathbf{m}}}{\partial\mathbf{h}^{T}} = \left(\frac{\partial\hat{m}_i}{\partial h_j}\right), \qquad \boldsymbol{\mathcal{X}}^{x} = \frac{\partial\hat{\mathbf{m}}}{\partial\mathbf{x}^{T}} = \left(\frac{\partial\hat{m}_i}{\partial x_j}\right). \tag{73}$$

The matrices $\boldsymbol{\mathcal{X}}^{h}$ and $\boldsymbol{\mathcal{X}}^{x}$ describe first-order changes of the common-image point as a result of changing, respectively, the half-offset vector and the CMP location, while the other entity (midpoint and half offset) is kept constant. The first-order change of the output trace location in the time-migration domain, $\hat{\bar{\mathbf{m}}}$, relative to the input trace location in the recording domain, $\bar{\mathbf{x}}$, is

$$\Delta\hat{\bar{\mathbf{m}}} = \begin{pmatrix} \mathbf{I} & \mathbf{O} \\ \boldsymbol{\mathcal{X}}^{h} & \boldsymbol{\mathcal{X}}^{x} \end{pmatrix}\Delta\bar{\mathbf{x}}. \tag{74}$$

In view of eqs (53) and (74) the time-migration spreading matrices $\boldsymbol{\mathcal{X}}^{h}$ and $\boldsymbol{\mathcal{X}}^{x}$ can be expressed in terms of the corresponding time-demigration spreading matrices as

$$\boldsymbol{\mathcal{X}}^{h} = -\left(\mathbf{X}^{m}\right)^{-1}\mathbf{X}^{h}, \qquad \boldsymbol{\mathcal{X}}^{x} = \left(\mathbf{X}^{m}\right)^{-1}. \tag{75}$$

Using eqs (54), (55), (75) and Appendix B, we formulate the time-migration spreading matrices in terms of reflection-time parameters of the recording domain as

$$\begin{aligned}
\boldsymbol{\mathcal{X}}^{h} &= \left(\mathbf{K}^{am} - \mathbf{U}^{aa}\right)^{-1}\left(\mathbf{M}^{hx} - \mathbf{K}^{ha}\right)^{T}, \\
\boldsymbol{\mathcal{X}}^{x} &= \left(\mathbf{K}^{am} - \mathbf{U}^{aa}\right)^{-1}\left(\mathbf{M}^{xx} - \mathbf{U}^{aa}\right).
\end{aligned} \tag{76}$$

9 KINEMATIC TIME MIGRATION/DEMIGRATION USING SINGLE-/DOUBLE-SQUARE-ROOT DIFFRACTION TIMES

Up to now, we have considered completely general schemes for kinematic time migration and demigration, which are independent of the choice of diffraction-time function and the parametrization of the time-migration velocity model. In the following, we turn to considering kinematic migration/demigration with specific conventionally used functions, namely, the single and double square-root approximations. For the double-square-root approximation at arbitrary offsets (eq. 21), it is not practical to write explicit expressions for the mapping operations, as these will become very extensive. Instead, we refer to the general mapping framework described above, where one should insert diffraction-time partial derivatives as specified in Appendix C.

9.1 Migration/demigration with single-square-root diffraction time

We consider kinematic migration an demigration using the single-square-root approximation to diffraction time (eq. 23). All required partial derivatives for this function are given in Appendix D.

Position and reflection time

Inserting the expressions for the partial derivatives given by eqs (D2), (D3) and (D4) into the consistency eq. (43) we obtain the relation

$$4S^{M}_{kj}\hat{a}_j - \mathcal{T}^{M}\psi^{m}_{k} - 2\left(\frac{\partial S^{M}_{ij}}{\partial m_k} + \psi^{m}_{k}\frac{\partial S^{M}_{ij}}{\partial\tau}\right)(\hat{a}_i\hat{a}_j + h_i h_j) = 0. \tag{77}$$

Eq. (77) can be used for demigration of the lateral input position $\mathbf{m}$ in the time-migration domain, by finding the aperture vector $\hat{\mathbf{a}}$ that corresponds to the time $\mathcal{T}^{M}$ and slope $\boldsymbol{\psi}^{m}$ of a reflection event identified in this domain. We observe that the equation is second order with respect to the components of vector $\hat{\mathbf{a}}$, which implies two potential roots. One of these is to be classified as 'non-physical'. If the variations of matrix $\mathbf{S}^{M}$ with $(\mathbf{m}, \tau)$ are neglected one obtains the solution

$$\hat{\mathbf{a}} = \frac{1}{4}\mathcal{T}^{M}\mathbf{S}^{M\,-1}\boldsymbol{\psi}^{m}. \tag{78}$$

The latter result, pertaining to a homogeneous time-migration velocity model, corresponds to Whitcombe's (1994) eq. (3) in the 2-D situation and to Soellner & Andersen's (2005) eq. (8) in the 3-D situation. When vector $\hat{\mathbf{a}}$ is known we use eq. (23) to obtain the demigrated reflection time, T^{X}.

For kinematic migration it is generally required to solve the equation system (68)–(69), thus implying a simultaneous estimation of aperture vector $\hat{\mathbf{a}}$ and migrated reflection time, $\mathcal{T}^{M}$. However, if the time-migration velocity model is homogeneous one can first compute $\hat{\mathbf{a}}$ by combining eqs (69) and (D2) and subsequently the migrated time $\mathcal{T}^{M}$ using eq. (23).

Reflection-time slopes and second derivatives; spreading matrices

Having obtained the aperture vector $\hat{\mathbf{a}}$ and the output (migrated/demigrated) reflection time, it is fairly straightforward to obtain all corresponding output slopes and second derivatives, by combining the above general formulations of kinematic migration/demigration with the explicit partial derivatives for the single-square-root diffraction-time function given in Appendix D.

For better insight and clarity, it may be instructive to neglect variations of matrix $\mathbf{S}^{M}$ with $(\mathbf{m}, \tau)$. As a result, we get simple relations

(i) between slope vectors in the recording and migration domains,

$$T^X \mathbf{p}^h = \mathcal{T}^M \boldsymbol{\psi}^h + 4\mathbf{S}^M \mathbf{h}, \tag{79}$$

$$T^X \mathbf{p}^x = \mathcal{T}^M \boldsymbol{\psi}^m, \tag{80}$$

(ii) between second-derivative matrices in the two domains,

$$\begin{aligned} T^X \mathbf{M}^{hh} + \mathbf{p}^h\ \mathbf{p}^{h\,T} &= \mathcal{T}^M \boldsymbol{\mathcal{M}}^{hh} + \boldsymbol{\psi}^h\ \boldsymbol{\psi}^{h\,T} + 4\mathbf{S}^M \\ &+ \left(\mathcal{T}^M \boldsymbol{\mathcal{M}}^{hm} + \boldsymbol{\psi}^h\ \boldsymbol{\psi}^{m\,T}\right)\left(\mathcal{T}^M \boldsymbol{\mathcal{M}}^{mm} + \boldsymbol{\psi}^m\ \boldsymbol{\psi}^{m\,T} + 4\mathbf{S}^M\right)^{-1} \\ &\times \left(\mathcal{T}^M \boldsymbol{\mathcal{M}}^{hm} + \boldsymbol{\psi}^h\ \boldsymbol{\psi}^{m\,T}\right)^T, \\ T^X \mathbf{M}^{hx} + \mathbf{p}^h\ \mathbf{p}^{x\,T} &= \left(\mathcal{T}^M \boldsymbol{\mathcal{M}}^{hm} + \boldsymbol{\psi}^h\ \boldsymbol{\psi}^{m\,T}\right) \\ &\times \left[\mathbf{I} + \frac{1}{4}\mathbf{S}^{M-1}\left(\mathcal{T}^M \boldsymbol{\mathcal{M}}^{mm} + \boldsymbol{\psi}^m\ \boldsymbol{\psi}^{m\,T}\right)\right]^{-1}, \\ \left[\mathbf{I} - \frac{1}{4}\mathbf{S}^{M-1}\left(T^X \mathbf{M}^{xx} + \mathbf{p}^x\ \mathbf{p}^{x\,T}\right)\right] &\\ \times \left[\mathbf{I} + \frac{1}{4}\mathbf{S}^{M-1}\left(\mathcal{T}^M \boldsymbol{\mathcal{M}}^{mm} + \boldsymbol{\psi}^m\ \boldsymbol{\psi}^{m\,T}\right)\right] &= \mathbf{I}, \end{aligned} \tag{81}$$

and

(iii) for the time-demigration spreading matrices,

$$\begin{aligned} \mathbf{X}^h &= \frac{1}{4}\mathbf{S}^{M-1}\left(\mathcal{T}^M \boldsymbol{\mathcal{M}}^{hm} + \boldsymbol{\psi}^h\ \boldsymbol{\psi}^{m\,T}\right), \\ \mathbf{X}^m &= \mathbf{I} + \frac{1}{4}\mathbf{S}^{M-1}\left(\mathcal{T}^M \boldsymbol{\mathcal{M}}^{mm} + \boldsymbol{\psi}^m\ \boldsymbol{\psi}^{m\,T}\right). \end{aligned} \tag{82}$$

To obtain corresponding time-migration spreading matrices, see eqs (75)–(76). For idealized migration focusing, we observe from eq. (82) that matrix $\mathbf{X}^h$ is zero for all offsets, while matrix $\mathbf{X}^m$ is invariant with offset. We emphasize that these properties of the time-demigration spreading matrices are not general—they belong specifically to the single-square-root function. The latter is therefore unable to take into account reflection-point smearing in the migration process, while the double-square-root function handles such smearing correctly when the medium is homogeneous and isotropic.

In the situation of demigration the slope vector $\mathbf{p}^x$ may be computed by eq. (80). Alternatively, it can be obtained by combining eqs (42) and (D2), which yields

$$\mathbf{p}^x = \frac{4}{T^X}\mathbf{S}^M \hat{\mathbf{a}}. \tag{83}$$

Eq. (83) has, in contrast to eq. (80), been derived without neglecting the variations of matrix $\mathbf{S}^M$ with $(\mathbf{m}, \tau)$.

9.2 Migration/demigration at zero offset

We recapitulate from above (see eqs 61–65) that the zero-offset situation always yields $\boldsymbol{\psi}^h = \mathbf{p}^h = \mathbf{0}$, $\boldsymbol{\mathcal{M}}^{hm} = \mathbf{M}^{hx} = \mathbf{O}$, and $\mathbf{X}^h = \boldsymbol{\mathcal{X}}^h = \mathbf{O}$. The double-square-root and single-square-root diffraction-time functions are identical at zero offset, with only one exception. The matrix $\mathbf{U}^{hh}$ is different for the two approximations, as shown in Appendix E. This difference has important consequences with respect to applicability, which is discussed in more detail below.

Migration/demigration of CMP/image-gather locations can be done with the procedure described in the previous sub-section, after substituting $\mathbf{h} = \mathbf{0}$ into eq. (77). For migration/demigration of reflection slopes and second-derivatives one can use the general framework with diffraction-time partial derivatives from Appendix E. If the time-migration velocity model is assumed homogeneous, slope mapping $\boldsymbol{\psi}^m \leftrightarrow \mathbf{p}^x$ and second-derivative mapping $\boldsymbol{\mathcal{M}}^{mm} \leftrightarrow \mathbf{M}^{xx}$ can be conducted using relevant relations in eqs (79)–(81). The time-demigration spreading matrix $\mathbf{X}^m$ is given in eq. (82).

9.3 Relating time-migration and NMO matrices

When considering the double-square-root approximation (eqs 5 and 21 in combination), it is of interest to relate time-migration velocity at the common-image point to NMO velocity at the CMP. For this we need diffraction-time partial derivatives at zero offset, which are specified in Appendix E.

Consider now eq. (E1) for the matrix $\mathbf{U}^{hh}$, and also eq. (65), which corresponds to a perfectly focused migration result at zero offset. Taking into account definitions of the time-migration and NMO matrices $\mathbf{S}^M$ and $\mathbf{S}^{\mathrm{NMO}}$ in eqs (19) and (31), we find the relation

$$\mathbf{S}^M = \mathbf{S}^{\mathrm{NMO}} + \frac{1}{4}\mathbf{p}^x\ \mathbf{p}^{x\,T}. \tag{84}$$

Eq. (84) can be used to estimate the matrix $\mathbf{S}^M$ from the matrix $\mathbf{S}^{\mathrm{NMO}}$ or vice versa. If we instead are using the single-square-root approximation, eq. (81) has the implication that

$$\mathbf{S}^M = \mathbf{S}^{\mathrm{NMO}}. \tag{85}$$

In other words, the single-square-root function predicts the time-migration matrix $\mathbf{S}^M$ at the common image-point location to be equal to the NMO matrix $\mathbf{S}^{\mathrm{NMO}}$ at the CMP location. Moreover, for any given direction, θ, the surface-specific NMO velocity is predicted equal to the corresponding time-migration velocity. As these results are obviously not exact even for an homogeneous isotropic medium, they demonstrate that the single-square-root approximation should be used with care. One cannot use the single-square-root approximation for estimating NMO velocity from time-migration velocity or vice versa. One can, however, use it for kinematic migration/demigration between the recording and migration domains as long as offsets and/or apertures are small.

10 ESTIMATION OF THE TIME-MIGRATION VELOCITY MODEL

We outline two routes by which the parameters of the time-migration velocity model can be estimated, using the methodology of kinematic time migration and demigration.

The first route is driven by known reflection-time parameters in the time-migration domain. One starts by time-migrating the seismic data set using a preliminary time-migration velocity model. In the migrated data set, reflection-time parameters are identified for a number of key reflections. Using the same preliminary time-migration velocity model as before, one kinematically demigrates the retrieved reflection-time parameters so that they become represented in the recording domain. One can now formulate an inversion scheme by which the time-migration velocity model is systematically updated by minimizing the slope parameter $\boldsymbol{\psi}^h$ for a range of offsets. If desirable, minimization of the second-derivative parameters $\boldsymbol{\mathcal{M}}^{hh}$ and $\boldsymbol{\mathcal{M}}^{hm}$ may be included in the procedure, as well.

The second route is driven by known reflection-time parameters in the recording domain. Assume, for example, that one takes as diffraction-time function the double-square-root function (eqs 17

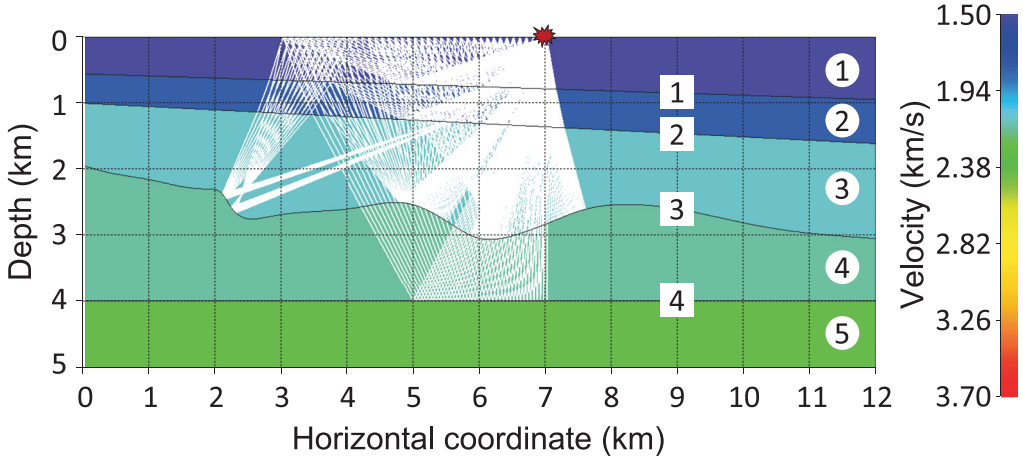

Figure 7. Example 1: 2-D depth model with five homogeneous isotropic layers (indices 1–5) and four interfaces (indices 1–4). The constant layer velocities are, from top to bottom, 1.5, 1.8, 2.1, 2.15 and 2.4 km s^{-1}. Reflection rays for the source point at horizontal location 7.0 km are superimposed. [Correction made after online publication 2012 April 26: the labelling in this figure has been corrected.]

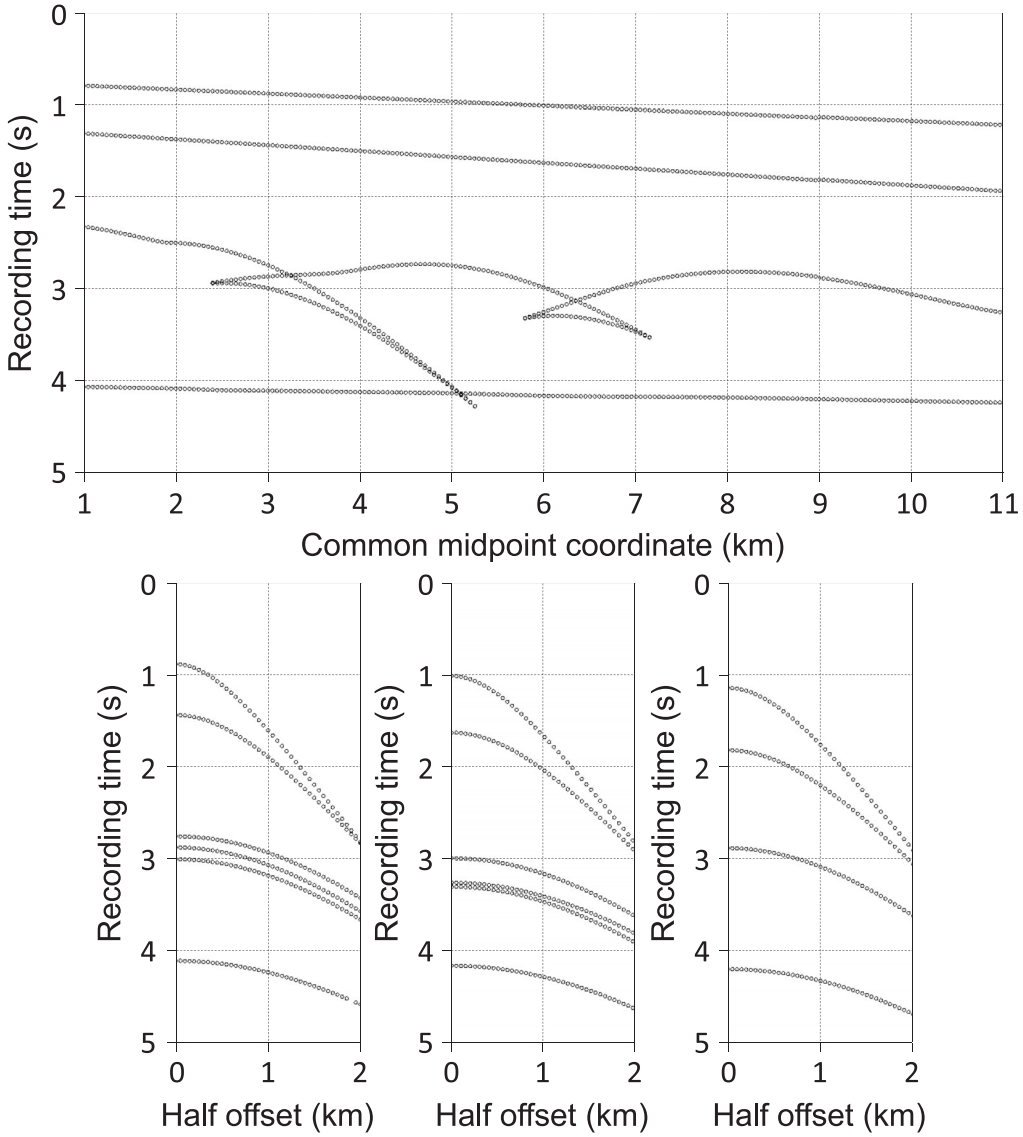

Figure 8. Example 1: reflection events simulated by ray tracing from 241 source points in the 2-D model (Fig. 7). Zero-offset gather (top panel) and common-midpoint gathers (bottom panel) corresponding to the locations 3.0, 6.0 and 9.0 km. The modulus of the half-offset vector is the horizontal coordinate of the common-midpoint gathers.

and 21 in combination). Let us further assume that for a given location $\mathbf{x}$ and zero offset, $\mathbf{h} = \mathbf{0}$, the reflection time T^X, the slope vector $\mathbf{p}^x$, and the NMO matrix, $\mathbf{S}^{\mathrm{NMO}}$, are known. Estimation of the latter from seismic data requires that observations are available for at least three different directions of the half-offset vector. A corresponding time-migration matrix, $\hat{\mathbf{S}}^M$, can then be estimated using eq. (84) , but we do not yet know its location $(\hat{\mathbf{m}}, \hat{\tau})$. For that, we can first use eq. (83), which applies to both the single- and double-square-root functions at zero offset, to obtain the aperture vector $\hat{\mathbf{a}}$ and then the image-gather location $\hat{\mathbf{m}} = \mathbf{x} - \hat{\mathbf{a}}$. Thereafter, we use eq. (23) with $\mathbf{h} = \mathbf{0}$ to compute the migration time, $\hat{\tau}$. Having applied this direct estimation procedure to yield a number of samples $(\hat{\mathbf{m}}, \hat{\tau}, \hat{\mathbf{S}}^M)$, the function $\mathbf{S}^M(\mathbf{m}, \tau)$ is finally established by regularization.

11 NUMERICAL EXAMPLES

The methodology presented above is illustrated by means of two numerical examples.

11.1 Example 1

Consider a 2-D depth model with five homogeneous isotropic layers (Fig. 7) separated by four interfaces. Layers and interfaces are numbered sequentially from top to bottom by indices 1-5 and 1-4, respectively. Interfaces 1 and 2 are planar and dipping, interface 3 has significant undulations, while interface 4 is planar and horizontal. The constant velocities in layers 1 through 5 are 1.5, 1.8, 2.1, 2.15 and 2.4 km s^{-1}. The velocity contrast across interface 3 is on purpose chosen to be very small, to avoid distorting the kinematic time migration corresponding to interface 4.

For each interface we simulated reflection events corresponding to a marine seismic survey with sources located at zero depth and between the horizontal locations 1.0 and 13.0 km. The source separation is 50 m (241 source points in total). The events were 'recorded' along a 4.0 km long towed receiver cable with receiver separation 50 m (81 receiver positions for each source point). Each simulated event is characterized by the following (minimum) information: the half-offset component, h_1, the midpoint coordinate,

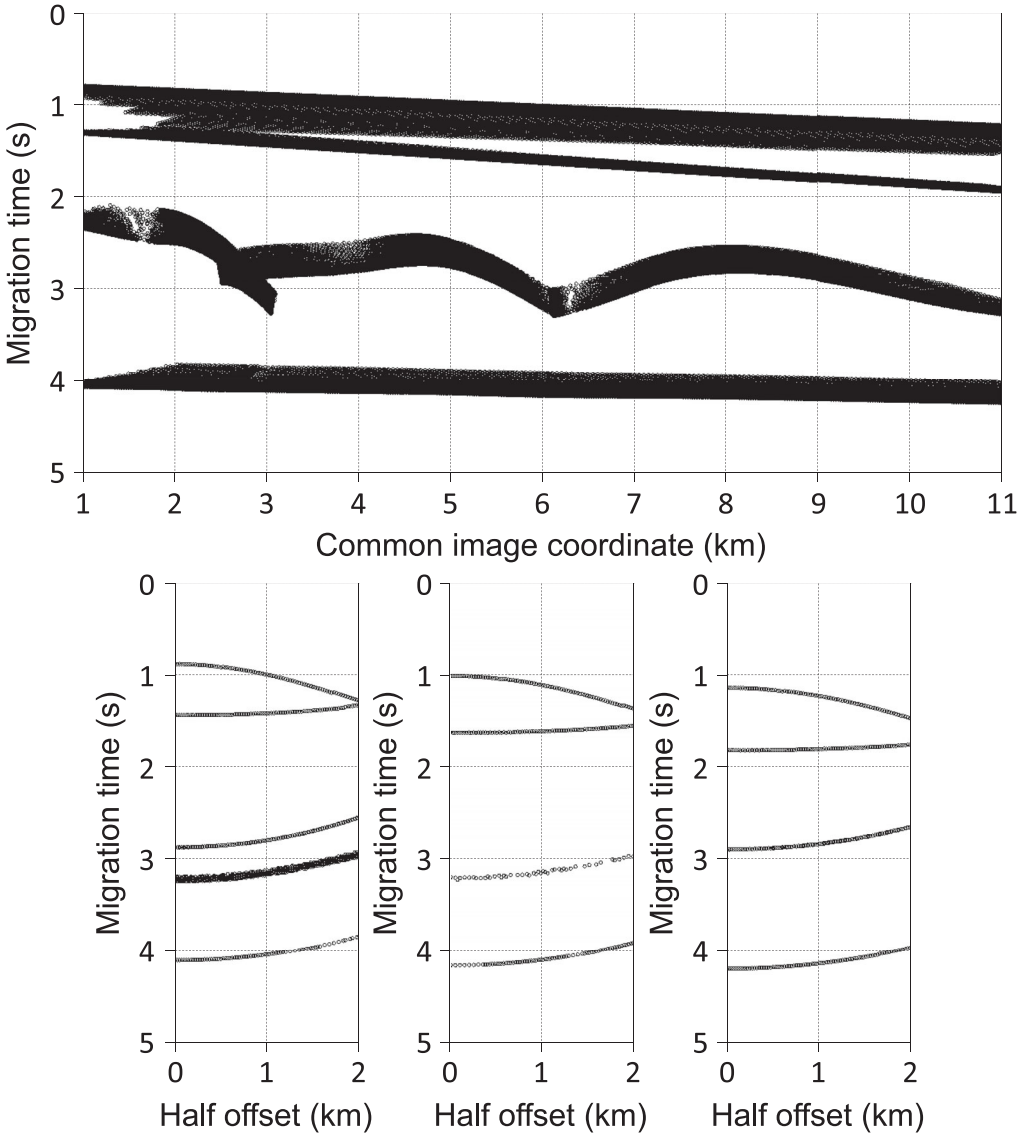

Figure 9. Example 1: reflection events after kinematic time migration using a constant migration velocity 1.6 km s^{-1} ($S^M_{11} = 0.390625$ s^2 km^{-2}). Projection of events for all offsets into the zero-offset section (top panel) and common-image gathers (bottom panel) corresponding to the locations 3.0, 6.0 and 9.0 km. The modulus of the half-offset vector is the horizontal coordinate of the common-image gathers.

x_1, the reflection time, T^X, and the reflection slope, p_1. A subset of the simulated reflection times is shown in Fig. 8. We observe that interface 3 gives rise to multiple arrivals.

The generated event data were pretended to be our seismic observations and we mapped them to the time-migration domain using the presented procedure for kinematic time migration. The inherent diffraction time was represented by the standard double-square root function (eqs 17 and 21). To start with the required time-migration velocity model was not known, so as a rough initial guess we let the time-migration velocity be constant and equal to 1.6 km s^{-1}. This corresponds to a squared time-migration slowness $S_{11}^M = 0.390625$ s^2 km^{-2}. Fig. 9 shows the reflection events after kinematic time migration using this homogeneous time-migration velocity model. In the upper subfigure all mapped events have been projected into the zero-offset section, while the three lower subfigures shows common-image gathers of the events at the horizontal locations 3.0, 6.0 and 9.0 km. Using these types of plots one can get a first indication of whether the time-migrated image will be well focused or not. It is obvious that our chosen initial time-migration velocity model is quite inadequate, in the sense that the events appear with significant residual moveout. Also, the triplications of the reflections from interface 3 have not been completely unfolded. On the other hand, the initial time-migration model is of sufficient quality to permit the identification of adequate single-valued reflection-time surfaces over most of the half-offset/image-gather area (Fig. 10).

From the reflection-time surfaces in Fig. 10 we estimated the reflection-time parameter $\mathcal{M}_{11}^{hh}$ at zero offset. This would correspond to applying a standard velocity analysis procedure (Taner & Koehler 1969) to common-image gathers of pre-stack time-migrated seismic data. In this way, we replaced the velocity analysis/event picking step (that would have to be included in the presence of real seismic data) with a surface fitting operation.

Having obtained the parameter $\mathcal{M}_{11}^{hh}$ we performed a kinematic time demigration at zero offset, which yielded the corresponding reflection-time parameter M_{11}^{hh} (eq. 64) and therefore also the squared NMO slowness, S_{11}^{NMO} (eq. 31). Knowing this entity, we took advantage of eq. (84) to estimate the corresponding squared time-migration slowness, S_{11}^M, and its associated image-gather and migration-time coordinates. After applying regularization and smoothing in these coordinates we obtained the updated result for S_{11}^M given in Fig. 11(a). The corresponding time-migration velocity is shown in Fig. 11(b).

Using the updated time-migration velocity model we applied again kinematic time migration to the full set of 'recorded' events. The result (Fig. 12) is to be compared to the one obtained using

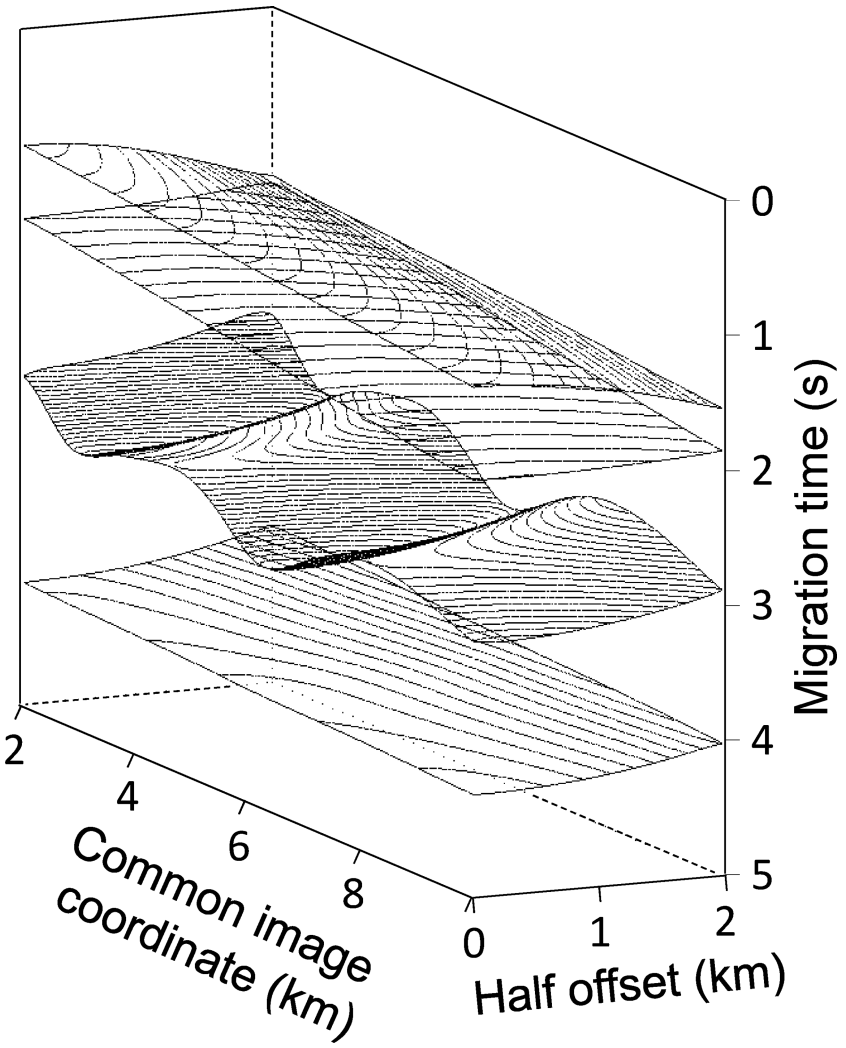

Figure 10. Example 1: reflection surfaces in the time-migration domain established from kinematically time-migrated events (Fig. 9). The vertical separation between contours is 25 ms.

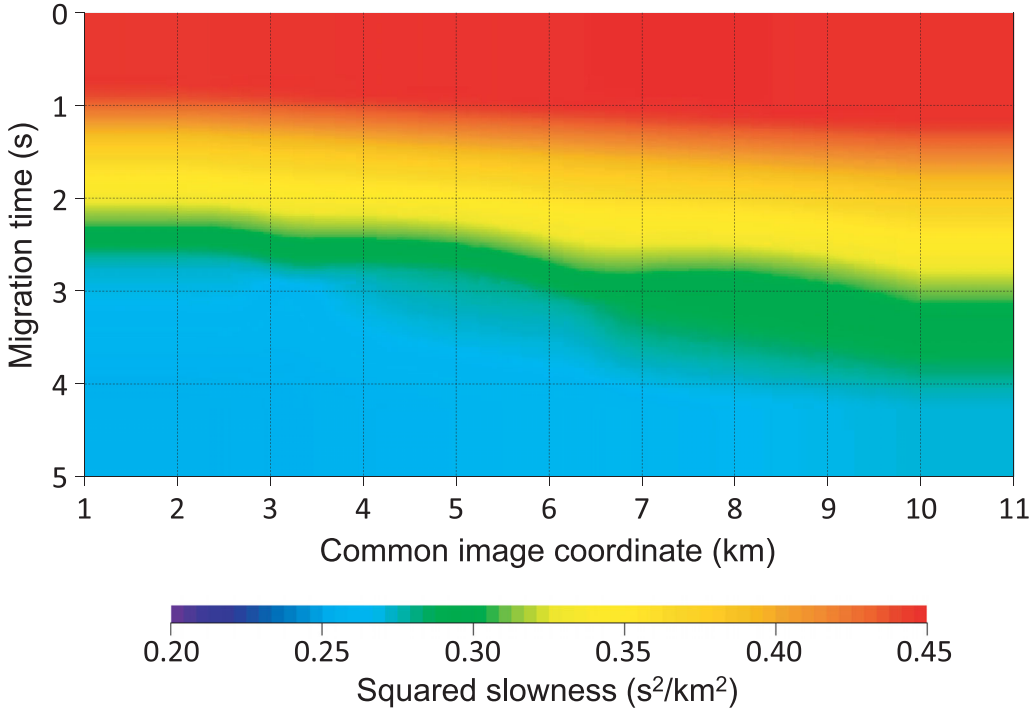

(a)

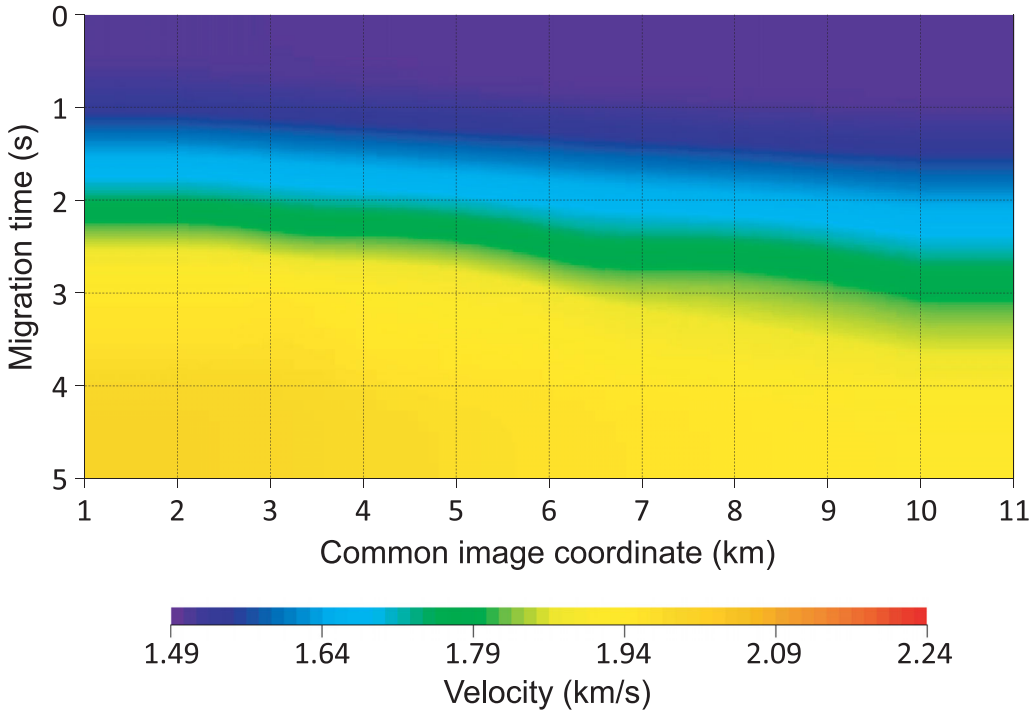

(b)

Figure 11. Example 1: (a) updated squared time-migration slowness S_{11}^{M} obtained after having 'measured' residual moveouts using reflection surfaces (Fig. 10) and (b) the corresponding time-migration velocity.

the initial homogeneous model (Fig. 9). For the two upper reflection surfaces there is still some residual moveout, but this appears only at very large offsets. The reason is probably a combination of errors introduced in the estimation of the parameter $\mathcal{M}_{11}^{hh}$, the regularization/smoothing procedure, and by the fact that diffraction times for interface 2 at very large offsets do not comply well with the standard double-square root function. For the two lowermost reflection surfaces one can observe a striking improvement of the imaging of the interface geometry as well as of the event flatness in common-image gathers. In a real data processing situation the

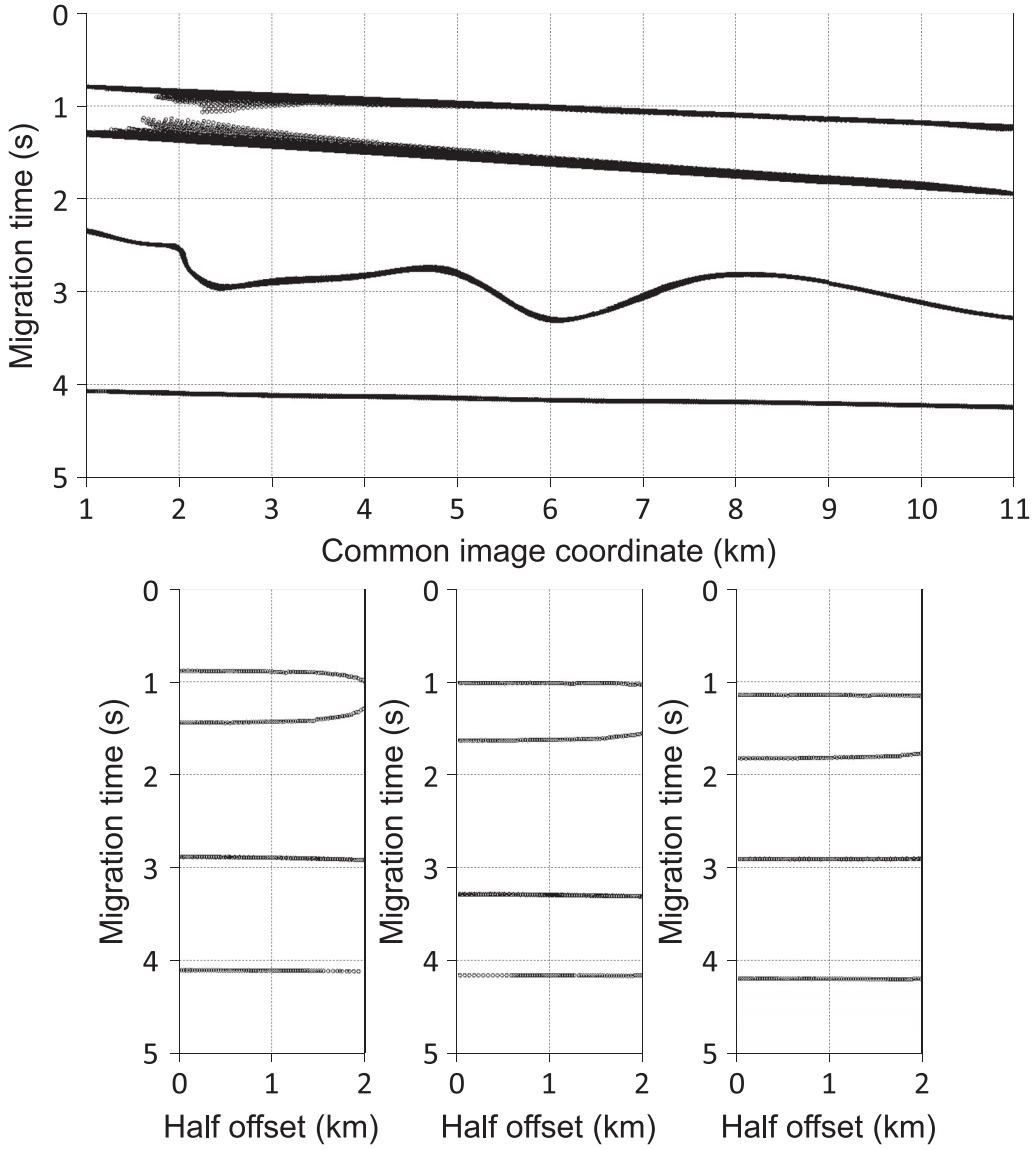

Figure 12. Example 1: reflection events after kinematic time migration using the updated S_{11}^M field in Fig. 11(a). Projection of events for all offsets into the zero-offset section (top panel) and common-image gathers (bottom panel) for the same locations as in Fig. 9.

far-offset shallow reflections are commonly muted. To be consistent with this practice we also applied a simple mute function to the reflection events before performing the kinematic time migration process. After these operations the 'image' of all four reflectors appears very well focused (Fig. 13).

As a final comment to example 1, observe that interface 4 is not imaged as exactly planar horizontal in the time-migration domain. This is an intrinsic effect of time migration which cannot be repaired by improving the time-migration velocity model.

11.2 Example 2

In example 1 the velocity contrast across interface 3 was very small, and kinematic time migration with respect to the reflections from interface 4 gave a nicely focused result. As a natural follow-up, we wanted to obtain a corresponding result in the situation where a larger velocity contrast appears across interface 3. We achieved this by introducing a linearly and laterally varying velocity function with a quite strong gradient, 0.1 s^{-1}, in layer 4 while the velocity at horizontal distance 0 km was the same as before, 2.15 km s^{-1}. For an impression of this modified model, see Fig. 14. As in Fig. 7 some ray paths are superimposed, but now only those corresponding to reflections at interface 4. The increasing velocity contrast along interface 3 is seen to yield significant focusing effects.

New reflection event data were generated for interface 4 (Fig. 15) and regularized data for the function S_{11}^M (see Fig. 16) were re-estimated by the same procedure as before. Using the updated S_{11}^M, the whole event data set was muted and thereafter kinematically migrated (Fig. 17).

We find the result in Fig. 17 very encouraging. The greater velocity contrast at interface 3 makes it difficult to estimate a consistent S_{11}^M in two regions with strong focusing effects. These regions are located below the troughs of interface 3 appearing approximately at the horizontal locations 2.5 and 6 km. The 'image' of interface 4 in these regions is observed to be somewhat more blurry than in example 1 (Fig. 13) but is by no means completely distorted.

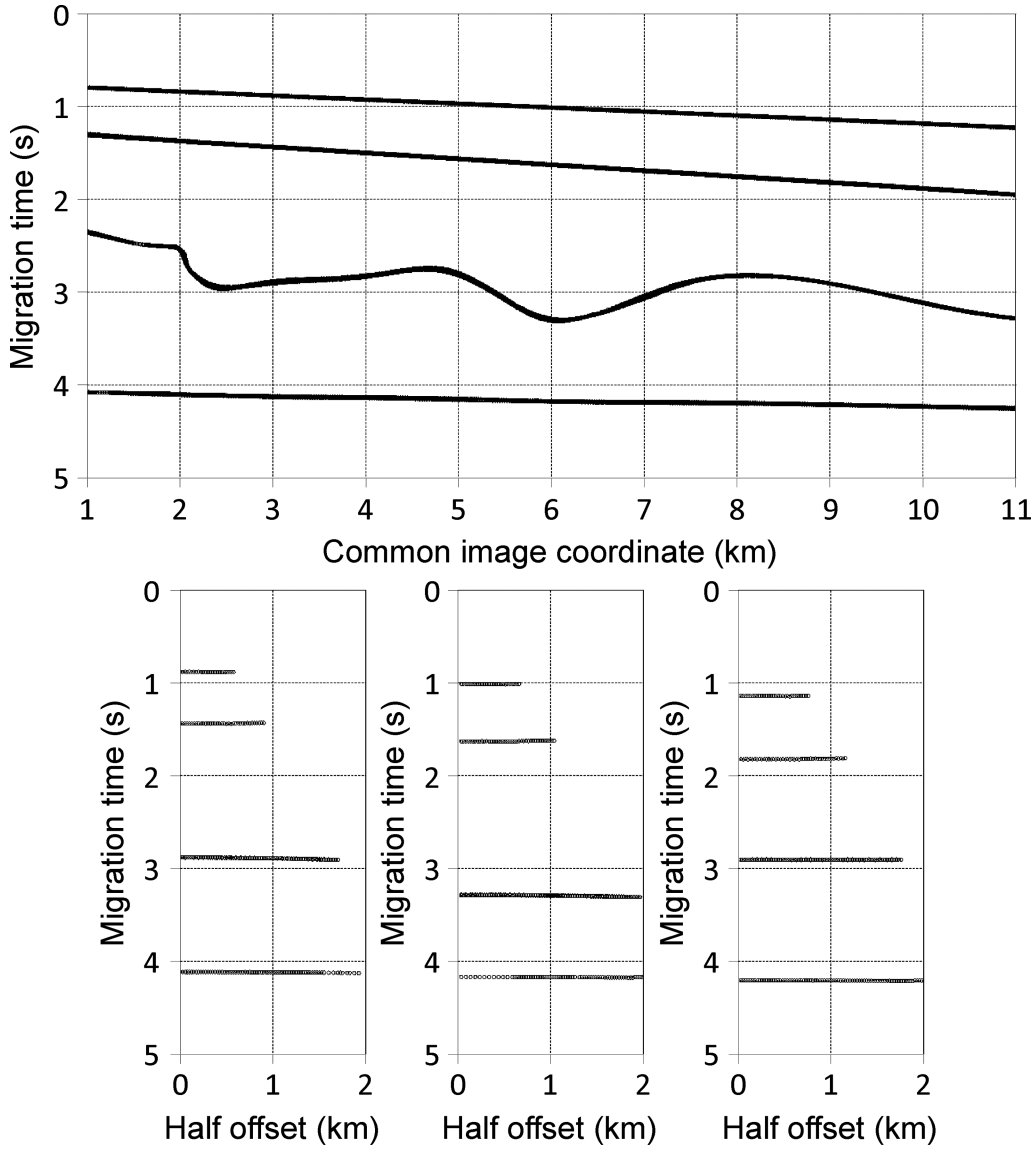

Figure 13. Example 1: reflection events after kinematic time migration as in Fig. 12, but with mute applied to the input events.

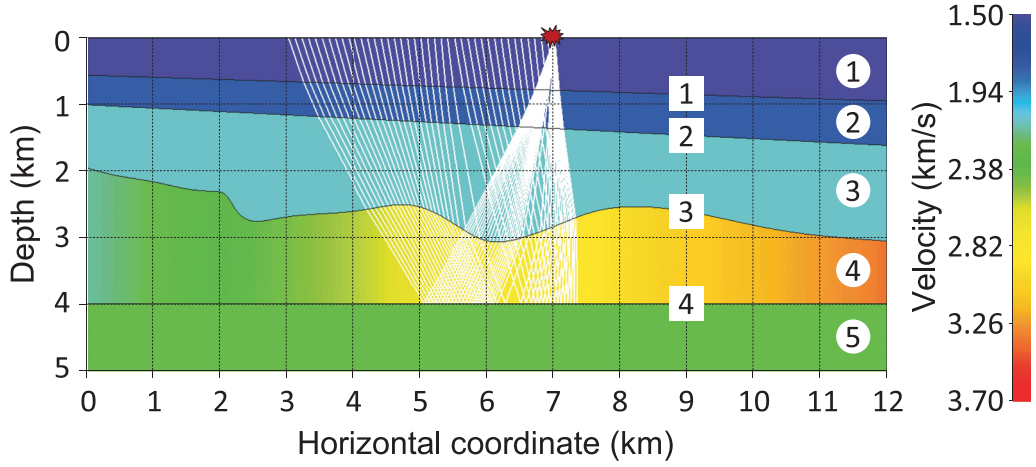

Figure 14. Example 2: modified 2-D depth model including a horizontal velocity gradient 0.1 s^{-1} in layer 4. Reflection rays for the source point at horizontal location 7.0 km and interface 4 are superimposed. For comparison with the original model, see Fig. 7. [Correction made after online publication 2012 April 26: the labelling in this figure has been corrected.]

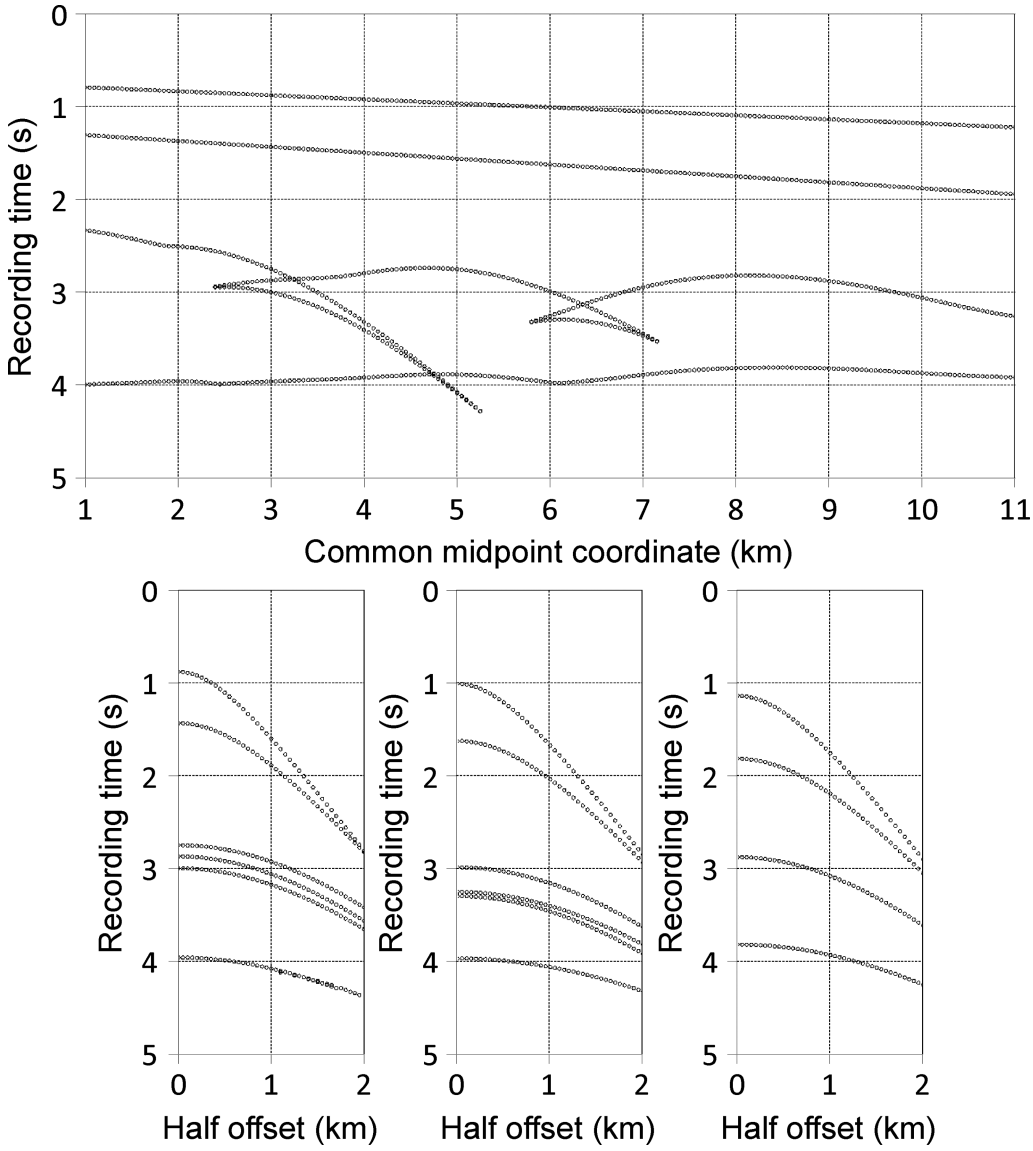

Figure 15. Example 2: reflection events simulated by ray tracing in the modified 2-D model (Fig. 14). The display is analogous to that in Fig. 8.

Furthermore, the result for interface 4 is characterized by typical pull-up and pull-down effects caused by strong lateral velocity variations in the overburden.

12 CONCLUSIONS

We present a generalization of kinematic time migration and demigration for arbitrary, constant, source–receiver offsets. The description is developed beyond mapping of reflection times and slopes, including also reflection curvatures. Local heterogeneity of the time-migration velocity model is accounted for, and the derived mapping equations do not depend specifically on the type of diffraction-time function and the parametrization of the velocity model. One fundamental requirement is that the diffraction-time field does not contain caustics. This ensures that the mapping between the time-migration domain and the depth-migration domain, which may be accomplished using image rays, is one-to-one. In this way, the results tie in with earlier work on estimating geological dips and curvatures from time-migrated zero-offset reflections.

The established mapping framework opens for interesting observations and interpretations. Mapping of reflection curvature in time-migration common-image coordinates to reflection curvature in CMP coordinates (or vice versa) represents the time-migration counterpart of the second duality theorem in Kirchhoff depth migration. We also show that the NIP-wave theorem follows naturally from the basic conditions involved in kinematic time migration and demigration. As a byproduct of the mapping operations we obtain time-migration and time-demigration spreading matrices, which have similarities with paraxial matrices known from ray theory. Regardless of the time-migration velocity model, some of the reflection-time parameters in the time-migration domain are always zero at zero offset, namely, the reflection-time slope with respect to offset and the reflection-time mixed second derivatives (with respect to offset and common-image coordinates).

We consider two specific examples of diffraction-time functions for time migration and demigration, namely, the classic single- and double-square-root functions. The single-square root function has limited applicability (offsets and apertures must be small) and is studied here because of its attention in the past and the simplicity of

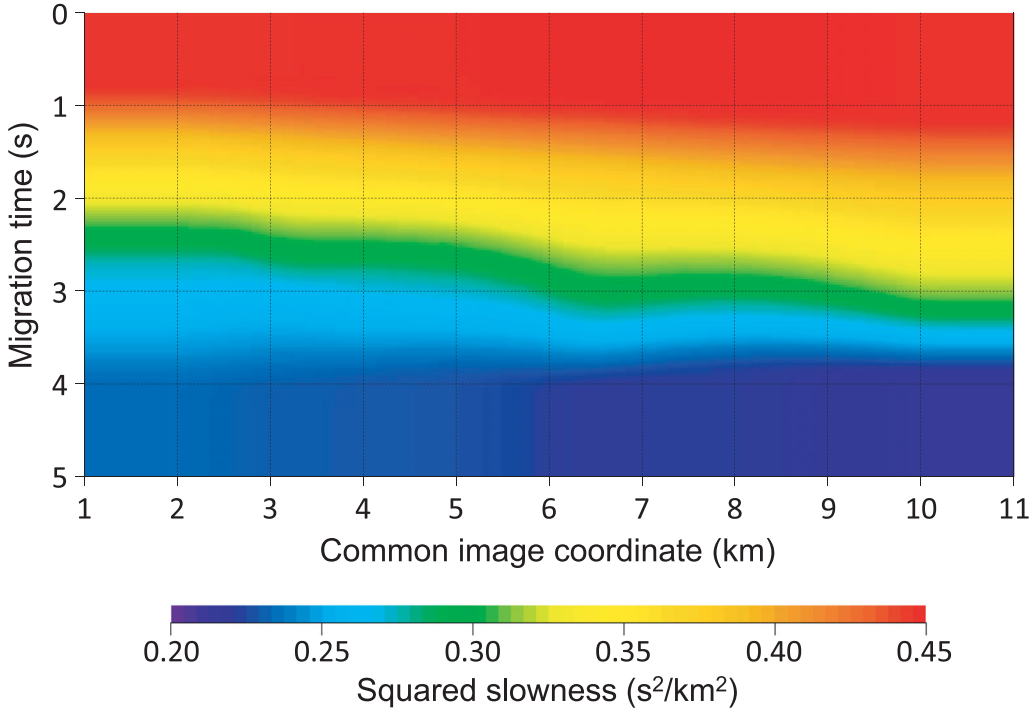

(a)

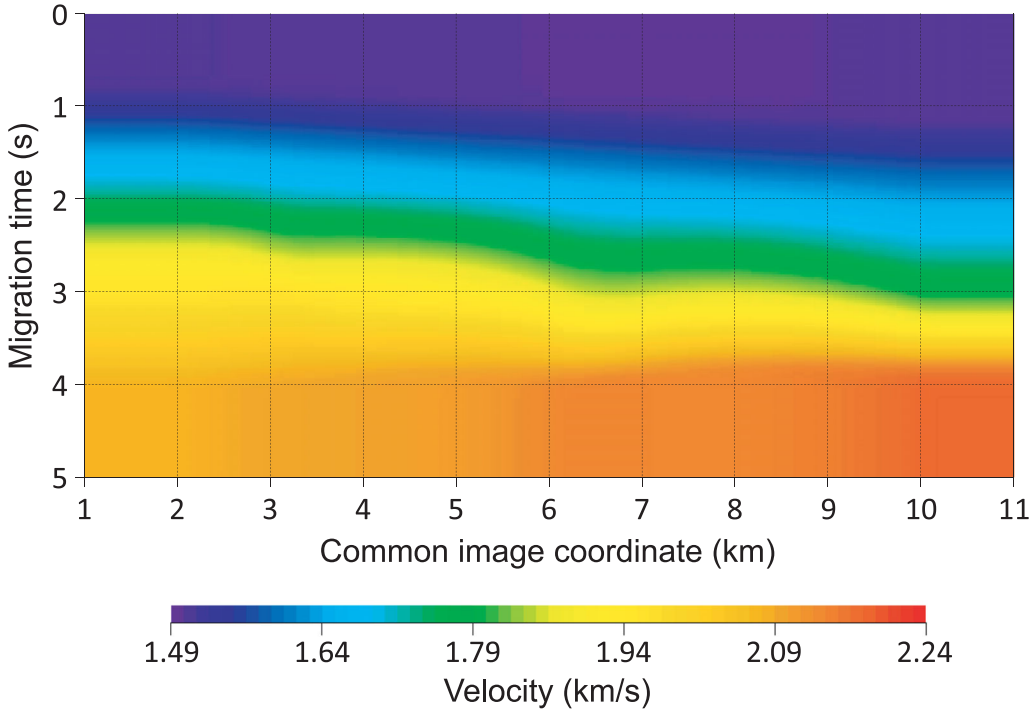

(b)

Figure 16. Example 2: (a) updated squared time-migration slowness S_{11}^{M} and (b) the corresponding time-migration velocity.

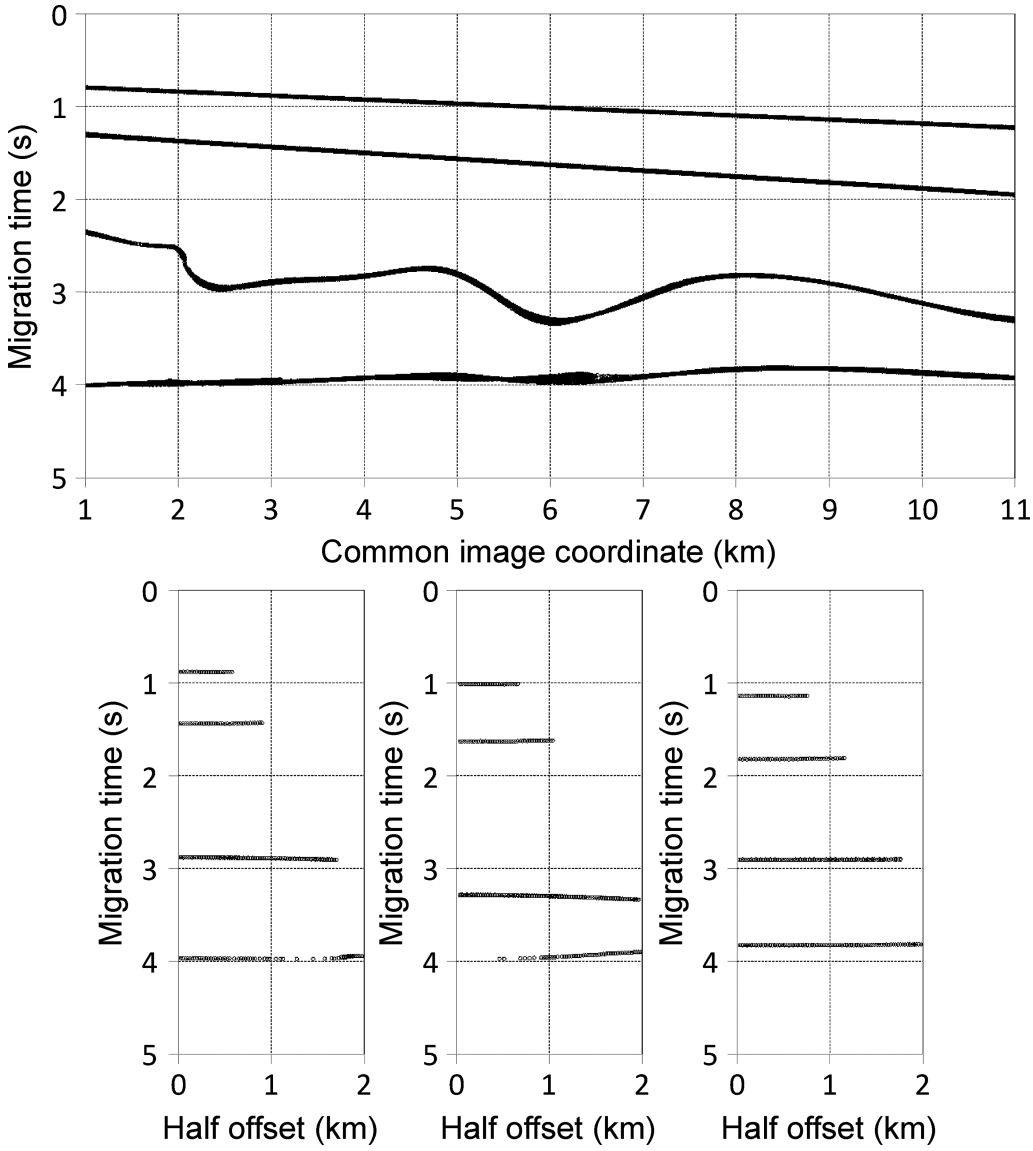

Figure 17. Example 2: reflection events after mute and kinematic time migration, as in Fig. 13.

its mapping relations. In new implementations of time migration, however, we see no reason not to describe diffraction time as an explicit sum of two one-way times.

We outline two routes to estimate the time-migration velocity model and associated time-migration velocity ellipses in a heterogeneous model setting, which signify the 'data' for non-linear velocity inversion. Applications of parameters insensitive to the time-migration velocity model include multi-midpoint stacking, kinematic depth migration, time-migration tomography, and depth-migration tomography. The developed concepts associated with time migration are foreseen to be of interest in reflection seismics as well as in global earth seismology. In two numerical examples we demonstrate the potential of kinematic time migration and demigration to become key processes in the construction of seismic time images and their associated velocity models.

13 ACKNOWLEDGMENTS

We acknowledge support by the Research Council of Norway via NORSAR's project 194064/I30 and the ROSE project, VISTA, the National Council of Scientific and Technological Development (CNPq), Brazil, the sponsors of the Wave Inversion Technology (WIT) Consortium, Germany and the members of the Geo-Mathematical Imaging Group, USA. We thank two anonymous reviewers for their constructive comments and questions, which were of great value during the revision of the paper.

REFERENCES

Alkhalifah, T., 2000. The offset-midpoint traveltime pyramid in transversely isotropic media, *Geophysics,* **65**(4), 1316–1325.

Bancroft, J.C., 2007. *A Practical Understanding of Pre- and Poststack Migrations, Volume 1 (Prestack),* SEG Course Notes Series No. 14, Society of Exploration Geophysicists, Tulsa, OK.

Bleistein, N., 1984. *Mathematical Methods for Wave Phenomena,* Academic Press, Inc, San Diego, CA.

Bleistein, N., Cohen, J.K. & Stockwell, J.W., Jr, 2001. *Mathematics of Multidimensional Seismic Imaging, Migration, and Inversion,* Springer, New York, NY.

Cameron, M.K., Fomel, S. & Sethian, J.A., 2007. Seismic velocity estimation from time migration, *Inverse Problems,* **23**(4), 1329–1369.

Chambers, K., Deuss, A. & Woodhouse, J., 2005. Reflectivity of the 410-km discontinuity from PP and SS precursors, *J. geophys. Res.,* **110**(B2), B02301.

Chernyak, V.S. & Gritsenko, S.A., 1979. Interpretation of the effective common-depth-point parameters for a three-dimensional system of homogeneous layers with curvelinear boundaries, *Soviet Geol. Geophys.,* **20,** 91–98.

Claerbout, J.F., 1985. *Imaging the Earth's Interior,* Blackwell Scientific Publications, Oxford.

Cooke, D., Bona, A. & Hansen, B., 2009. Simultaneous time imaging, velocity estimation, and multiple suppression using local event slopes, *Geophysics,* **74**(6), WCA65–WCA73.

de Hoop, M.V., Le Rousseau, J.H. & Biondi, B.L., 2003. Symplectic structure of wave-equation imaging: a path-integral approach based on the double-square-root equation, *Geophys. J. Int.,* **153**(1), 52–74.

Dell, S. & Gajewski, D., 2011. Common-reflection-surface-based workflow for diffraction imaging, *Geophysics,* **76**(5), S187–S195.

Deuss, A., Woodhouse, J.H., Paulssen, H. & Trampert, J., 2000. The observation of inner core shear waves, *Geophys. J. Int.,* **142**(1), 67–73.

Douma, H. & de Hoop, M.V., 2006. Explicit expressions for prestack map time migration in isotropic and VTI media and the applicability of map depth migration in heterogeneous anisotropic media, *Geophysics,* **71**(1), S13–S28.

Duveneck, E., 2004. 3D tomographic velocity model estimation with kinematic wavefield attributes, *Geophys. Prospect.,* **52**(6), 535–545.

Flanagan, M. & Shearer, P., 1998. Global mapping of topography on transition zone velocity discontinuities by stacking SS precursors, *J. geophys. Res.,* **103**(B2), 2673–2692.

Fomel, S., 2003. Velocity continuation and the anatomy of residual prestack time migration, *Geophysics,* **68**(5), 1650–1661.

Fomel, S., 2007. Velocity-independent time-domain seismic imaging using local event slopes, *Geophysics,* **72**(3), S139–S147.

Gjøystdal, H. & Ursin, B., 1981. Inversion of reflection times in three-dimensions, *Geophysics,* **46**(7), 972–983.

Gjøystdal, H., Reinhardsen, J.E. & Ursin, B., 1984. Traveltime and wavefront curvature calculations in three-dimensional inhomogeneous layered media with curved interfaces, *Geophysics,* **49**(9), 1466–1494.

Grechka, V. & Tsvankin, I., 2002. NMO-velocity surfaces and Dix-type formulas in anisotropic heterogeneous media, *Geophysics,* **67**(3), 939–951.

Grigis, A. & Sjöstrand, J., 1994. *Microlocal Analysis for Differential Operators. An Introduction,* Cambridge University Press, Cambridge.

Hubral, P., 1977. Time migration—some ray theoretical aspects, *Geophys. Prospect.,* **25**(4), 738–745.

Hubral, P. & Krey, T., 1980. *Interval Velocities from Seismic Reflection Time Measurements,* Society of Exploration Geophysicists, Tulsa, OK.

Hubral, P., Schleicher, J. & Tygel, M., 1996. A unified approach to 3-D seismic reflection imaging, part I: basic concepts, *Geophysics,* **61**(3), 742–758.

Iversen, E., 2004. The isochron ray in seismic modeling and imaging, *Geophysics,* **69**(4), 1053–1070.

Iversen, E., 2006. Amplitude, Fresnel zone, and NMO velocity for PP and SS normal-incidence reflections, *Geophysics,* **71**(2), W1–W14.

Iversen, E. & Gjøystdal, H., 1996. Event-oriented velocity estimation based on prestack data in time or depth domain, *Geophys. Prospect.,* **44**(4), 643–686.

Iversen, E. & Tygel, M., 2008. Image-ray tracing for joint 3D seismic velocity estimation and time-to-depth conversion, *Geophysics,* **73**(3), P99–P114.

Jäger, R., Mann, J., Höcht, G. & Hubral, P., 2001. Common-reflection-surface stack: image and attributes, *Geophysics,* **66**(1), 97–109.

Jones, I.F., 2010. *An Introduction To: Velocity Model Building,* European Association of Geoscientists and Engineers, Houten.

Kleyn, A.H., 1977. On the migration of reflection time contour maps, *Geophys. Prospect.,* **25**(1), 125–140.

Lindsey, J.P. & Hermann, A., 1970. Digital migration, *Oil Gas J.,* **38,** 112–115.

Lu, L. & Riabinkin, L.A., 1991. Fundamentals of resolving power of controlled directional reception (CDR) of seismic waves, in *Slant Stack Processing,* pp. 36–60, eds Gardner, G.H.F. & Lu, L., Society of Exploration Geophysicists, Tulsa, OK.

Mayne, W.H., 1962. Common reflection point horizontal data stacking techniques, *Geophysics,* **27**(6), 927–938.

Rieber, F., 1936. A new reflection system with controlled directional sensitivity, *Geophysics,* **1**(1), 97–106.

Robein, E., 2003. *Velocities, Time Imaging and Depth Imaging in Reflection Seismics. Principles and Methods,* European Association of Geoscientists and Engineers, Houten.

Schleicher, J., Tygel, M. & Hubral, P., 2007. *Seismic True-Amplitude Imaging,* Society of Exploration Geophysicists, Tulsa, OK.

Schleicher, J., Costa, J.C., Santos, L.T., Novais, A. & Tygel, M., 2009. On the estimation of local slopes, *Geophysics,* **74**(4), P25–P33.

Shah, P.M., 1973. Use of wavefront curvature to relate seismic data with subsurface parameters, *Geophysics,* **38**(5), 812–825.

Shearer, P., 1991. Imaging global body wave phases by stacking long-period seismograms, *J. geophys. Res.,* **96**(B12), 20 353–20 364.

Söllner, W. & Andersen, E., 2005. Kinematic time migration and demigration in a 3D visualization system, *J. Seism. Explor.,* **14**(2–3), 255–270.

Stamnes, J.J., 1986. *Waves in Focal Regions,* Adam Hilger, Bristol.

Stolk, C.C., de Hoop, M.V. & Symes, W.W., 2009. Kinematics of shot-geophone migration, *Geophysics,* **74**(6), WCA19–WCA34.

Taner, M.T. & Koehler, F., 1969. Velocity spectra—digital computer derivation applications of velocity functions, *Geophysics,* **34**(6), 859–881.

Treves, F., 1980. *Introduction to Pseudodifferential and Fourier Integral Operators,* Vol. 2, Plenum Press, New York, NY.

Tsvankin, I., 2005. *Seismic Signatures and Analysis of Reflection Data in Anisotropic Media,* Elsevier, Oxford.

Tygel, M., Schleicher, J. & Hubral, P., 1994. Pulse distortion in depth migration, *Geophysics,* **59**(10), 1561–1569.

Tygel, M., Schleicher, J. & Hubral, P., 1996. A unified approach to 3-D seismic reflection imaging, part II: theory, *Geophysics,* **61**(3), 759–775.

Tygel, M., Ursin, B., Iversen, E. & de Hoop, M.V., 2012. Estimation of geological dip and curvature from time-migrated zero-offset reflections in heterogeneous anisotropic media, *Geophys. Prospect.,* **60**(2), 201–216.

Ursin, B., 1982a. Quadratic wavefront and travel time approximations in inhomogeneous layered media with curved interfaces, *Geophysics,* **47**(3), 1012–1021.

Ursin, B., 1982b. Time-to-depth migration using wavefront curvature, *Geophys. Prospect.,* **30**(3), 261–280.

Ursin, B. & Stovas, A., 2006. Traveltime approximations for a layered transversely isotropic medium, *Geophysics,* **71**(2), D23–D33.

Whitcombe, D.N., 1994. Fast model building using demigration and single-step ray migration, *Geophysics,* **59**(3), 439–449.

Yilmaz, O., 2000. *Seismic Data Analysis Vol. 1,* Society of Exploration Geophysicists, Tulsa, OK.

Yilmaz, O., 2001. *Seismic Data Analysis Vol. 2,* Society of Exploration Geophysicists, Tulsa, OK.

Zhang, Y., Bergler, S. & Hubral, P., 2001. Common-reflection-surface (CRS) stack for common offset, *Geophys. Prospect.,* **49**(6), 709–718.

APPENDIX A: MICROLOCAL ANALYSIS OF TIME MIGRATION AND DEMIGRATION

This appendix elaborates on the dynamic aspects of time migration and demigration, using concepts and notation from microlocal analysis (e.g. Grigis & Sjöstrand 1994; de Hoop *et al.* 2003). Such concepts started developing as part of the study of linear partial differential equations.

The notion of a wavefront set appeared in reflection seismology as early as in the work of Rieber (1936); see also the reprinted article Lu & Riabinkin (1991). The wavefront set of a distribution detects orientation as well as position of singularities. An element in the wavefront set of reflection data can thus be identified, locally, as an event with its slope.

In the context of single-scattering based seismic imaging, the notion of *propagation of singularities* coincides essentially with map migration and demigration using, respectively, the slopes in the data and the dips in the reflectivity or image. For a historical overview, see the introduction of Douma & de Hoop (2006). In the following, propagation of singularities is utilized in the context of time migration and demigration: in time migration one generates time-migrated data $d^M(\mathbf{h}, \mathbf{m}, \tau)$ from recorded data $d(\mathbf{h}, \mathbf{x}, t)$; in time demigration one transforms $d^M(\mathbf{h}, \mathbf{m}, \tau)$ back to the recording domain, resulting in the time-demigrated data $\tilde{d}(\mathbf{h}, \mathbf{x}, t)$.

The extended time-demigration operator, F, associated with eq. (7) can be written in the form $\tilde{d}(\mathbf{h}, \mathbf{x}, t) = (Fd^M)(\mathbf{h}, \mathbf{x}, t)$, where

$$\tilde{d}(\mathbf{h}, \mathbf{x}, t) = \iiint W(\mathbf{h}, \mathbf{x}, \mathbf{m}, \tau, \omega) \exp[\imath\phi(\mathbf{h}, \mathbf{x}, t, \mathbf{m}, \tau, \omega)] \times d^M(\mathbf{h}, \mathbf{m}, \tau)\, \mathrm{d}\mathbf{m}\, \mathrm{d}\tau\, \mathrm{d}\omega, \tag{A1}$$

with phase function

$$\phi(\mathbf{h}, \mathbf{x}, t, \mathbf{m}, \tau, \omega) = \omega\,[T^D(\mathbf{h}, \mathbf{x} - \mathbf{m}, \mathbf{m}, \tau) - t] \tag{A2}$$

and frequency-dependent weight function $W(\mathbf{h}, \mathbf{x}, \mathbf{m}, \tau, \omega)$. In principle, W can be derived from the Born approximation and asymptotic ray theory, while d^M can be related to reflectivity using image-ray coordinates. Details concerning how W can be estimated are, however, outside the scope of this paper. Eq. (8) outlines that W can be connected with a frequency-independent weight function similar to the one used by Schleicher *et al.* (2007, p. 195, eq. 5).

The extended time-migration operator, F^*, is obtained by taking the adjoint of F. The time-migrated data can then be expressed as

$$\begin{aligned} d^M(\mathbf{h}, \mathbf{m}, \tau) &= \iiint W^*(\mathbf{h}, \mathbf{x}, \mathbf{m}, \tau, \omega) \\ &\quad \times \exp[-\imath\phi(\mathbf{h}, \mathbf{x}, t, \mathbf{m}, \tau, \omega)]\, d(\mathbf{h}, \mathbf{x}, t)\, \mathrm{d}\mathbf{x}\, \mathrm{d}t\, \mathrm{d}\omega \\ &= \iiint W^*(\mathbf{h}, \mathbf{m} + \mathbf{a}, \mathbf{m}, \tau, \omega) \\ &\quad \times \exp[-\imath\phi(\mathbf{h}, \mathbf{m} + \mathbf{a}, t, \mathbf{m}, \tau, \omega)] \\ &\quad \times d(\mathbf{h}, \mathbf{m} + \mathbf{a}, t)\, \mathrm{d}\mathbf{a}\, \mathrm{d}t\, \mathrm{d}\omega, \end{aligned} \tag{A3}$$

introducing (relative) aperture coordinates, $\mathbf{a} = \mathbf{x} - \mathbf{m}$. Corrections to the amplitude of F^* are obtained upon considering the composition F^*F and constructing its asymptotic inverse. The operator F is the time demigration analogue of the surface-offset extension of the single scattering operator considered by Stolk *et al.* (2009). In the absence of caustics, operator F is asymptotically invertible.

The propagation of singularities by the operator F follows from evaluating the set of points,

$$\left(\mathbf{h}, \mathbf{x}, t, \frac{\partial\phi}{\partial\mathbf{h}}, \frac{\partial\phi}{\partial\mathbf{x}}, \frac{\partial\phi}{\partial t}; \mathbf{h}, \mathbf{m}, \tau, -\frac{\partial\phi}{\partial\mathbf{h}}, -\frac{\partial\phi}{\partial\mathbf{m}}, -\frac{\partial\phi}{\partial\tau}\right) \text{ at } \frac{\partial\phi}{\partial\omega} = 0, \tag{A4}$$

signifying the *stationary point set*, and is described by the so-called *canonical relation* (Grigis & Sjöstrand 1994)

$$\begin{aligned} \Lambda_\phi = \Bigg\{\Bigg[&\mathbf{h}, \mathbf{x}, T^D(\mathbf{h}, \mathbf{x} - \mathbf{m}, \mathbf{m}, \tau), \omega\frac{\partial T^D}{\partial\mathbf{h}}(\mathbf{h}, \mathbf{x} - \mathbf{m}, \mathbf{m}, \tau), \\ &\omega\frac{\partial T^D}{\partial\mathbf{a}}(\mathbf{h}, \mathbf{x} - \mathbf{m}, \mathbf{m}, \tau), -\omega; \\ &\mathbf{h}, \mathbf{m}, \tau, -\omega\frac{\partial T^D}{\partial\mathbf{h}}(\mathbf{h}, \mathbf{x} - \mathbf{m}, \mathbf{m}, \tau), \\ &-\omega\frac{\partial T^D}{\partial\mathbf{m}}(\mathbf{h}, \mathbf{x} - \mathbf{m}, \mathbf{m}, \tau), -\omega\frac{\partial T^D}{\partial\tau}(\mathbf{h}, \mathbf{x} - \mathbf{m}, \mathbf{m}, \tau)\Bigg]\Bigg\}. \end{aligned} \tag{A5}$$

The propagation of singularities reads that $(\mathbf{h}, \mathbf{x}, t, \mathbf{p}^h, \mathbf{p}^x, \omega)$ belongs to the wavefront set of the recorded or time-demigrated seismic data (i.e. corresponds with an event) if there exists a $(\mathbf{h}, \mathbf{m}, \tau, \boldsymbol{\psi}^h, \boldsymbol{\psi}^m, \upsilon)$ such that $(\mathbf{h}, \mathbf{x}, t, \mathbf{p}^h, \mathbf{p}^x, \omega; \mathbf{h}, \mathbf{m}, \tau, \boldsymbol{\psi}^h, \boldsymbol{\psi}^m, \upsilon)$ belongs to Λ_ϕ and $(\mathbf{h}, \mathbf{m}, \tau, \boldsymbol{\psi}^h, \boldsymbol{\psi}^m, \upsilon)$ is contained in the wavefront of the extended time-migrated image. The scalar υ can be interpreted as a frequency variable associated with the time-migration domain. In fact, Λ_ϕ is the graph of an invertible transformation, Θ, which prescribes the propagation of singularities. We note that $\mathbf{h}$ plays the role of a *parameter*; it is constant under the application of the transformation Θ. In eq. (A5), $\partial T^D/\partial\tau$ signifies the 'coordinate stretch' between migration time and recording time; it is the quantity u defined in eq. (10). For the corresponding coordinate stretch between migration depth and recording time, see, for example, Tygel *et al.* (1994).

If the singular support of the extended time-migrated image can be described (locally) by a level set function $\mathcal{T}$, that is, $\tau = \mathcal{T}(\mathbf{h}, \mathbf{m})$, one can define a time-demigration map from $(\mathbf{h}, \mathbf{m})$ to $\mathbf{x}$, through a projection of the elements of the wavefront set obtained from $[\mathbf{h}, \mathbf{m}, \mathcal{T}(\mathbf{h}, \mathbf{m}), -\partial\mathcal{T}(\mathbf{h}, \mathbf{m})/\partial\mathbf{h}, -\partial\mathcal{T}(\mathbf{h}, \mathbf{m})/\partial\mathbf{m}, 1]$ using the canonical relation; in the main text this map is denoted by $\hat{\mathbf{x}}$. The singular support of the time-demigrated data can be correspondingly described (locally) by a level set function T, that is, $t = T(\mathbf{h}, \mathbf{x})$, so that

$$T\,[\mathbf{h}, \hat{\mathbf{x}}(\mathbf{h}, \mathbf{m})] = T^D\,[\mathbf{h}, \hat{\mathbf{x}}(\mathbf{h}, \mathbf{m}) - \mathbf{m}, \mathbf{m}, \mathcal{T}(\mathbf{h}, \mathbf{m})]\,; \tag{A6}$$

moreover, the dual to $\mathbf{x}$ in the canonical relation gives the correspondence

$$\frac{\partial T}{\partial\mathbf{x}}\,[\mathbf{h}, \hat{\mathbf{x}}(\mathbf{h}, \mathbf{m})] = \frac{\partial T^D}{\partial\mathbf{a}}\,[\mathbf{h}, \hat{\mathbf{x}}(\mathbf{h}, \mathbf{m}) - \mathbf{m}, \mathbf{m}, \mathcal{T}(\mathbf{h}, \mathbf{m})]\,. \tag{A7}$$

Eqs (A6)–(A7) coincide with eqs (41)–(42).

The propagation of singularities by time migration is straightforwardly described by $\Lambda_\phi{}^*$. The singular support of the recorded data and the extended time-migrated image then correspond, respectively, to the level set functions $t = T(\mathbf{h}, \mathbf{x})$ and $\tau = \mathcal{T}(\mathbf{h}, \mathbf{m})$. One defines a time-migration map from $(\mathbf{h}, \mathbf{x})$ to $\mathbf{m}$ through a projection of the elements of the wavefront set of the extended image obtained from $[\mathbf{h}, \mathbf{x}, T(\mathbf{h}, \mathbf{x}), \partial T(\mathbf{h}, \mathbf{x})/\partial\mathbf{h}, \partial T(\mathbf{h}, \mathbf{x})/\partial\mathbf{x}, -1]$; in the main text this map is denoted by $\hat{\mathbf{m}}$. This yields

$$T(\mathbf{h}, \mathbf{x}) = T^D\left\{\mathbf{h}, \mathbf{x} - \hat{\mathbf{m}}(\mathbf{h}, \mathbf{x}), \hat{\mathbf{m}}(\mathbf{h}, \mathbf{x}), \mathcal{T}[\mathbf{h}, \hat{\mathbf{m}}(\mathbf{h}, \mathbf{x})]\right\} \tag{A8}$$

according to the canonical relation (A5).

APPENDIX B: TRANSFORMATIONS BETWEEN DERIVATIVES OF REFLECTION TIME IN THE MIGRATION AND RECORDING DOMAINS

The topic of this appendix is derivation of transformations between derivatives of reflection time in the migration and recording domains, both being considered in their common-offset representations.

B1 First-order partial derivatives

Consider first eq. (38). Differentiation with respect to half-offset coordinates h_k and position components m_k in the time-migration domain yields

$$\frac{\partial\hat{a}_i}{\partial h_k} = \frac{\partial\hat{x}_i}{\partial h_k}, \tag{B1}$$

$$\frac{\partial \hat{a}_i}{\partial m_k} = \frac{\partial \hat{x}_i}{\partial m_k} - \delta_{ik}. \tag{B2}$$

Now we take derivatives of the basic condition in eq. (41) with respect to position components m_k. The result is

$$\frac{\partial \hat{x}_i}{\partial m_k}\frac{\partial T}{\partial x_i} = \frac{\partial T^D}{\partial m_k} + \frac{\partial \mathcal{T}}{\partial m_k}\frac{\partial T^D}{\partial \tau} + \frac{\partial \hat{a}_i}{\partial m_k}\frac{\partial T^D}{\partial a_i}. \tag{B3}$$

In the last equation we recognize the components, $\partial \hat{x}_i/\partial m_k$, of the time-demigration spreading matrix $\mathbf{X}^m$ (eq. 52). Using eqs (42) and (B2) in eq. (B3) yields

$$\frac{\partial T}{\partial x_i} = \frac{\partial T^D}{\partial m_i} + \frac{\partial \mathcal{T}}{\partial m_i}\frac{\partial T^D}{\partial \tau}. \tag{B4}$$

This equation relates the first derivatives of reflection time $\partial \mathcal{T}/\partial m_i$ and $\partial T/\partial x_i$. Using eq. (42) in eq. (B4) results in the so-called consistency equation,

$$\frac{\partial T^D}{\partial a_i} - \frac{\partial T^D}{\partial m_i} = \frac{\partial \mathcal{T}}{\partial m_i}\frac{\partial T^D}{\partial \tau}. \tag{B5}$$

It is given as eq. (43) in the main text.

Differentiation of eq. (41) with respect to half-offset components h_k yields

$$\frac{\partial \hat{x}_i}{\partial h_k}\frac{\partial T}{\partial x_i} + \frac{\partial T}{\partial h_k} = \frac{\partial T^D}{\partial h_k} + \frac{\partial \mathcal{T}}{\partial h_k}\frac{\partial T^D}{\partial \tau} + \frac{\partial \hat{a}_i}{\partial h_k}\frac{\partial T^D}{\partial a_i}. \tag{B6}$$

Applying eq. (B1) and the basic condition (42), we find that the derivatives $\partial \mathcal{T}/\partial h_i$ and $\partial T/\partial h_i$ are related by the equation

$$\frac{\partial T}{\partial h_i} = \frac{\partial T^D}{\partial h_i} + \frac{\partial \mathcal{T}}{\partial h_i}\frac{\partial T^D}{\partial \tau}. \tag{B7}$$

B2 Second-order partial derivatives

The basic condition in eq. (42) is differentiated with respect to coordinates m_k to yield

$$\frac{\partial \hat{x}_j}{\partial m_k}\frac{\partial^2 T}{\partial x_j \partial x_i} = \frac{\partial^2 T^D}{\partial m_k \partial a_i} + \frac{\partial \mathcal{T}}{\partial m_k}\frac{\partial^2 T^D}{\partial \tau \partial a_i} + \frac{\partial \hat{a}_j}{\partial m_k}\frac{\partial^2 T^D}{\partial a_j \partial a_i}. \tag{B8}$$

We also differentiate eq. (B4) with respect to m_k, which gives

$$\begin{aligned}\frac{\partial \hat{x}_j}{\partial m_k}\frac{\partial^2 T}{\partial x_j \partial x_i} = {} & \frac{\partial^2 T^D}{\partial m_k \partial m_i} + \frac{\partial^2 \mathcal{T}}{\partial m_k \partial m_i}\frac{\partial T^D}{\partial \tau} + \frac{\partial \mathcal{T}}{\partial m_k}\frac{\partial^2 T^D}{\partial \tau \partial m_i} \\ & + \frac{\partial \mathcal{T}}{\partial m_i}\frac{\partial^2 T^D}{\partial \tau \partial m_k} + \frac{\partial \mathcal{T}}{\partial m_i}\frac{\partial \mathcal{T}}{\partial m_k}\frac{\partial^2 T^D}{\partial \tau^2} + \frac{\partial \hat{a}_j}{\partial m_k} \\ & \times \left(\frac{\partial^2 T^D}{\partial a_j \partial m_i} + \frac{\partial \mathcal{T}}{\partial m_i}\frac{\partial^2 T^D}{\partial a_j \partial \tau}\right).\end{aligned} \tag{B9}$$

Using that the right-hand sides of eqs (B8) and (B9) have to be equal, and also taking into account eq. (B2), we obtain

$$\begin{aligned}\left(\frac{\partial^2 T^D}{\partial a_i \partial a_j} - \frac{\partial^2 T^D}{\partial m_i \partial a_j} - \frac{\partial \mathcal{T}}{\partial m_i}\frac{\partial^2 T^D}{\partial a_j \partial \tau}\right)\frac{\partial \hat{x}_j}{\partial m_k} = {} & \frac{\partial^2 \mathcal{T}}{\partial m_i \partial m_k}\frac{\partial T^D}{\partial \tau} \\ & + \frac{\partial^2 T^D}{\partial a_i \partial a_k} + \frac{\partial^2 T^D}{\partial m_i \partial m_k} + \frac{\partial^2 T^D}{\partial \tau \partial m_i}\frac{\partial \mathcal{T}}{\partial m_k} + \frac{\partial^2 T^D}{\partial \tau \partial m_k}\frac{\partial \mathcal{T}}{\partial m_i} \\ & + \frac{\partial \mathcal{T}}{\partial m_i}\frac{\partial \mathcal{T}}{\partial m_k}\frac{\partial^2 T^D}{\partial \tau^2} - \left(\frac{\partial^2 T^D}{\partial a_i \partial m_k} + \frac{\partial^2 T^D}{\partial \tau \partial a_i}\frac{\partial \mathcal{T}}{\partial m_k}\right) \\ & - \left(\frac{\partial^2 T^D}{\partial a_k \partial m_i} + \frac{\partial^2 T^D}{\partial \tau \partial a_k}\frac{\partial \mathcal{T}}{\partial m_i}\right).\end{aligned} \tag{B10}$$

Using the definitions in eq. (11) and (49), the equivalent matrix form of eq. (B10) is

$$-\left(\mathbf{K}^{am} - \mathbf{U}^{aa}\right)^T \mathbf{X}^m = u\,\boldsymbol{\mathcal{M}}^{mm} - \mathbf{Y}. \tag{B11}$$

Eq. (B11) can be used for computation of the time-demigration spreading matrix $\mathbf{X}^m$; the final expression for it is given in eq. (55).

A minor rearrangement of terms in eq. (B8) yields

$$\left(\frac{\partial^2 T}{\partial x_i \partial x_j} - \frac{\partial^2 T^D}{\partial a_i \partial a_j}\right)\frac{\partial \hat{x}_j}{\partial m_k} = \frac{\partial^2 T^D}{\partial a_i \partial m_k} + \frac{\partial^2 T^D}{\partial \tau \partial a_i}\frac{\partial \mathcal{T}}{\partial m_k} - \frac{\partial^2 T^D}{\partial a_i \partial a_k}, \tag{B12}$$

or in matrix form,

$$\left(\mathbf{M}^{xx} - \mathbf{U}^{aa}\right)\mathbf{X}^m = \mathbf{K}^{am} - \mathbf{U}^{aa}. \tag{B13}$$

By combining eqs (B11) and (B13) matrix $\mathbf{X}^m$ is eliminated, and we obtain the explicit formula for matrix $\mathbf{M}^{xx}$ in eq. (48).

Our next task is to find an expression for the mixed-term second-derivative matrix belonging to the recording domain, $\mathbf{M}^{hx} = (\partial^2 T/\partial h_i \partial x_j)$. We proceed by differentiating eq. (B7) with respect to m_k,

$$\begin{aligned}\frac{\partial \hat{x}_j}{\partial m_k}\frac{\partial^2 T}{\partial x_j \partial h_i} = {} & \frac{\partial^2 T^D}{\partial m_k \partial h_i} + \frac{\partial \mathcal{T}}{\partial m_k}\frac{\partial^2 T^D}{\partial \tau \partial h_i} + \frac{\partial \hat{a}_j}{\partial m_k}\frac{\partial^2 T^D}{\partial a_j \partial h_i} \\ & + \frac{\partial^2 \mathcal{T}}{\partial m_k \partial h_i}\frac{\partial T^D}{\partial \tau} + \frac{\partial \mathcal{T}}{\partial h_i} \\ & \times \left(\frac{\partial^2 T^D}{\partial \tau \partial m_k} + \frac{\partial \mathcal{T}}{\partial m_k}\frac{\partial^2 T^D}{\partial \tau^2} + \frac{\partial \hat{a}_j}{\partial m_k}\frac{\partial^2 T^D}{\partial a_j \partial \tau}\right),\end{aligned} \tag{B14}$$

which can be restated as

$$\begin{aligned}\left(\frac{\partial^2 T}{\partial h_i \partial x_j} - \frac{\partial^2 T^D}{\partial h_i \partial a_j} - \frac{\partial \mathcal{T}}{\partial h_i}\frac{\partial^2 T^D}{\partial a_j \partial \tau}\right)\frac{\partial \hat{x}_j}{\partial m_k} = {} & \frac{\partial^2 \mathcal{T}}{\partial h_i \partial m_k}\frac{\partial T^D}{\partial \tau} \\ & + \frac{\partial^2 T^D}{\partial h_i \partial m_k} + \frac{\partial^2 T^D}{\partial \tau \partial h_i}\frac{\partial \mathcal{T}}{\partial m_k} + \frac{\partial \mathcal{T}}{\partial h_i}\frac{\partial^2 T^D}{\partial \tau \partial m_k} + \frac{\partial \mathcal{T}}{\partial h_i}\frac{\partial \mathcal{T}}{\partial m_k}\frac{\partial^2 T^D}{\partial \tau^2} \\ & - \frac{\partial^2 T^D}{\partial h_i \partial a_k} - \frac{\partial \mathcal{T}}{\partial h_i}\frac{\partial^2 T^D}{\partial a_k \partial \tau}.\end{aligned} \tag{B15}$$

Applying the definitions in eq. (11) and (49), we rewrite eq. (B15) in matrix form as follows,

$$\left(\mathbf{M}^{hx} - \mathbf{K}^{ha}\right)\mathbf{X}^m = u\,\boldsymbol{\mathcal{M}}^{hm} + \mathbf{L}^{hm} - \mathbf{K}^{ha}. \tag{B16}$$

Combination of the last result with eq. (B11) eliminates matrix $\mathbf{X}^m$ and yields eq. (47) for matrix $\mathbf{M}^{hx}$.

Differentiation of eq. (42) with respect to half-offset component h_k gives

$$\frac{\partial \hat{x}_j}{\partial h_k}\frac{\partial^2 T}{\partial x_j \partial x_i} + \frac{\partial^2 T}{\partial h_k \partial x_i} = \frac{\partial^2 T^D}{\partial h_k \partial a_i} + \frac{\partial \mathcal{T}}{\partial h_k}\frac{\partial^2 T^D}{\partial \tau \partial a_i} + \frac{\partial \hat{a}_j}{\partial h_k}\frac{\partial^2 T^D}{\partial a_j \partial a_i}, \tag{B17}$$

which can be rewritten as

$$\left(\frac{\partial^2 T}{\partial x_i \partial x_j} - \frac{\partial^2 T^D}{\partial a_i \partial a_j}\right)\frac{\partial \hat{x}_j}{\partial h_k} = -\frac{\partial^2 T}{\partial x_i \partial h_k} + \frac{\partial^2 T^D}{\partial a_i \partial h_k} + \frac{\partial^2 T^D}{\partial \tau \partial a_i}\frac{\partial \mathcal{T}}{\partial h_k} \tag{B18}$$

with the corresponding matrix form

$$\left(\mathbf{M}^{xx} - \mathbf{U}^{aa}\right)\mathbf{X}^h = -\left(\mathbf{M}^{hx} - \mathbf{K}^{ha}\right)^T. \tag{B19}$$

We observe that the time-demigration spreading matrix $\mathbf{X}^h$ (see eq. 52) can be determined from eq. (B19). Utilizing also the relations (47)–(48) leads to eq. (54), which relates matrix $\mathbf{X}^h$ solely to

diffraction-time partial derivatives and reflection-time parameters belonging to the time-migration domain.

To obtain the second-derivative matrix $\mathbf{M}^{hh} = (\partial^2 T/\partial h_i \partial h_j)$, we differentiate eq. (B7) with respect to h_k,

$$\begin{aligned}\frac{\partial \hat{x}_j}{\partial h_k}\frac{\partial^2 T}{\partial x_j \partial h_i} + \frac{\partial^2 T}{\partial h_k \partial h_i} &= \frac{\partial^2 T^D}{\partial h_i \partial h_k} + \frac{\partial \mathcal{T}}{\partial h_k}\frac{\partial^2 T^D}{\partial \tau \partial h_i} \\ &+ \frac{\partial \hat{a}_j}{\partial h_k}\frac{\partial^2 T^D}{\partial a_j \partial h_i} + \frac{\partial^2 \mathcal{T}}{\partial h_k \partial h_i}\frac{\partial T^D}{\partial \tau} \\ &+ \frac{\partial \mathcal{T}}{\partial h_i}\left(\frac{\partial^2 T^D}{\partial \tau \partial h_k} + \frac{\partial \mathcal{T}}{\partial h_k}\frac{\partial^2 T^D}{\partial \tau^2} + \frac{\partial \hat{a}_j}{\partial h_k}\frac{\partial^2 T^D}{\partial a_j \partial \tau}\right), \end{aligned} \tag{B20}$$

which can be restated as

$$\begin{aligned}\frac{\partial^2 T}{\partial h_i \partial h_k} &= \frac{\partial^2 \mathcal{T}}{\partial h_i \partial h_k}\frac{\partial T^D}{\partial \tau} + \frac{\partial^2 T^D}{\partial h_i \partial h_k} + \frac{\partial^2 T^D}{\partial \tau \partial h_i}\frac{\partial \mathcal{T}}{\partial h_k} \\ &+ \frac{\partial \mathcal{T}}{\partial h_i}\frac{\partial^2 T^D}{\partial \tau \partial h_k} + \frac{\partial \mathcal{T}}{\partial h_i}\frac{\partial \mathcal{T}}{\partial h_k}\frac{\partial^2 T^D}{\partial \tau^2} \\ &- \left(\frac{\partial^2 T}{\partial h_i \partial x_j} - \frac{\partial^2 T^D}{\partial h_i \partial a_j} - \frac{\partial \mathcal{T}}{\partial h_i}\frac{\partial^2 T^D}{\partial a_j \partial \tau}\right)\frac{\partial \hat{x}_j}{\partial h_k}, \end{aligned} \tag{B21}$$

or equivalently,

$$\mathbf{M}^{hh} = u\,\boldsymbol{\mathcal{M}}^{hh} + \mathbf{L}^{hh} - \left(\mathbf{M}^{hx} - \mathbf{K}^{ha}\right)\mathbf{X}^h. \tag{B22}$$

Taking into account eq. (B16) and already derived time-demigration spreading matrices in eqs (54)–(55), we obtain the formula for matrix $\mathbf{M}^{hh}$ in eq. (46).

APPENDIX C: PARTIAL DERIVATIVES OF THE DOUBLE-SQUARE-ROOT FUNCTION

The double-square-root function is given by the combination of eq. (5) with eq. (21). In this appendix we specify all its partial derivatives up to second order.

C1 First-order partial derivatives

$$\begin{aligned}\frac{\partial T^S}{\partial h_k} &= -\frac{1}{T^S}S^M_{kj}(a_j - h_j), \\ \frac{\partial T^R}{\partial h_k} &= \frac{1}{T^R}S^M_{kj}(a_j + h_j), \end{aligned} \tag{C1}$$

$$\begin{aligned}\frac{\partial T^S}{\partial a_k} &= \frac{1}{T^S}S^M_{kj}(a_j - h_j), \\ \frac{\partial T^R}{\partial a_k} &= \frac{1}{T^R}S^M_{kj}(a_j + h_j), \end{aligned} \tag{C2}$$

$$\begin{aligned}\frac{\partial T^S}{\partial m_k} &= \frac{1}{2T^S}\frac{\partial S^M_{ij}}{\partial m_k}(a_i - h_i)(a_j - h_j), \\ \frac{\partial T^R}{\partial m_k} &= \frac{1}{2T^R}\frac{\partial S^M_{ij}}{\partial m_k}(a_i + h_i)(a_j + h_j), \end{aligned} \tag{C3}$$

$$\begin{aligned}\frac{\partial T^S}{\partial \tau} &= \frac{1}{T^S}\left[\frac{\tau}{4} + \frac{1}{2}\frac{\partial S^M_{ij}}{\partial \tau}(a_i - h_i)(a_j - h_j)\right], \\ \frac{\partial T^R}{\partial \tau} &= \frac{1}{T^R}\left[\frac{\tau}{4} + \frac{1}{2}\frac{\partial S^M_{ij}}{\partial \tau}(a_i + h_i)(a_j + h_j)\right]. \end{aligned} \tag{C4}$$

C2 Second-order partial derivatives

$$\begin{aligned}\frac{\partial^2 T^S}{\partial h_k \partial h_l} &= \frac{1}{T^S}\left(S^M_{kl} - \frac{\partial T^S}{\partial h_k}\frac{\partial T^S}{\partial h_l}\right), \\ \frac{\partial^2 T^R}{\partial h_k \partial h_l} &= \frac{1}{T^R}\left(S^M_{kl} - \frac{\partial T^R}{\partial h_k}\frac{\partial T^R}{\partial h_l}\right), \end{aligned} \tag{C5}$$

$$\begin{aligned}\frac{\partial^2 T^S}{\partial a_k \partial a_l} &= \frac{1}{T^S}\left(S^M_{kl} - \frac{\partial T^S}{\partial a_k}\frac{\partial T^S}{\partial a_l}\right), \\ \frac{\partial^2 T^R}{\partial a_k \partial a_l} &= \frac{1}{T^R}\left(S^M_{kl} - \frac{\partial T^R}{\partial a_k}\frac{\partial T^R}{\partial a_l}\right), \end{aligned} \tag{C6}$$

$$\begin{aligned}\frac{\partial^2 T^S}{\partial m_k \partial m_l} &= \frac{1}{T^S}\left[\frac{1}{2}\frac{\partial^2 S^M_{ij}}{\partial m_k \partial m_l}(a_i - h_i)(a_j - h_j) - \frac{\partial T^S}{\partial m_k}\frac{\partial T^S}{\partial m_l}\right], \\ \frac{\partial^2 T^R}{\partial m_k \partial m_l} &= \frac{1}{T^R}\left[\frac{1}{2}\frac{\partial^2 S^M_{ij}}{\partial m_k \partial m_l}(a_i + h_i)(a_j + h_j) - \frac{\partial T^R}{\partial m_k}\frac{\partial T^R}{\partial m_l}\right], \end{aligned} \tag{C7}$$

$$\begin{aligned}\frac{\partial^2 T^S}{\partial h_k \partial a_l} &= -\frac{1}{T^S}\left(S^M_{kl} + \frac{\partial T^S}{\partial h_k}\frac{\partial T^S}{\partial a_l}\right), \\ \frac{\partial^2 T^R}{\partial h_k \partial a_l} &= \frac{1}{T^R}\left(S^M_{kl} - \frac{\partial T^R}{\partial h_k}\frac{\partial T^R}{\partial a_l}\right), \end{aligned} \tag{C8}$$

$$\begin{aligned}\frac{\partial^2 T^S}{\partial h_k \partial m_l} &= -\frac{1}{T^S}\left[\frac{\partial S^M_{kj}}{\partial m_l}(a_j - h_j) + \frac{\partial T^S}{\partial h_k}\frac{\partial T^S}{\partial m_l}\right], \\ \frac{\partial^2 T^R}{\partial h_k \partial m_l} &= \frac{1}{T^R}\left[\frac{\partial S^M_{kj}}{\partial m_l}(a_j + h_j) - \frac{\partial T^R}{\partial h_k}\frac{\partial T^R}{\partial m_l}\right], \end{aligned} \tag{C9}$$

$$\begin{aligned}\frac{\partial^2 T^S}{\partial a_k \partial m_l} &= \frac{1}{T^S}\left[\frac{\partial S^M_{kj}}{\partial m_l}(a_j - h_j) - \frac{\partial T^S}{\partial a_k}\frac{\partial T^S}{\partial m_l}\right], \\ \frac{\partial^2 T^R}{\partial a_k \partial m_l} &= \frac{1}{T^R}\left[\frac{\partial S^M_{kj}}{\partial m_l}(a_j + h_j) - \frac{\partial T^R}{\partial a_k}\frac{\partial T^R}{\partial m_l}\right], \end{aligned} \tag{C10}$$

$$\begin{aligned}\frac{\partial^2 T^S}{\partial h_k \partial \tau} &= -\frac{1}{T^S}\left[\frac{\partial S^M_{kj}}{\partial \tau}(a_j - h_j) + \frac{\partial T^S}{\partial h_k}\frac{\partial T^S}{\partial \tau}\right], \\ \frac{\partial^2 T^R}{\partial h_k \partial \tau} &= \frac{1}{T^R}\left[\frac{\partial S^M_{kj}}{\partial \tau}(a_j + h_j) - \frac{\partial T^R}{\partial h_k}\frac{\partial T^R}{\partial \tau}\right], \end{aligned} \tag{C11}$$

$$\begin{aligned}\frac{\partial^2 T^S}{\partial a_k \partial \tau} &= \frac{1}{T^S}\left[\frac{\partial S^M_{kj}}{\partial \tau}(a_j - h_j) - \frac{\partial T^S}{\partial a_k}\frac{\partial T^S}{\partial \tau}\right], \\ \frac{\partial^2 T^R}{\partial a_k \partial \tau} &= \frac{1}{T^R}\left[\frac{\partial S^M_{kj}}{\partial \tau}(a_j + h_j) - \frac{\partial T^R}{\partial a_k}\frac{\partial T^R}{\partial \tau}\right], \end{aligned} \tag{C12}$$

$$\begin{aligned}\frac{\partial^2 T^S}{\partial m_k \partial \tau} &= \frac{1}{T^S}\left[\frac{1}{2}\frac{\partial^2 S^M_{ij}}{\partial m_k \partial \tau}(a_i - h_i)(a_j - h_j) - \frac{\partial T^S}{\partial m_k}\frac{\partial T^S}{\partial \tau}\right], \\ \frac{\partial^2 T^R}{\partial m_k \partial \tau} &= \frac{1}{T^R}\left[\frac{1}{2}\frac{\partial^2 S^M_{ij}}{\partial m_k \partial \tau}(a_i + h_i)(a_j + h_j) - \frac{\partial T^R}{\partial m_k}\frac{\partial T^R}{\partial \tau}\right], \end{aligned} \tag{C13}$$

$$\frac{\partial^2 T^S}{\partial \tau^2} = \frac{1}{T^S}\left[\frac{1}{4} + \frac{1}{2}\frac{\partial^2 S_{ij}^M}{\partial \tau^2}(a_i - h_i)(a_j - h_j) - \left(\frac{\partial T^S}{\partial \tau}\right)^2\right],$$

$$\frac{\partial^2 T^R}{\partial \tau^2} = \frac{1}{T^R}\left[\frac{1}{4} + \frac{1}{2}\frac{\partial^2 S_{ij}^M}{\partial \tau^2}(a_i + h_i)(a_j + h_j) - \left(\frac{\partial T^R}{\partial \tau}\right)^2\right]. \tag{C14}$$

APPENDIX D: PARTIAL DERIVATIVES OF THE SINGLE-SQUARE-ROOT FUNCTION

The single-square-root function, see eq. (23), has first- and second order partial derivatives as specified in the following.

D1 First-order partial derivatives

$$q_k^h = \frac{\partial T^D}{\partial h_k} = \frac{4}{T^D} S_{kj}^M h_j, \tag{D1}$$

$$q_k^a = \frac{\partial T^D}{\partial a_k} = \frac{4}{T^D} S_{kj}^M a_j, \tag{D2}$$

$$q_k^m = \frac{\partial T^D}{\partial m_k} = \frac{2}{T^D}\frac{\partial S_{ij}^M}{\partial m_k}(a_i a_j + h_i h_j), \tag{D3}$$

$$u = \frac{\partial T^D}{\partial \tau} = \frac{1}{T^D}\left[\tau + 2\frac{\partial S_{ij}^M}{\partial \tau}(a_i a_j + h_i h_j)\right]. \tag{D4}$$

D2 Second-order partial derivatives

$$U_{kl}^{hh} = \frac{\partial^2 T^D}{\partial h_k \partial h_l} = \frac{1}{T^D}\left(4S_{kl}^M - \frac{\partial T^D}{\partial h_k}\frac{\partial T^D}{\partial h_l}\right), \tag{D5}$$

$$U_{kl}^{aa} = \frac{\partial^2 T^D}{\partial a_k \partial a_l} = \frac{1}{T^D}\left(4S_{kl}^M - \frac{\partial T^D}{\partial a_k}\frac{\partial T^D}{\partial a_l}\right), \tag{D6}$$

$$U_{kl}^{mm} = \frac{\partial^2 T^D}{\partial m_k \partial m_l} = \frac{1}{T^D}\left[2\frac{\partial^2 S_{ij}^M}{\partial m_k \partial m_l}(a_i a_j + h_i h_j) - \frac{\partial T^D}{\partial m_k}\frac{\partial T^D}{\partial m_l}\right], \tag{D7}$$

$$U_{kl}^{ha} = \frac{\partial^2 T^D}{\partial h_k \partial a_l} = -\frac{1}{T^D}\frac{\partial T^D}{\partial h_k}\frac{\partial T^D}{\partial a_l}, \tag{D8}$$

$$U_{kl}^{hm} = \frac{\partial^2 T^D}{\partial h_k \partial m_l} = \frac{1}{T^D}\left(4\frac{\partial S_{kj}^M}{\partial m_l}h_j - \frac{\partial T^D}{\partial h_k}\frac{\partial T^D}{\partial m_l}\right), \tag{D9}$$

$$U_{kl}^{am} = \frac{\partial^2 T^D}{\partial a_k \partial m_l} = \frac{1}{T^D}\left(4\frac{\partial S_{kj}^M}{\partial m_l}a_j - \frac{\partial T^D}{\partial a_k}\frac{\partial T^D}{\partial m_l}\right), \tag{D10}$$

$$u_k^h = \frac{\partial^2 T^D}{\partial h_k \partial \tau} = \frac{1}{T^D}\left(4\frac{\partial S_{kj}^M}{\partial \tau}h_j - \frac{\partial T^D}{\partial h_k}\frac{\partial T^D}{\partial \tau}\right), \tag{D11}$$

$$u_k^a = \frac{\partial^2 T^D}{\partial a_k \partial \tau} = \frac{1}{T^D}\left(4\frac{\partial S_{kj}^M}{\partial \tau}a_j - \frac{\partial T^D}{\partial a_k}\frac{\partial T^D}{\partial \tau}\right), \tag{D12}$$

$$u_k^m = \frac{\partial^2 T^D}{\partial m_k \partial \tau} = \frac{1}{T^D}\left[2\frac{\partial^2 S_{ij}^M}{\partial m_k \partial \tau}(a_i a_j + h_i h_j) - \frac{\partial T^D}{\partial m_k}\frac{\partial T^D}{\partial \tau}\right], \tag{D13}$$

$$u^\tau = \frac{\partial^2 T^D}{\partial \tau^2} = \frac{1}{T^D}\left[1 + 2\frac{\partial^2 S_{ij}^M}{\partial \tau^2}(a_i a_j + h_i h_j) - \left(\frac{\partial T^D}{\partial \tau}\right)^2\right]. \tag{D14}$$

APPENDIX E: PARTIAL DERIVATIVES OF THE SINGLE/DOUBLE SQUARE-ROOT FUNCTIONS AT ZERO OFFSET

At zero offset, the first and second derivatives of the single and double square-root forms of the diffraction-time function are identical, with one important exception. When using the double-square-root form we obtain

$$U_{kl}^{hh} = \frac{\partial^2 T^D}{\partial h_k \partial h_l} = \frac{1}{T^D}\left(4S_{kl}^M - \frac{\partial T^D}{\partial a_k}\frac{\partial T^D}{\partial a_l}\right), \tag{E1}$$

while the corresponding relation for the single-square-root function is

$$U_{kl}^{hh} = \frac{\partial^2 T^D}{\partial h_k \partial h_l} = \frac{4}{T^D} S_{kl}^M. \tag{E2}$$

Relations for the remaining derivatives, which are identical to the two representations in the zero-offset situation, are listed in the following.

E1 First-order partial derivatives

$$q_k^h = \frac{\partial T^D}{\partial h_k} = 0, \tag{E3}$$

$$q_k^a = \frac{\partial T^D}{\partial a_k} = \frac{4}{T^D} S_{kj}^M a_j, \tag{E4}$$

$$q_k^m = \frac{\partial T^D}{\partial m_k} = \frac{2}{T^D}\frac{\partial S_{ij}^M}{\partial m_k}a_i a_j, \tag{E5}$$

$$u = \frac{\partial T^D}{\partial \tau} = \frac{1}{T^D}\left(\tau + 2\frac{\partial S_{ij}^M}{\partial \tau}a_i a_j\right). \tag{E6}$$

E2 Second-order partial derivatives

$$U_{kl}^{aa} = \frac{\partial^2 T^D}{\partial a_k \partial a_l} = \frac{1}{T^D}\left(4S_{kl}^M - \frac{\partial T^D}{\partial a_k}\frac{\partial T^D}{\partial a_l}\right), \tag{E7}$$

$$U_{kl}^{mm} = \frac{\partial^2 T^D}{\partial m_k \partial m_l} = \frac{1}{T^D}\left(2\frac{\partial^2 S_{ij}^M}{\partial m_k \partial m_l}a_i a_j - \frac{\partial T^D}{\partial m_k}\frac{\partial T^D}{\partial m_l}\right), \tag{E8}$$

$$U_{kl}^{ha} = \frac{\partial^2 T^D}{\partial h_k \partial a_l} = 0, \tag{E9}$$

$$U_{kl}^{hm} = \frac{\partial^2 T^D}{\partial h_k \partial m_l} = 0, \tag{E10}$$

$$U_{kl}^{am} = \frac{\partial^2 T^D}{\partial a_k \partial m_l} = \frac{1}{T^D}\left(4\frac{\partial S_{kj}^M}{\partial m_l}a_j - \frac{\partial T^D}{\partial a_k}\frac{\partial T^D}{\partial m_l}\right), \tag{E11}$$

$$u_k^h = \frac{\partial^2 T^D}{\partial h_k \partial \tau} = 0, \tag{E12}$$

$$u_k^a = \frac{\partial^2 T^D}{\partial a_k \partial \tau} = \frac{1}{T^D}\left(4\frac{\partial S_{kj}^M}{\partial \tau}a_j - \frac{\partial T^D}{\partial a_k}\frac{\partial T^D}{\partial \tau}\right), \tag{E13}$$

$$u_k^m = \frac{\partial^2 T^D}{\partial m_k \partial \tau} = \frac{1}{T^D}\left(2\frac{\partial^2 S_{ij}^M}{\partial m_k \partial \tau}a_i a_j - \frac{\partial T^D}{\partial m_k}\frac{\partial T^D}{\partial \tau}\right), \tag{E14}$$

$$u^\tau = \frac{\partial^2 T^D}{\partial \tau^2} = \frac{1}{T^D}\left[1 + 2\frac{\partial^2 S_{ij}^M}{\partial \tau^2}a_i a_j - \left(\frac{\partial T^D}{\partial \tau}\right)^2\right]. \tag{E15}$$